Model-Based Mitigation of Biodynamic Feedthrough for Touchscreen Dragging Tasks in Turbulence

A. Khoshnewiszadeh

12 February 2020

TU Delft

Model-Based Mitigation of Biodynamic Feedthrough for Touchscreen Dragging Tasks in Turbulence

Master of Science Thesis

For obtaining the degree of Master of Science in Aerospace Engineering at Delft University of Technology

A. Khoshnewiszadeh

12 February 2020

Cover image [1]

Delft University of Technology

Delft University Of Technology
Department Of
Control and Simulation

The undersigned hereby certify that they have read and recommend to the Faculty of Aerospace Engineering for acceptance a thesis entitled "**Model-Based Mitigation of Biodynamic Feedthrough for Touchscreen Dragging Tasks in Turbulence**" by A. Khoshnewiszadeh in partial fulfillment of the requirements for the degree of Master of Science.

Dated: 12 February 2020

Readers:

prof.dr.ir. M. Mulder

dr.ir. D.M. Pool

dr.ir. R. Happee

Acknowledgements

By delivering this MSc thesis work my time in Delft has come to an end. The road has at times been long and hard, but also fun, educational and beyond anything I could have imagined when I left my native Norway. There are many people who have supported me on the way who deserve recognition for their help, weather they know it or not. Firstly, the atmosphere you have created at the Control & Simulation department is unique and I believe an envy of fellow students. Not only is the academic staff kind, knowledgeable and approachable. Together you have create a culture that brings the best out of each students. Max, through your invaluable (and passionate!) supervision I have noticed your dedication to the work you all do. Keep inspiring more students! I also want to thank Olaf who supervised me during the experiment and made sure SIMONA always was working. Off course, the participants who let me shake them around in the name of science deserve their credit for their time and patients. I want to extent my appreciation to Simon who took time from his own thesis work to help me accomplish my goals. Thank you!

Importantly I want to thank Daan for agreeing to be my supervisor. Whoever I met talked about you in glowing terms. You are not only great at brainstorming and giving feedback, you also truly care about your students and it shows. Even during the tougher weeks of the thesis, I without exception left our meetings feeling positive, with many ideas to pursue.

There are many friends I want to thank, but I especially want to make sure Victor and Oana know how important they have been. As many students know, the thesis process can be solitary and lonely at times. Having friends around was the best antidote to long days in front of the screen. Thank you to my friends, the Heijnsteiners and the people at MB6. My parents and brother have been invaluable. I could always count on them on being there for me. Pouran and Behzad, your own hardships of arriving in a new country and making something of yourself has always inspired me and kept me going.

Arwin
Delft, 12 February 2020

Contents

List of Figures

List of Tables

Nomenclature

List of Abbreviations

APU	Auxiliary Power Unit
ARMA	Autoregressive Moving Average
ARP	Aerospace Recommended Practise
BDFT	Biodynamic Feedthrough
CDU	Control Display Unit
CNS	Central Nervous System
DOF	Degree Of Freedom
FMS	Flight Management System
FAA	Federal Aviation Administration
FRF	Frequency Response Function
MDTT	Multi-Directional Tapping Test
NMS	Neuromuscular System
OSFA	One-Size-Fits-All
PFD	Primary Flight Display
PSD	Power Spectral Density
RMS	Root Mean Square
SA	Subject Average
SIMONA	SImulation, MOtion and NAvigation Institute
SRS	SIMONA Research Simulator
VAF	Variance Accounted For

Chapter 1

Introduction

Aircraft flight decks have had a major evolution from analog displays and mechanical controls to the digital flight deck. The classical cockpits tended to display information on dedicated gauges and with controls executing one task (Figure 1-1a). In contrast, modern aircraft have an even larger amount of information that needs to be accessed by the pilots, but with the cockpit surface area remaining almost the same [12]. This has been solved by integrating data and displaying it in new ways (Figure 1-1b). The introduction of computers has also allowed organizing data in folder structures such as on the Control Display Unit (CDU) which is the main way to interface with the Flight Management System (FMS) [13]. This evolution is continuing, with touchscreens soon taking over the commercial cockpit.

With touchscreen technology ubiquitous in everyday life, in the aviation industry they are seen as a novelty. In 2009, with their G3000 integrated avionics system, Garmin was the first to introduce touch in the cockpit of private and business aircraft. In 2018 Gulfstream introduced its G500/G600 business aircraft with 10 touchscreens taking over the functions of a large number of knobs, buttons and controls [14]. Most recently the commercial aircraft manufacturers Airbus and Boeing will soon introduce touchscreens in their A350 and 777X line of aircraft [15, 16]. It is still early days for touch technology on the flight deck, but with their many potential benefits, aircraft manufacturers and airlines are likely to continue its integration on the flight deck [17].

(a) Classic flight deck on the McDonnell Douglas DC-10.

(b) Modern flight deck on the Airbus A350.

Figure 1-1: The cockpit evolution

There are several advantages of introducing touchscreens on the flight deck. They have the ability to make human-computer interaction more intuitive by using direct manipulation and when coupled with new visualisation methods can improve task performance [18]. This can lead to a potential of reduction of pilot workload and increased task speed compared to conventional input methods [19–21]. However, touchscreens also bring new challenges such as inadvertent touch due to turbulence, no direct feedback and the possibility of glare [9, 14, 18, 22–25].

Previous research has shown that turbulence causes biodynamic feedthrough (BDFT), the involuntary limb movement due to vibrations [26, 27]. There is however a lack of research into ways to reduce the effect of BDFT. This leads to the motivation and objective of the thesis:

Objective: Mitigating BDFT can have a positive effect on the pilot performance and motivate the introduction of touchscreens on the flight deck. Currently aircraft manufacturers have solved this by letting pilots brace on the touchscreens bezels (frame) and edges [14, 16, 28], but with introduction of larger screens this strategy can make certain tasks difficult and make parts of the screen hard to reach. Mobertz, a previous master thesis student at the Control & Simulation department at the Aerospace Faculty at TU Delft, quantified and modelled BDFT and recommended further research into using a model-based approach for mitigation [27].

This thesis has therefore continued that work by looking at a software solution to mitigating BDFT by using a model-based approach.

Research Question: The following research question was answered in the AIAA Paper and is a modification of the research question posed at conclusion of the Preliminary Report in Chapter 7. The change emphasises that both continuous and step tracking tasks were investigated for model-based BDFT cancellation.

> To what extent can biodynamic feedthrough be mitigated using a model-based approach whilst performing a 2D continuous pursuit dragging task and a point-to-point (step) dragging task on a touchscreen display located at a typical flight deck PFD position?

Thesis Report outline:

Experiment Results

AIAA Paper
This paper deals with human-in-the-loop experiment conducted in the SIMONA Research Simulator (SRS) to answer the main research question presented in this introduction. The experiment looked into model-based mitigation of BDFT for a continuous pursuit dragging task and a point-to-point (step) dragging task.

Literature

Chapter 2: Preliminary Research Question
The literature study started with a preliminary research question to guide the study. The Preliminary Report concluded with a research proposal based on the literature and data analysis.

Chapter 3: Touchscreens on the Flight Deck
Different aspects of introducing touchscreens on the flight deck were investigated, their advantages, challenges, properties and tasks.

Chapter 4: BDFT Mitigation and Modelling
This chapter took a closer look at BDFT by defining what it is and investigating different ways of mitigating it. The chapter then shifted to BDFT modelling in the context of model-based BDFT mitigation.

Data Analysis

Chapter 5: Offline Model-Based Cancellation
Data from research conducted by Mobertz, a previous MSc student at the Control & Simulation department the Aerospace Faculty of the TU Delft was used to perform an offline model-based BDFT cancellation to investigate its feasibility.

Pilot Experiment

Chapter 6: Pilot Experiment: Online Model-Based BDFT Cancellation
Building on the previous chapter, a pilot experiment was performed in the SRS. It investigated model-based BDFT cancellation using a step task, which more closely resembled a realistic precision touchscreen task.

Future experiment and Conclusion

Chapter 7: Research Proposal
Based on literature, offline cancellation and pilot experiment this chapter proposed a research question and experiment to be conducted in the SRS. This research question was slightly modified after the completion of the Preliminary Report.

Chapter 8: Preliminary Report Conclusion
Finally, the conclusion about the work performed in the Preliminary Report is presented.

Additional Information

Appendices
The appendices provide additional information and results and analysis from both the Preliminary Report and AIAA Paper

Part I

AIAA Paper

Model-Based Mitigation of Biodynamic Feedthrough for Touchscreen Dragging Tasks in Turbulence

Arwin Khoshnewiszadeh*
Delft University of Technology
Delft, the Netherlands

The anticipated arrival of touchscreens on the commercial flight deck will make pilots vulnerable to erroneous screen inputs under vibration, creating a potential safety hazard. Biodynamic feedthrough (BDFT) has shown to be a key obstacle in continuous touchscreen dragging tasks under simulated turbulence, disrupting task performance. This research therefore focuses on the implementation of a model-based approach to mitigate the adverse effects of BDFT. A human-in-the-loop experiment with 18 participants was performed. The experiment consisted of two simulator sessions, the first with the goal of collecting data used for identifying two BDFT models: a subject-average (SA) and a one-size-fits-all (OSFA) model. In the second session these two models were tested for their ability to cancel BDFT in the same two-dimensional pursuit task they were identified from, and in an additional point-to-point dragging task emulating a waypoint modification. The model-based BDFT cancellation approach was tested for two combinations of motion disturbance axis and touchscreen input direction: sway (side-to-side motion) with horizontal screen inputs and heave (up-down motion) with vertical screen inputs. The results showed it is possible to cancel between 80-90% of the BDFT in both cases despite poor cancellation for certain specific participants. The point-to-point dragging task showed much less BDFT than the continuous task used for BDFT model development, however, making the cancellation ineffective. Overall, the results show that while model-based BDFT cancellation is possible, it is crucial to account for individual variability and the specific touchscreen task.

Nomenclature

Symbols

A_d	Multisine disturbance amplitude, [m/s^2]	ω_{BDFT}	BDFT model natural frequency, [rad/s]
A_t	Multisine target amplitude, [mm]	ω_d	Motion disturbance frequencies, [rad/s]
$e_{y,z}$	Tracking error pursuit task, [mm]		
$f_{t_{y,z}}$	Target signal, [mm]	*Abbreviations*	
$f_{d_{y,z}}$	Motion disturbance signal, [m/s^2]		
G_{BDFT}	BDFT model gain, [mm/(m/s^2)]	BDFT	Biodynamic feedthrough
$\hat{H}_{BDFT}$	BDFT frequency response, [-]	BMI	Body Mass Index
H_{BDFT}	Identified BDFT dynamics, [-]	CNS	Central nervous system
$n_{d,t}$	Multisine integer multiples, [-]	FAA	Federal Aviation Agency
s	Laplace operator, [-]	FRF	Frequency response function
T_m	Measurement time, [s]	OSFA	One-size-fits-all
$u_{y,z}$	Touchscreen input, [mm]	PFD	Primary flight display
$u_{y,z}^{can}$	Cancelled touchscreen input, [mm]	PFD	Primary flight display
$u_{f_d}^{meas}$	Measured BDFT, [mm]	PSD	Power Spectral Density
$u_{f_d}^{mod}$	Modelled BDFT, [mm]	SA	Subject Average
ζ_{BDFT}	BDFT model damping ratio, [-]	SRS	SIMONA Research Simulator
τ_{BDFT}	BDFT model delay, [s]	VAF	Variance Accounted For
$\phi_{d,t}$	Multisine phase, [rad]		

*MSc Student, Control and Simulation Section, Faculty of Aerospace Engineering, P.O. Box 5058, 2600GB Delft, The Netherlands; a.khoshnewiszadeh@student.tudelft.nl

I. Introduction

The next evolution of the commercial flight deck will introduce touchscreen devices to replace physical controls such as buttons and switches. Both Airbus and Boeing have announced touchscreens in the cockpit of their coming airliners[1,2] with Gulfstream's business jet G500/600 already including ten touchscreen controllers.[3] The possible advantages of touchscreens such as their direct manipulation capabilities, reduction of workload, cost and efficient space usage have been motivations for their introduction.[4,5] However, one important challenge is their operation in vibrating environments, such as turbulence, which has shown to increase workload, cause more task errors, and to increase fatigue.[6,7]

One key reason for decreased task performance is biodynamic feedthrough (BDFT), the involuntary movement of limbs due to vibration.[8,9] BDFT causes the body to move in an unintentional manner, resulting in unwanted touchscreen inputs. Although BDFT so far has received little attention in regard to touchscreen tasks, it has been extensively investigated and shown to decrease task performance in aircraft and helicopters control tasks,[8,10–13] hydraulic excavators,[14] and electric wheelchairs.[15] Hence, the mitigation of BDFT will benefit the pilot's interaction with touchscreens on the flight deck and result in fewer input errors.

Several methods have been proposed for mitigating BDFT or reducing its effects on task performance. The most simple methods involve different types of hand support. Examples include adding high friction materials around the screen bezels or making it possible to grip around the edge of the screen.[3,7,16,17] A rather novel approach relies on resting all fingers on the screen while using the index finger for tapping.[18] While these methods can be useful for tapping tasks, they can be limiting for continuous dragging tasks envisioned for touchscreen applications on the flight deck.[19–22] A completely different software-based approach, which is explored in this paper, is model-based BDFT cancellation. This approach uses a model that only describes the involuntary hand movements caused by the vehicle acceleration. The modelled BDFT output can then, in the gesture interpretation software, be subtracted from the total touchscreen control input. In literature this method has been demonstrated with physical control inceptors.[23–25] A downside of this method is that it relies on the fidelity of the BDFT model for successful cancellation.[26] Only one previous study by Mobertz et al.[9] has focused on the quantification of BDFT when using a touchscreen. The authors showed that feedthrough was strongest when the vehicle motion and screen input were along the same axis, resulting in a high signal-to-noise ratio. Simple transfer function BDFT models were then identified for these conditions, but were not used for cancellation. Hence, applying these models to perform model-based BDFT cancellation is a promising next step.

Two types of BDFT can be distinguished: closed-loop[24,25] and open-loop.[27] If the control actions of the operator changes the state of the vehicle BDFT is considered closed-loop. An example is a pilot's input to the control inceptor under turbulence. With open-loop BDFT the state of the vehicle does not change with the control inputs. Touchscreen operations typically do not intend to directly control the vehicle. A waypoint modification, as simulated in this study, is such an example.

The goal of this paper is to assess the feasibility of open-loop model-based BDFT cancellation for touchscreen applications under simulated turbulence. Specifically, the paper looks into how much cancellation is feasible with this approach, if BDFT models should be individualized, and finally, if the BDFT model used in the paper can be effective on two different types of touchscreen tasks. This was accomplished by performing a human-in-the-loop experiment using the SIMONA Research Simulator (SRS) at Delft University of Technology. A two-dimensional multisine pursuit dragging task was first performed by all 18 participants with a multisine motion disturbance signal in either the vertical or lateral axis, mimicking turbulence. This allowed for the identification of two BDFT models: a subject-average model (SA) and a one-size-fits-all (OSFA) solution based on the average of all participants, making it possible to assess how between-subject differences affect model-based cancellation. The models were then applied as a software solution on a second evaluation day, including the same pursuit task and an additional point-to-point (step task), simulating a more realistic dragging task. Because the two tasks differed in how the finger moved over the screen, the generalizability of the model across tasks could be determined.

First, in Section II a background on how to perform BDFT cancellation is given. Then, in Section III the method of the experiment is presented, including the details of the touchscreen tasks, the motion disturbance signal, the BDFT models and the setup of the experiment. In Section IV the results of the BDFT cancellation are presented. The results are then discussed in Section V before the paper's conclusion in Section VI.

II. BDFT Cancellation

BDFT is the involuntary limb movement caused by vibration and is different than voluntary control action, as shown in Figure 1. The voluntary actions come from the central nervous system (CNS) which in order to achieve the goals of the control task applies cognitive commands to the neuromuscular system.[26,28] Although the two can be separated, the voluntary actions do affect the involuntary contributions to the total control input indirectly. For example, by cognitively changing the neuromuscular setting, tightening or loosening muscles, the susceptibility to BDFT will also change.[11,29]

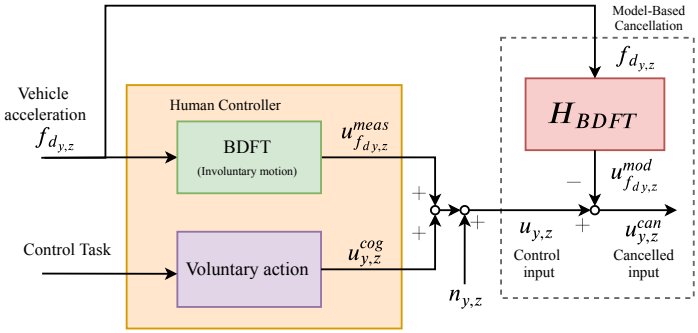

Figure 1: Definition of open-loop BDFT and model-based BDFT cancellation.

The control signal, $u_{y,z}$, therefore has several contributions. One part of the input signal can be attributed to the motion disturbance, $u^{meas}_{f_{d\,y,z}}$, while the other part is the cognitive input, $u^{cog}_{y,z}$. Additionally there is the remnant, $n_{y,z}$, which is the component not linearly correlated with the tracking signal or motion disturbance.[8] The goal of model-based BDFT cancellation is to remove the contribution of the motion disturbance. This can be done by subtracting the modelled BDFT contribution, $u^{mod}_{f_{d\,y,z}}$ from the total control input, $u_{y,z}$. The cancelled screen input signal and can therefore be described according to Equation (1).

$$u^{can}_{y,z} = u_{y,z} - u^{mod}_{f_{d\,y,z}} = u^{cog}_{y,z} + n_{y,z} + u^{meas}_{f_{d\,y,z}} - u^{mod}_{f_{d\,y,z}} \tag{1}$$

Because the BDFT cancellation is taking place in the software, the pilots are not directly aware of it taking place, making the registered touch point unpredictable. Another method to cancel the BDFT is to move the screen image a distance corresponding to the modelled BDFT. The advantage is the operator's awareness of the cancellation, which includes them in the cancellation loop.[26] However, this method was not used in the current research because of the possibility of visual blurring and the possible change in the participants' control strategy based on the movement of the screen image.

III. Method

A. Control Tasks

Two different touchscreen tasks were considered for the human-in-the-loop experiment: a pursuit task and a step task (target acquisition). While the former was used for the identification of BDFT models, both tasks were used for performing model-based BDFT cancellation while under the influence of a motion disturbance signal. Figure 2 shows a block diagram of the performed tracking tasks. For the pursuit task the horizontal (f_{t_y}) and vertical (f_{t_z}) target signals were multisine signals, resulting in a continuous movement across the screen. The pursuit task was identical to the one used in the work of Mobertz et al.[9] It was decided to use the same task since their work had shown that enough BDFT was present for successful system identification of a BDFT model. For the step task, the target signals 'jumped' between predetermined screen locations. For both tasks, constant contact with the screen was required. Additionally, the displays were identical, with the only difference being the target signals. The display (see Figure 3 and Figure 4) had two markers, one purple marker showed the touch position u_y and u_z, while the white marker displayed the target signals f_{t_y} and f_{t_z}. Both markers had attached horizontal and vertical lines, aiding participants in case of their arm or hand blocked their view. The touchscreen was in an upright position directly in front of the participant, typical of a

primary flight display (PFD). For both the pursuit and step tasks the experiment runs lasted 90 seconds per condition, of which the measurement time for the pursuit task is defined as the last $T_m = 81.92$ seconds.

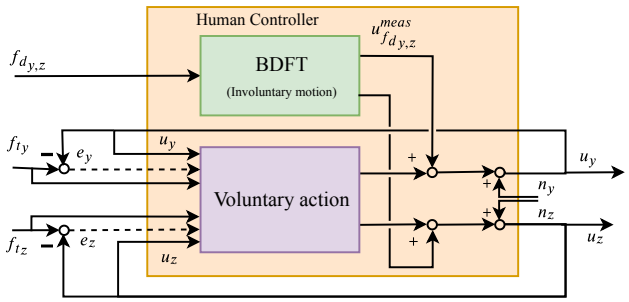

Figure 2: Quasi-linear human operator model for both the pursuit and step tracking tasks.

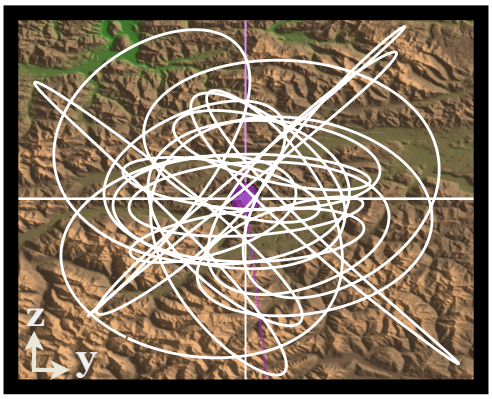

Figure 3: Path of forcing function for pursuit target across the touchscreen.

1. Forcing Functions: Disturbance Signal and Pursuit Task

Both the disturbance signal and touchscreen pursuit task were quasi-random sum-of-sines created using Equation (2) and were also used in the work by Mobertz et al.[9] The disturbance signal had the goal of simulating a realistic turbulence signal while at the same time only having power at predetermined frequencies. The same disturbance signal was applied separately in the lateral (Y) and vertical (Z) motion axes. On the other hand, the two-dimensional touchscreen target signals were meant to create a continuous and unpredictable task for the operator, without being too challenging. Figure 3 shows an example realization of the pursuit task forcing functions across the touchscreen. The horizontal and vertical tracking errors (e_y, e_z) were to be minimized by the participants, with the error defined as the difference between the target signals (f_{t_y}, f_{t_z}) and the control signal (u_y, u_z), also called the touchscreen input.

The signals were defined by the amplitude ($A_{d,t}$), phase ($\phi_{d,t}$) and frequency ($\omega_{d,t}$) with the subscripts d and t indicating the disturbance and pursuit target signal, respectively. By choosing the disturbance and target frequencies as multiples (n_d and n_t) of the base frequency, $\omega_m = 2\pi/T_m = 0.0767$ rad/s, spectral leakage was prevented. The parameters used to define Equation (2) can be found in Table 1.

$$f_{d,t}(t) = \sum_{k=1}^{N_{d,t}} A_{d,t}[k] \sin\left(\omega_{d,t}[k]t + \phi_{d,t}[k]\right) \tag{2}$$

The disturbance signals which have been used in previous research[9,30] were based on $N_d = 10$ sum-of-sines frequencies between 0.38 and 17.33 rad/s for the lateral (f_{d_y}) and vertical motion axis (f_{d_z}). In this paper the motion disturbance refers to the cabin acceleration, but in Table 1 the signals are reported as position signals, f_d^{pos}. Because the motion simulator required an acceleration input, f_d^{pos} had to be differentiated twice to obtain acceleration signals. More details can be found in Ref. 9. The amplitude distribution was created by a low-pass filter resulting in a lower power at higher frequencies. To limit peaks in the time domain, the phases were chosen using a cresting technique.[9]

The target signals in horizontal (f_{t_y}) and vertical (f_{t_z}) screen directions both consisted of three distinct frequencies. Only having a limited number of low frequencies risked the participants learning the path of the target. This risk was reduced by mirroring the signals in both horizontal and vertical screen directions between consecutive tracking runs, creating four different time realizations of the same set of two multisine signals. The horizontal and vertical target signals were first scaled to have the same power before being normalized. To use the full extent of the touchscreen the vertical target was then scaled by 360 px (106.92 mm) and the horizontal with 480 px (142.56mm). For reference, in Table 1 the amplitudes are given in millimeters since the pixel pitch can vary between screens.

Table 1: Multisine properties used for the disturbance and pursuit target signal.

	Disturbance, $f^{pos}_{d_{y,z}}$				Target, f_{t_y}				Target, f_{t_z}			
k	n_d	ω_d	A_d	ϕ_d	n_{t_y}	ω_{t_y}	A_{t_y}	ϕ_{t_y}	n_{t_z}	ω_{t_z}	A_{t_z}	ϕ_{t_z}
-	-	rad/s	m	rad	-	rad/s	mm	rad	-	rad/s	mm	rad
1	5	0.384	$1.067 \cdot 10^{-1}$	-0.269	3	0.230	32.767	1.445	2	0.153	22.771	0.308
2	11	0.844	$8.069 \cdot 10^{-2}$	4.016	7	0.537	39.777	0.000	13	0.997	39.775	-0.431
3	23	1.764	$4.019 \cdot 10^{-2}$	-0.806	19	1.457	71.354	-1.825	17	1.304	47.511	-1.591
4	37	2.838	$2.048 \cdot 10^{-2}$	4.938								
5	51	3.912	$1.246 \cdot 10^{-2}$	5.442								
6	71	5.446	$7.568 \cdot 10^{-2}$	2.274								
7	101	7.747	$4.735 \cdot 10^{-3}$	1.636								
8	137	10.508	$3.424 \cdot 10^{-3}$	2.973								
9	171	13.116	$2.856 \cdot 10^{-3}$	3.429								
10	226	17.334	$2.416 \cdot 10^{-3}$	3.486								

2. Step Task

The step task was used to explicitly assess the generalizability of the model-based BDFT approach for different touchscreen input tasks. That is, can BDFT models identified using the mutlisine pursuit task be successful in cancelling a more realistic point-to-point step task? For a drag-and-drop task, only the final touchscreen input position is of importance, therefore only the BDFT cancellation at the endpoint was assessed. Compared to the pursuit task, the step task simulated a realistic precision dragging task between two locations. This can be a touchscreen flightplan modification where the operator must drag a waypoint to an alternate location. Conversely to the pursuit task, which had a smooth movement across the screen, the step task jumped between four predetermined locations. The endpoints were concentric with respect to the center of the touchscreen, Figure 4 shows the four possible endpoint locations which were a distance of 500 px (148.5 mm) apart. The marker would stay at the location for 3 seconds before shifting to one of the three other endpoints, as shown in the example time traces in Figure 5, with the shaded area being the data used for the analysis. It was empirically found that subjects needed between 1.0 - 1.5 seconds to move to the endpoint location, and since only the endpoint performance was evaluated, the last 1.5 seconds of each step was used to assess the BDFT cancellation performance.

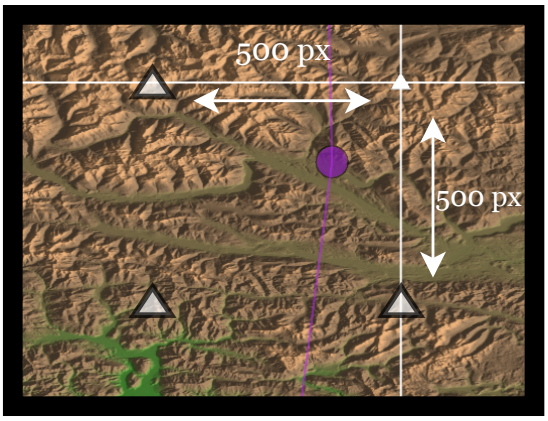

Figure 4: Visual display with target endpoint location defined for the step task.

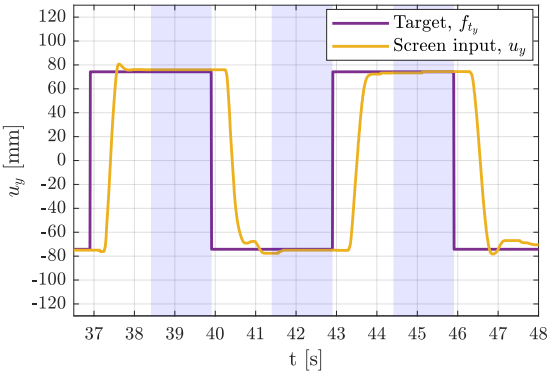

Figure 5: Example forcing function f_{t_y} and touchscreen input u_y time traces for step task.

The velocity profile when dragging across the screen was different than for the pursuit task. The maximum velocity is experienced around the half point between the starting location and the endpoint. Because of the nature of the task, the dragging speed was not controlled between subjects. However, they were asked to use natural dragging movements. With the four possible endpoint locations in Figure 4, screen movements were limited to only vertical, horizontal and diagonal movements.

B. BDFT Models

1. System Identification

Because of the success in modelling BDFT by Mobertz et al., the same linear modelling approach was used in the current work. The BDFT models were identified and then applied to two conditions: sway (lateral) motion disturbance with horizontal touchscreen input (denoted: HOR) and heave (vertical) motion disturbance with vertical input (denoted: VER). These conditions were chosen for two reasons. First, aircraft turbulence is mostly present in sway and heave.[31] Additionally, Mobertz et al.[9] showed that strong biodynamic feedthrough is present in both of these conditions and that this enables reliable system identification of BDFT dynamics.

The multisine disturbance and target signals have the benefit of having a discrete frequency spectrum. The contributions from these two signals can therefore be separated using frequency domain identification techniques.[32,33] Any power at the motion disturbance frequencies (ω_d) in the control signal ($u_{y,z}$) can therefore be attributed to the disturbance signal. The frequency response function (FRF) between the disturbance signal and the control signal then gives a non-parametric estimate of the BDFT dynamics at the disturbance frequencies (Equation (3)). This estimate is obtained from the ratio of the cross-spectral density between the motion disturbance and the control signal ($S_{f_d,u_{y,z}}(j\omega_d)$) with the auto-spectral density of the motion disturbance ($S_{f_{d_{y,z}},f_{d_{y,z}}}(j\omega_d)$). The model therefore has an acceleration input and as output the relative finger position caused by motion disturbance:

$$\hat{H}_{BDFT_{y,z}}(j\omega_d) = \frac{S_{f_d,u_{y,z}}(j\omega_d)}{S_{f_{d_{y,z}},f_{d_{y,z}}}(j\omega_d)} \tag{3}$$

2. BDFT Model and Parameter Estimates

By analyzing the FRFs it was decided to use a mass-spring-damper system with an additional gain and time delay as the model structure to model the BDFT dynamics (Equation (4)). The model consist of a gain (G_{BDFT}), natural frequency (ω_{BDFT}), damping ratio (ζ_{BDFT}) and time delay (τ_{BDFT}). The gain G_{BDFT} was added to be able to capture the magnitude of the BDFT, which is different between experiment conditions and individual participants. Additionally, the time delay τ_{BDFT} was added because the frequency responses showed a decrease in phase at higher frequencies and resulted in a higher model fit. Unfortunately, the model parameters can not be directly compared to the work by Mobertz et al.[9] While they also used a second-order BDFT model (without a time delay), by employing three model coefficients: a mass, spring and a damper, instead of natural frequency and damping ratio, their system was over-determined. The resulting parameters were therefore not unique. Because the model describes all effects between the input acceleration and the relative finger position, the model parameters must be seen as lumped, consisting of several contributing systems such as seat, spine and arm dynamics acting in parallel:

$$H_{BDFT}(s) = G_{BDFT} \cdot \frac{\omega_{BDFT}^2}{s^2 + 2\zeta_{BDFT}\omega_{BDFT} \cdot s + \omega_{BDFT}^2} e^{-s\tau_{BDFT}} \tag{4}$$

$$J(\theta) = \sum_{k=1}^{N_d} \left| \frac{\hat{H}_{BDFT}(j\omega_d) - H_{BDFT}(j\omega_d|\theta)}{\hat{H}_{BDFT}(j\omega_d)} \right| \tag{5}$$

The system identification was performed using an standard interior-point optimization in the frequency domain using Matlab's `fmincon` function using the cost function in Equation (5). The parameter limits and initial conditions used are listed in Table 2.

Table 2: Limits and initial conditions for the BDFT parameter estimation.

	G_{BDFT} [mm/(m/s^2)]	ω_{BDFT} [rad/s]	ζ_{BDFT} [-]	τ_{BDFT} [s]
Lower limit	0.0	0.0	0.0	0.0
Upper limit	35.0	15.0	2.0	2.0
Initial condition	20.0	6.0	0.6	0.1

3. BDFT Model Averaging: SA and OSFA Models

To evaluate the necessity of individualization, two types of BDFT cancellation models were created from the models estimated from participants' individual trial data: a subject-average (SA) and a one-size-fits-all (OSFA) model. These two types of models were created for both the HOR and VER conditions. The SA, or individualized model, is derived from the mean of the identified BDFT model parameters for every participant. The OSFA models then resulted by taking the mean of each subjects's SA parameters. The Variance Accounted For (VAF) was used for model validation. The VAF indicates how much of the measured variance of the BDFT signal can be explained by the modelled BDFT, with 100% meaning that the two signals are identical. Figure 6 shows a typical Bode plot of the model fit for HOR. Both the SA and OSFA models are estimated, with the SA model leading to having a better model fit than the OSFA model.

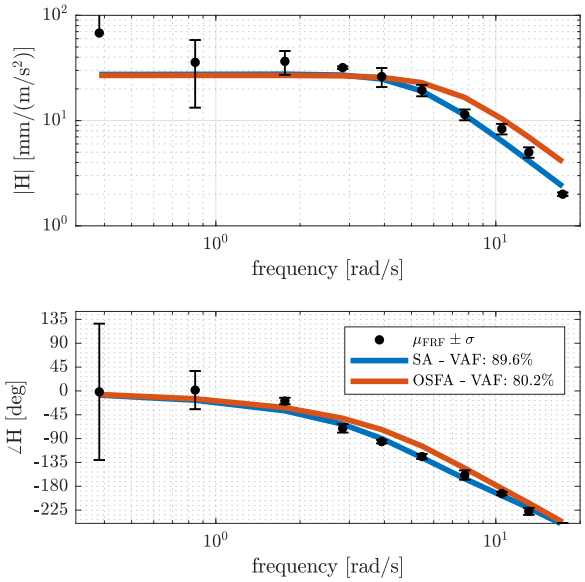

Figure 6: Frequency response and model fit for the subject-average (SA) and one-size-fits-all (OSFA) BDFT models for Subject 1 in the HOR condition.

To confirm the validity of this approach, the data from the BDFT touchscreen experiment by Mobertz et al.[9] were used to identify SA and OSFA BDFT models as defined in Equation (4). The VAF for the HOR condition showed that both the SA (M = 87.87%, SD = 3.92%) and OSFA models (M = 79.53%, SD = 16.92%) could be modelled with a high accuracy and small spread between subjects. The VER condition showed that the SA (M = 74.04%, SD = 16.54%) and especially OSFA (M = 24.61%, SD = 67.88%) having worse model fit with a higher spread. These findings suggest the feasibility of using the SA models for successful BDFT cancellation, while limited success is expected from the OSFA models.

C. Apparatus

The experiment was performed in the SIMONA Research Simulator (SRS) at Delft University of Technology. This 6-degree-of-freedom hexapod research simulator, shown in Figure 7, is hydraulically actuated with a reported motion delay of around 30 ms.[34] Experiment data were collected at 100 Hz update rate. The experimental setup inside the SRS is shown in Figure 8. The adjustable seat was equipped with a five-point harness, restricting the movement of the participants, but still allowing the upper body to lean forward. The light in the cabin was kept on throughout the experiment to reduce eye strain.

A 15" Iiyama ProLite TF1534MC-B1X capacitive touchscreen was installed directly in front of the pilot seat and was tilted 18° with respect to the vertical plane. It had a 1024×768 pixel resolution, a pixel pitch of 0.297 mm/px and a tap response time of 8 ms. The drag latency of the screen was measured with a custom test bench and was found to be a function of input speed, see Figure 9.[35] The vertical line and shaded area show the mean velocity and standard deviation of the the multisine target signals. A drag delay between 70 and 80 ms was therefore experienced. For the step task only the endpoint portion of the dataset was used for the BDFT cancellation analysis. At the endpoint locations the finger

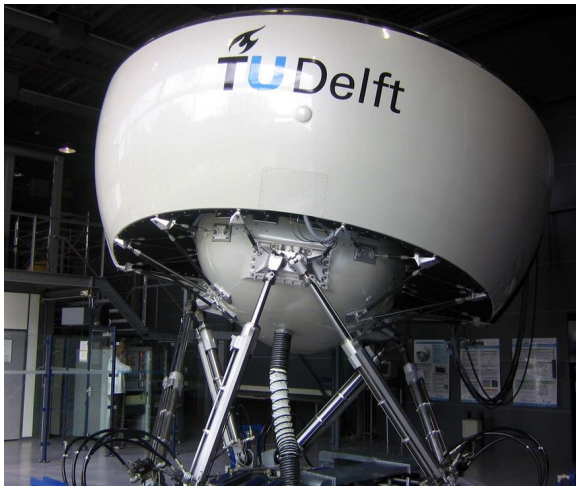

Figure 7: SIMONA Research Simulator (SRS) at Delft University of Technology.

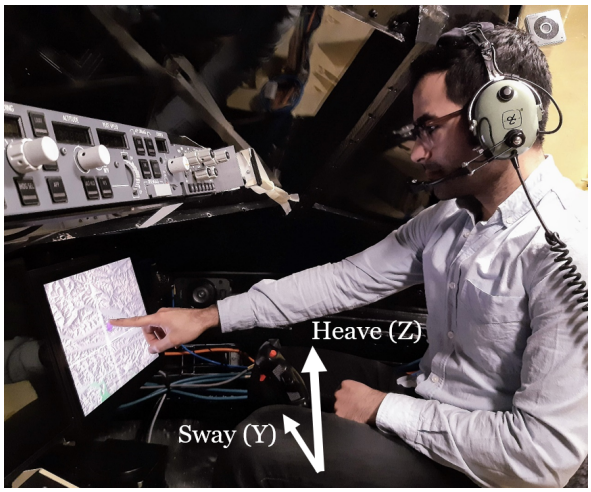

Figure 8: Flight deck experiment setup.

velocity is close to zero. For this condition the experienced drag latency was therefore close to 80 ms. The additional delay in the real time software was measured to be between 1 ms and 6 ms. To reduce friction and finger fatigue, the participants wore anti-static gloves for the duration of the experiment (EN338 performance level 2242, NEN-EN-IEC 61340-5-1 ESD rated).

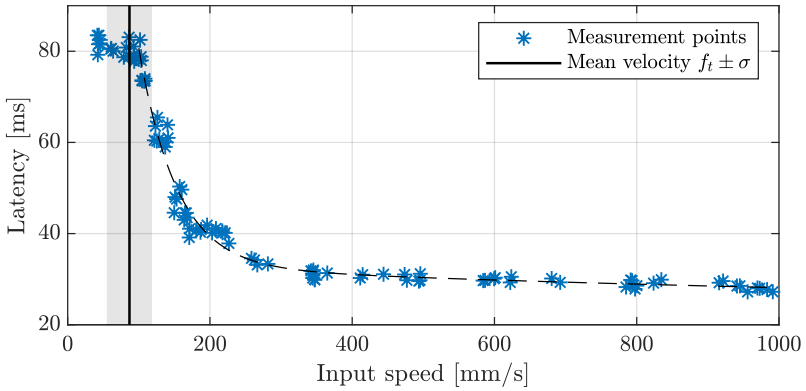

Figure 9: Drag latency of the Iiyama ProLite TF1534MC-B1X capacitive touchscreen.

D. Participants

The experiment was performed by 18 participants (M = 27, SD = 4.77 years) of which 15 were male and 3 female. They were recruited from the student population at Delft University of Technology and most were familiar with manual tracking tasks from previous experiments. For reference, the participants' height (M = 179.71, SD = 7.32 cm) and weight (M = 78.45, SD = 12.70 kg) were measured and used to derive the Body-Mass-Index (BMI) (M = 24.27, SD = 3.64 kg/m^2). The participants also estimated the number of years of experience they had with touchscreen use (M = 9.10, SD = 2.45 years). Participants were asked to use their dominant hand during the experiment, with one participant using the left hand while the 17 remaining used their right hand. All subjects signed a consent form agreeing to take part in the experiment.

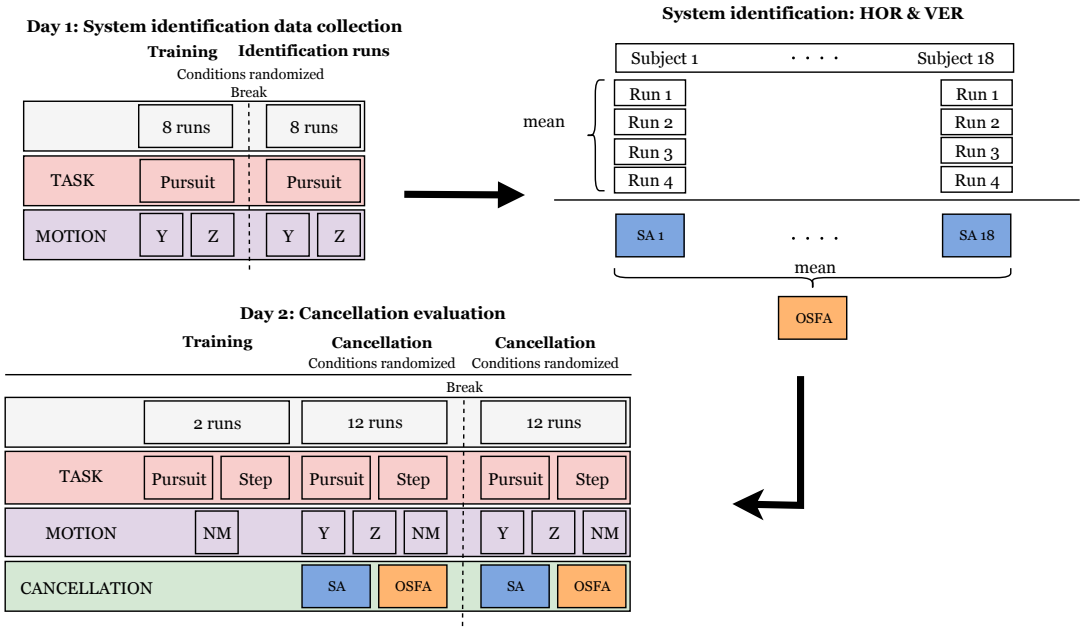

Figure 10: Experiment conditions and procedures.

E. Procedure

A written briefing was sent to the participants a couple of days before the experiment, detailing the tasks and experiment procedures. They were only told the research was related to measuring the effect of BDFT while using a touchscreen, while any mention of system identification and cancellation was left out to avoid any influence on the task performance. They were also informed about the amount of runs for each day, but the exact experiment conditions were not known except for the presence of different motion conditions and a no-motion condition.

Figure 10 shows the details of the experiment procedure as they were performed for each subject. The experiment was split over two days: day one had the goal of collecting data for system identification of the BDFT models, while the second day was used to evaluate the identified models. The first experiment day consisted of 16 runs with a break of around fifteen minutes halfway. Because the control task was simple to perform, only eight training runs were used. The participants were not informed that only the runs after the break were used for the system identification, while the the first eight runs were used for training. All participants first performed this part of the experiment to allow for the identification of the OSFA models. Between the two experiment days, the collected data were used to identify the SA and OSFA models for both the HOR and VER conditions.

The goal of the second experiment day was to evaluate the quality of model-based mitigation achieved with the identified BDFT models. The number of days between the two experiment days varied between participants from a minimum of 3 days to a maximum of 14 days. In total, there were 24 experiment runs and an additional 2 training runs with no motion (NM) to get familiar with the pursuit task from the first experiment day, as well as the new step task. The combination of task (pursuit and step task) and motion condition (Y, Z, NM) gave six experiment conditions. The BDFT models identified from HOR was only applied with Y motion while the VER models were used for Z motion only. Each of the six conditions were repeated four times using a randomized Latin square. The participants were never aware of the BDFT cancellation taking place since no feedback was given to the operators.

Throughout the experiment no numerical feedback was given to participants regarding their performance, but encouragement was given to perform better, especially with subjects that were having a more difficult time focusing or experiencing arm fatigue. For the same reason the breaks between the runs varied in length between a few seconds to maximum of a 2-3 minutes.

F. Dependent Measures

The goal of the paper is to assess the effectiveness of model-based BDFT cancellation for different tasks, and also to investigate possible reasons for differences seen between peoples BDFT dynamics. To achieve this, several dependent measures were calculated from the recorded touchscreen input and motion disturbance data.

- **The BDFT model parameters:** G_{BDFT}, ω_{BDFT}, ζ_{BDFT}, τ_{BDFT} define the dynamics of the BDFT model and were the results of the system identification. The parameters were identified for each of the four runs per experiment condition before being averaged to the SA and OSFA models, see Figure 10. The parameters were then used to assess the variability in BDFT dynamics observed between participants. To validate the BDFT models, VAF was used as a goodness-of-fit measure.
- **Power Spectral Densities (PSDs):** for the multisine pursuit task data, the power spectral densities (PSDs) of both the original ($u_{y,z}$) and cancelled screen input signal ($u^{can}_{y,z}$) were used to estimate the feedthrough caused by the motion disturbance (f_d). Power observed at the disturbance frequencies signifies the presence of BDFT.
- **BDFT cancellation pursuit task:** the main measure for the cancellation performance is given in Equation (6) and is a relative percentage change of the biodynamic feedthrough of the cancelled control signal, $u^{can}_{f_d}$, with respect to the feedthrough with no cancellation, $u^{meas}_{f_d}$.

$$\Delta\sigma^2_{u_{f_d}} = \frac{\mathrm{Var}\left(u^{meas}_{f_d}\right) - \mathrm{Var}\left(u^{can}_{f_d}\right)}{\mathrm{Var}\left(u^{meas}_{f_d}\right)} \cdot 100[\%] \tag{6}$$

- **BDFT cancellation step task:** the step target signal does not have a discrete power spectrum, which means touchscreen input power at ω_d can not only be attributed to the disturbance frequencies. Because of these limitations of spectral methods with the step task, the standard deviation of the horizontal (σ_{u_y}) and vertical (σ_{u_z}) screen input signals are used as a measure of BDFT. After cancellation the horizontal ($\sigma^{can}_{u_y}$) and vertical ($\sigma^{can}_{u_z}$) deviations are a performance measure of the cancellation. A lower standard deviation for the cancelled signal implies that the cancellation is attenuating the BDFT.

G. Hypothesis

The following hypotheses were formulated for the current experiment:

H1: *The motion disturbance component of the touchscreen input signal, $u^{meas}_{f_{d\,y,z}}$, will have an average cancellation up to 88% for the pursuit task:*
Mobertz et al.[9] found that BDFT could be modelled with a median VAF of 75%. However, for a better model fit at higher frequencies the current BDFT model also includes a time delay, τ_{BDFT}, which in Section III.B showed can provide a better model fit. Since the quality-of-fit of the BDFT can be considered the upper limit for the extent to which $u^{meas}_{f_{d\,y,z}}$ can be cancelled, a successful cancellation close to 88% was expected.

H2: *Individualized BDFT models will result in improved cancellation compared to the one-size-fits-all models:*
Because the task variables (e.g., forcing functions), procedural (e.g., instructions, training) and environmental variables (e.g., temperature, lighting) have been controlled to a large extent, it was expected that differences in BDFT dynamics seen within subjects are smaller than those seen between subjects.[36,37] Moreover, model-based BDFT mitigation in an earlier study focusing on BDFT with sidestick manipulators showed that individualized models were up to 35% more effective in BDFT cancellation as compared to OSFA models.[29]

H3: *BDFT cancellation for the step task will be ineffective when compared to the pursuit task:*
Model-based BDFT mitigation has shown to be dependent on the task in the context of sidestick manipulators.[29] The study showed that BDFT models were only successful for the task they were identified from because the tasks required different neuromuscular settings. Although no studies have been found on the relationship between neuromuscular settings and touchscreen tasks, the difference between the pursuit and step task is likely to affect the cancellation. Moreover, as the screen input velocity goes towards zero, as in the step task, there is a possibility of nonlinear stick-slip, which can make the BDFT model less applicable.[38] The participants used a touchscreen glove to control for the friction effects, but cancellation was still expected to decrease notably when compared to the multisine task.

IV. Results

A. BDFT Identification

1. BDFT Model Validation

Figure 11 shows the VAF of the subject-average (SA) models in blue and one-size-fits-all (OSFA) models in orange. The validation is presented for both the HOR and VER conditions. The SA models for both HOR and VER are more accurate than the OSFA models. While the SA models have a median fit of above 90%, the OSFA models explains less of the measured BDFT with a median VAF between 85%-90%. Although both the SA and OSFA show a good model fit, it is also clear that the spread is smaller for the SA than the OSFA models. The interquartile range of the SA models is between 2%-3% VAF, while it is between 4%-7% for the OSFA. However, the OSFA also has several outliers, especially for the VER condition. These results were anticipated since the between-subject differences were expected to be larger than the within-subject differences, consistent with previous research.[29] This suggests that SA models will be more successful than the OSFA model during the model-based BDFT cancellation.

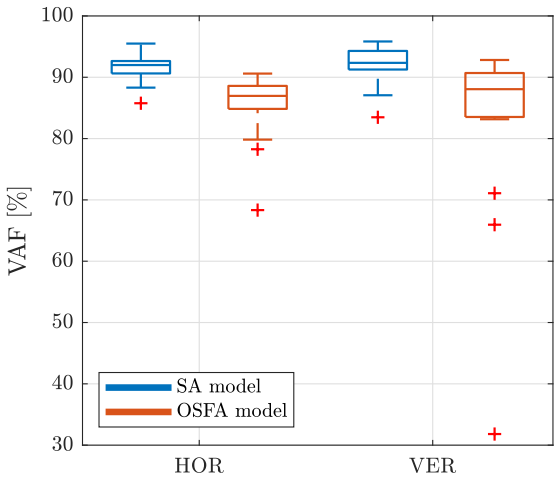

Figure 11: BDFT model validation from system identification.

2. BDFT Parameter Analysis

Figure 12 shows the estimated parameters of the BDFT model in Equation (4) for both the HOR and VER conditions. Each box-plot shows the variation of the SA model parameters with the OSFA values also displayed, i.e., the mean of the SA parameters indicated with red diamonds.

In Figure 12a the lower gain, G_{BDFT}, for the VER condition is in line with previous research where it was found that sway motion disturbance resulted in stronger feedthrough to horizontal screen input (HOR) than heave acceleration to vertical screen input (VER).[9] On the other hand, the BDFT natural frequency ω_{BDFT} (see Figure 12b) has a similar median value, close to 7 rad/s, for the two conditions, but with VER showing a larger spread between subjects. The larger variation for VER suggests a higher range of effective stiffness values between the subjects, and therefore a larger spread in the model bandwidth. The damping ratio ζ_{BDFT} shows considerable difference between conditions (see Figure 12c). A median value of $\zeta_{BDFT} = 0.7$ was found for HOR compared to $\zeta_{BDFT} = 0.9$ for VER. Lastly, the time delay τ_{BDFT} also shows the HOR models having a 50% higher delay than the VER model, or 0.03s.

Because the estimated parameters represent the lumped BDFT dynamics it is difficult to pinpoint the exact reason for the differences seen between the HOR and VER conditions. However, vibrations in sway has shown to be fundamentally different than vertical vibration because of the movement of the hip joint and bending of the spine.[10] This difference can indeed explain the higher effective delay, τ_{BDFT}, and lower damping ratio, ζ_{BDFT} observed for the HOR condition.

Table 3 shows in percentage terms, the relative spread of the BDFT model parameters. The relative change is calculated as the fraction of the standard deviation of each parameter and is with respect to the corresponding mean value

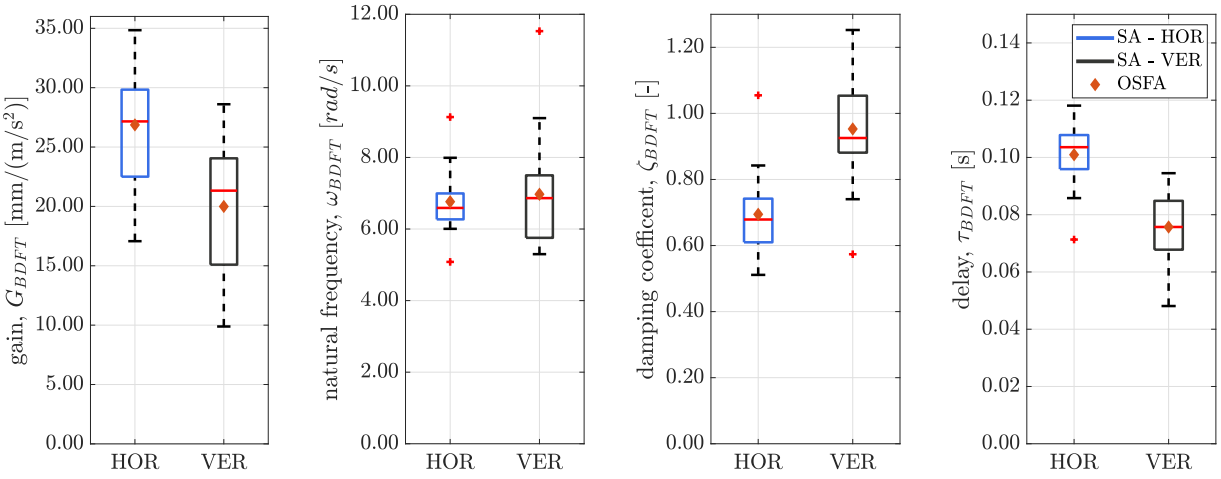

(a) G_{BDFT} **(b)** ω_{BDFT} **(c)** ζ_{BDFT} **(d)** τ_{BDFT}

Figure 12: Estimated BDFT model parameters for SA and OSFA.

of the estimated parameters. In this way, the between-subject differences for each parameter become more apparent. The largest difference between the HOR and VER conditions is observed for ω_{BDFT}, while for ζ_{BDFT} the spread is equivalent for both conditions. The largest spread is seen for the G_{BDFT}, while the time delay has the smallest between-subject differences.

Table 3: Relative spread of estimated BDFT model parameters.

	G_{BDFT}	ω_{BDFT}	ζ_{BDFT}	τ_{BDFT}
HOR	19.27%	13.08%	18.19%	11.71%
VER	25.42%	22.18%	16.63%	15.25%

Table 4: Linear correlation between BDFT, anthropometric measures, and estimated BDFT model parameters.

	$\sigma^2_{u_{f_d}}/\sigma^2_u$		G_{BDFT}		ω_{BDFT}		ζ_{BDFT}		τ_{BDFT}	
	HOR	VER	HOR	VER	HOR	VER	HOR	VER	HOR	VER
$\sigma^2_{u_{f_d}}/\sigma^2_u$	1.0	1.0	0.77	0.67	-0.11	-0.01	-0.38	-0.26	0.62	0.24
Height	0.06	0.22	-0.10	0.03	0.12	0.29	-0.31	0.02	0.03	0.38
Weight	0.19	0.13	0.13	0.24	-0.22	-0.09	-0.28	0.08	-0.13	0.44
BMI	0.18	0.04	0.19	0.25	-0.29	-0.24	-0.13	0.09	-0.15	0.29

3. Between-Subject Variability

To investigate possible reasons for differences seen between the subjects, Table 4 shows the correlation between the estimated BDFT model parameters and the amount of BDFT ($\sigma^2_{u_{f_d}}/\sigma^2_u$), and participants' height, weight and BMI. BMI is defined as the weight over the height squared (kg/m^2) and is a measure used to categorize people as under- or overweight.[39] The anthropometric measures of height, weight and BMI seem to have a weak or no linear correlation with any of the model parameters nor the feedthrough. This suggests that the between-subject differences largely originate from other sources such as differences in task strategy and muscular tension.[37] Although differences in mass will change the operator's dynamics, there seems to be no evidence this affects BDFT. Conversely, as expected, the BDFT has a strong relationship with G_{BDFT} for both HOR and VER. Higher feedthrough means a higher amplitude signal caused by the motion disturbance, which is modelled by the G_{BDFT} parameter. However, the correlation does not explain why certain individuals have a higher feedthrough than others.

B. BDFT Cancellation: Pursuit Task

Figure 13 shows the subject-averaged PSDs of the screen input signal for the HOR and VER conditions as measured in the evaluation session of the experiment for the pursuit task. The green line shows the raw input $u_{y,z}$ with the peaks at the motion disturbance frequencies indicating the presence of BDFT, but this constitutes only a small part of the total

power. Most of the power in $u_{y,z}$ comes from the participants following the target signal marked in purple. This is evident from the significant higher amplitude peaks than visible for the raw touchscreen input. Also shown are the cancelled screen input signals observed using both the SA (blue) and OSFA (orange) models. The HOR condition in Figure 13a shows that at the disturbance frequencies a considerable decrease in power is achieved, indicating a successful cancellation. Both the SA and OSFA models result in similar cancellation, with the SA achieving slightly higher BDFT attenuation. Figure 13b shows that for the HOR condition, a similar decrease in power with respect to the raw screen input signal was achieved. However, the SA models show better cancellation than the OSFA, as seen from the lower power at the disturbance frequencies. This is likely explained by the higher between-subject variability of the BDFT model parameters for the VER condition. This indicates that the OSFA model could be too "generalized" to accurately describe each individual subjects' dynamics.

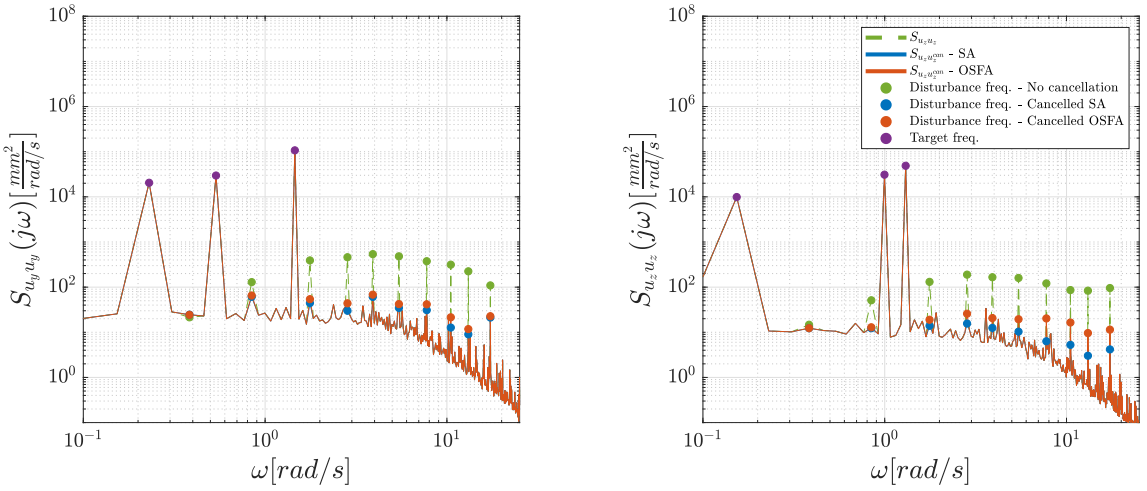

(a) Sway with horizontal screen input (HOR).

(b) Heave with vertical screen input (VER).

Figure 13: Power Spectral Density of touchscreen inputs signal before and after BDFT cancellation.

Another way to quantify the BDFT cancellation effectiveness is by calculating the relative decrease of BDFT after cancellation using Equation (6). This measure describes the reduction of variance achieved of the cancelled feedthrough u_{fd}^{can} with respect to the variance of the measured feedthrough u_{fd}^{meas}. Figure 14a and Figure 14b show this BDFT cancellation measure per subject for the HOR and VER conditions, SA cancellation indicated with blue and OSFA with orange. The shaded areas show the standard deviations across the four runs performed per condition by each participant. The HOR condition in Figure 14a, shows a median cancellation of 90% for SA, with the OSFA slightly worse at 88%. For the VER condition, Figure 14b show that the SA has a median cancellation just above 90% and the OSFA a considerably worse cancellation of 85%. Overall, there is a high average cancellation of above 80% for both HOR and VER with a difference of around 6% between the SA and OSFA models.

It is clear from Figure 14 that for most subjects the SA models provide better BDFT cancellation than the OSFA model. Subject 18 is a notable exception in HOR, where the mean SA cancellation is around 75% compared to 90% for the OSFA. The opposite is observed for Subjects 6, 9 and 16 for HOR and 6, 9, 17 for VER, where the OSFA model results in considerably worse cancellation than their respective SA models. Although it is expected that the OSFA model would be less successful in BDFT cancellation as a result of between-subject differences, it still raises the question of why these specific subjects have such a bad cancellation? Looking at the amount of BDFT observed for each individual subject is helpful in answering the question.

Figure 15 shows the scatter plots of the average observed BDFT between the system identification and evaluation session for each subject for both the HOR and VER conditions. For HOR (Figure 15a), Subject 18 showed the largest difference in feedthrough between the two experiment sessions. Thus, this subject's SA model has a gain paramter, G_{BDFT}, that is too high for effective cancellation of his evaluation session data, making the OSFA model (with a lower gain) more successful. Moreover, Subjects 6, 9, 16 and 17 have low feedthrough ($\sigma^2_{u_{fd}}/\sigma^2_u$) in the evaluation sessions, resulting in the higher gain OSFA model having a too high gain for effective cancellation.

It is clear that the amount of BDFT for individual participants varies within a subject to a degree that makes a BDFT

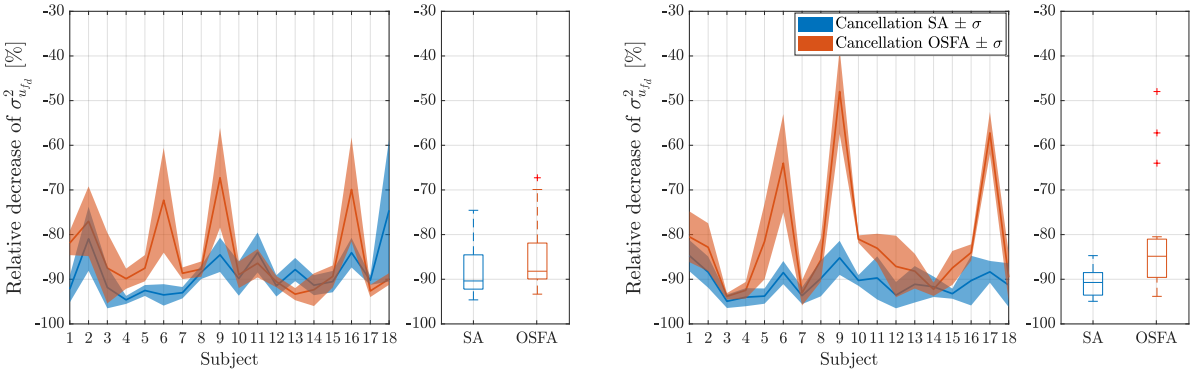

(a) Sway with horizontal screen input (HOR). **(b) Heave with vertical screen input (VER).**

Figure 14: BDFT cancellation for the pursuit task with the shaded areas showing the standard deviation across the four runs.

model with a constant set of parameters ineffective for feedthrough cancellation.

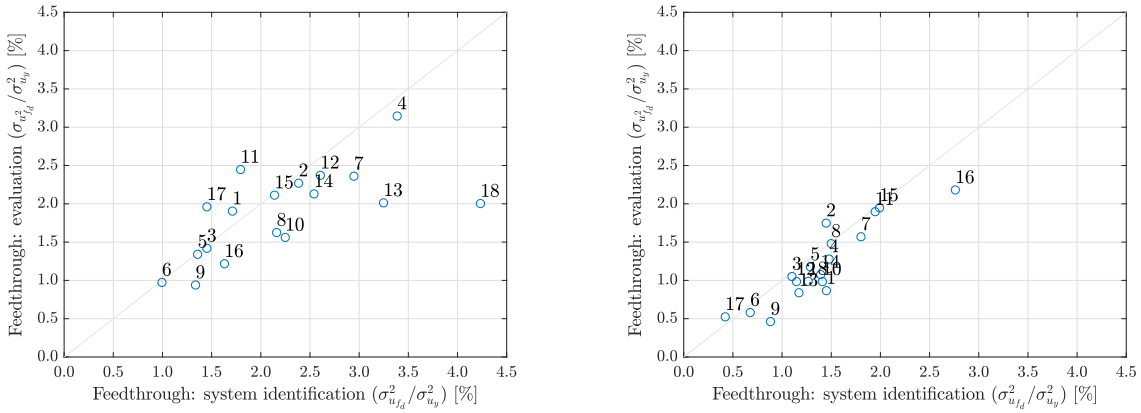

(a) Sway with horizontal screen input (HOR). **(b) Heave with vertical screen input (VER).**

Figure 15: Difference in BDFT between the system identification and evaluation session, for each subject.

C. BDFT Cancellation: Step Task

1. Cancellation Performance

In Section IV.B, BDFT models that were identified from a multisine pursuit task data, were applied for BDFT cancellation in that same task, resulting in an effective reduction of the biodynamic feedthrough. Here, the same BDFT models are applied for cancellation in the step task presented in Section IV.C to verify if the model-based cancellation can be successful independent of the task.

Figure 16 shows an example time trace of a typical subject, with the target signal in purple, the raw touchscreen input in yellow and the cancelled input of the SA model in blue. Even though each step lasted 3 seconds, only the last 1.5 seconds were used for this analysis since the subjects needed about the same time to reach the endpoint. The data used for the analysis is displayed as the three shaded areas of the plot. The raw input shows the subject being able to hold the finger steady at the endpoint location, as desired for the step task. Only a small overshoot is observed, making the subject successful in stabilizing the finger without the need for model-based BDFT cancellation. Since the cancelled input signal ($u^{can}_{y,z}$) equals the predicted BDFT model output (u^{mod}_{fd}) deducted from the raw input ($u_{y,z}$), this results in an amplification of errors in the raw input.

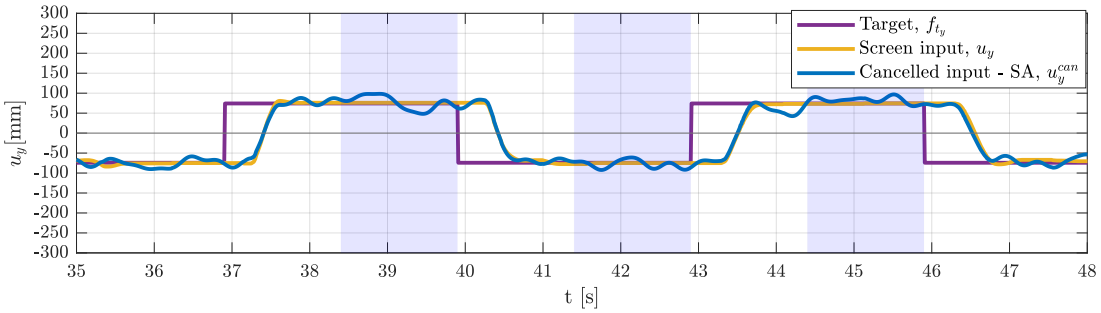

Figure 16: Typical time traces for the step task with BDFT cancellation in HOR (Subject 18, Run 1).

Figure 17 shows the variation of the finger position for the step task at the four possible endpoint locations averaged across runs. This plot compares the condition when the motion disturbance was off (no-motion) with three motion on conditions: BDFT cancellation off and cancellation on with either the SA or OSFA model. Both the SA and OSFA models show a median standard deviation of around $\sigma_{u_y} \approx 7$ mm for the HOR condition in Figure 17a, which is considerably higher than the $\sigma_{u_y} \approx 3.5$ mm when BDFT cancellation was off. The same is seen for the VER condition in Figure 17b, where the cancellation resulted in increased endpoint variation. ($\sigma_{u_z} \approx 4.5$ mm) than when cancellation was off ($\sigma_{u_z} \approx 2$ mm). However, comparing the no-motion condition to when cancellation was turned off, it is clear that some feedthrough is still present. Overall, the results indicate that the BDFT cancellation is, in fact, doing more harm than good at the endpoint locations.

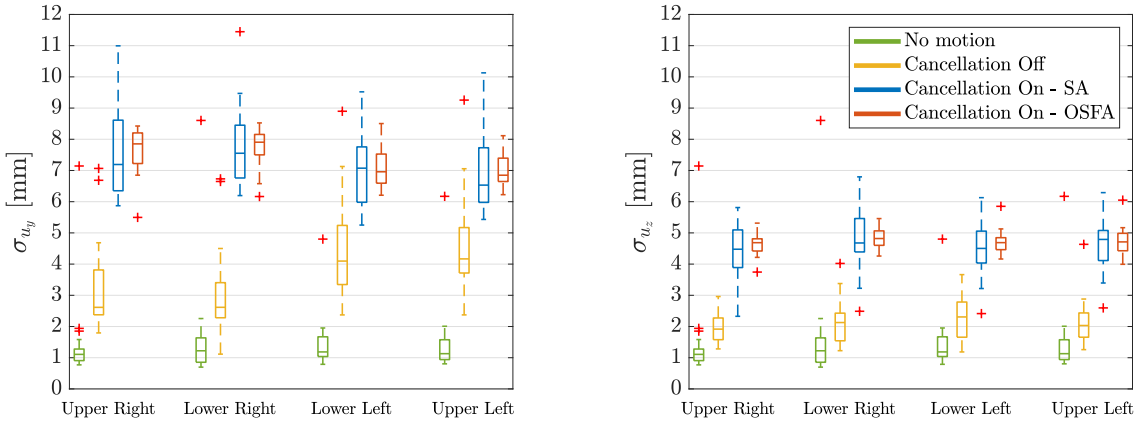

(a) Sway with horizontal screen input (HOR).

(b) Heave with vertical screen input (VER).

Figure 17: Step task endpoint variation for the four possible target locations.

2. Gain Optimization

The previous section showed that the BDFT is still present for the step task, but that neither the SA or OSFA models were able to cancel the feedthrough since participants were able to successfully stabilize their hands. The BDFT models therefore have a G_{BDFT} parameter to large for successful cancellation. By lowering the gain the of the models can still be possible.

Figure 18 shows the averaged variation $\sigma_{u_{y,z}}$ across the four endpoint conditions, but with G_{BDFT} for the OSFA models varied over a representative range. The shaded areas represents the standard deviation across four experiment runs. Both for the HOR condition in Figure 18a and Figure 18b the standard deviation at the endpoint locations decrease with lower BDFT model gain. For HOR an optimum is reached at $G_{BDFT} = 5$ mm/m s^{-2}, while for VER the optimum is at $G_{BDFT} = 3$ mm/m s^{-2}. Both constitute a 12% decrease of compared to when the BDFT cancellation is turned off.

The lowering of the gain, as identified from the pursuit task, can therefore substantially improve the BDFT cancellation. However, the goal is to achieve a high reduction of feedthrough compared to when BDFT cancellation is turned off, which from the current analysis is not accomplished.

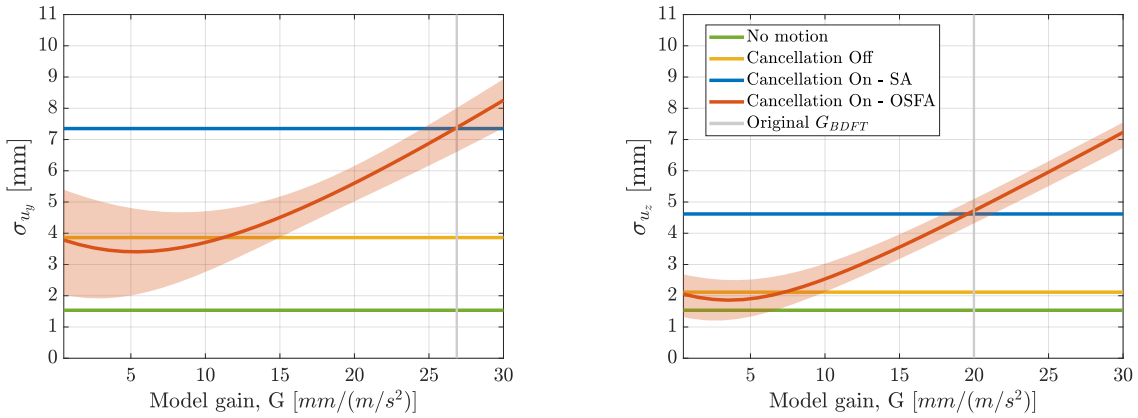

(a) Sway with horizontal screen input (HOR).

(b) Heave with vertical screen input (VER).

Figure 18: Step task endpoint variation while varying G_{BDFT} for the OSFA models.

V. discussion

This paper described a human-in-the-loop experiment performed to test the feasibility of model-based BDFT cancellation on touchscreens under turbulent conditions. Although BDFT has been extensively investigated with physical control inceptors, it is only recently that BDFT was quantified and modelled for a touchscreen task.[9] Building on this work, 18 participants performed a two-dimensional pursuit dragging task under the influence of a multisine motion disturbance signal resembling turbulence, allowing for the identification of two BDFT models: an individualized subject-average (SA) model based on the average model parameters of a single subject, and a one-size-fits-all (OSFA) model defined as the average across all subjects. An evaluation experiment used the identified models to perform BDFT cancellation in the same multisine pursuit task. Additionally, a step task was also tested, as this better represents a realistic precision input task such as a flightplan modification using direct manipulation.[21] This allowed for investigation of the three main goals of the paper: the potential of model-based BDFT cancellation, the need for individualization, and the effectiveness of cancellation across different touchscreen tasks.

The previous work by Mobertz et al.[9] showed that BDFT touchscreen inputs could be modelled at high accuracy using a linear transfer function model. To achieve a better model fit to the current experiment data, a time delay was added to the BDFT model. Based on these results the first hypothesis **H1** predicted that a median cancellation up to 88% would be possible for the pursuit task. The experiment data showed that the SA models had a median cancellation of above 90% for both the HOR and VER conditions, outperforming the prediction. The OSFA models showed a 88% and 85% cancellation for condition HOR and VER, respectively. This shows that a large part of the BDFT can in fact be cancelled for the pursuit task, for both lateral motion with horizontal touchscreen input and vertical motion with vertical screen inputs, and for SA and OSFA models. However, from the data analysis presented in Section III.B based on previous experiment data from Mobertz et al., the VER condition showed a low VAF and a large spread (M = 25%, SD = 68%), indicating a low performance if used for model-based cancellation. A possible explanation for this difference with the current experiment data is the length of the experiment sessions performed by Mobertz, where each subject performed 64 runs (also 90 seconds), only taking a break half way. This contrasts with the current study, where the system identification session consisted of a total of 16 runs, including a break after 8 runs. Since some less reliable system identification results were obtained for Mobertz' data, especially for the VER condition, fatigue is a possible culprit. This suggest the human operator being more susceptible to fatigue with heave turbulence. Because both the SA and OSFA models exceeded the expectation for BDFT cancellation, the hypothesis is accepted. As mentioned in literature, BDFT is a complex phenomenon[40] and other variables, such as fatigue, play a role in successful system identification and thus effective model-based cancellation.

Two types of models were used in this paper, one based on the average model parameters of each subject, and an

other based on the grand average of all subjects' parameters. Hypothesis **H2**, predicted individualized models to provide better cancellation than the OSFA models, even expectantly that between-subject differences would make the OSFA models, ineffective, as seen for analysis of Mobertz' data in Section III.B. The BDFT model validation did indeed show a larger variation between subjects for the VER condition. Furthermore, as expected, the cancellation of the pursuit task was worse for the OSFA than the SA model, with a large variation of the mean cancellation between 50% and 95% across subjects. This is in contrast to the SA model, which not only gave a seven percentage points better cancellation, but also had lower variation between 85% and 95% across subjects.

Although some of the variation between the subjects' dynamics (and thus BDFT cancellation) can be explained by the anthropometric measures of height, weight and BMI, there is little evidence for the current dataset that points to a strong relationship between them and BDFT, which is consistent with previous research.[41,42] Using height, weight or BMI to predict or account for differences in BDFT is therefore not viable. Although, as expected, the strength of the feedthrough is positively related to the BDFT model gain, this does not explain the underlying reasons for the differences observed between subjects, but some variation can be attributed to differences is task strategy and muscle activity.[37] The variation in the cancellation does not only originate from between-subject differences but also within-subjects. Between the system identification and evaluation sessions the differences in mean BDFT were larger for the HOR condition than for VER. This can explain the corresponding spread in cancellation performance for the former condition. It is important to note that the amount of days between the two sessions varied from a minimum of 3 to a maximum of 14 days, but no correlation was found between BDFT and days between sessions (see Appendix C). In conclusion, the hypothesis is partially accepted. The individualized models indeed have a higher cancellation with a lower spread between subjects than the OSFA models. However, it was also observed that for certain individuals even the SA models can result in bad cancellation performance due to within-subject variability.

The experiment demonstrated that model-based BDFT cancellation in fact is possible for the multisine pursuit task. The BDFT model was identified in the same task, raising the question of how effective the model would be in cancelling a different more realistic, precision dragging task? Hypothesis **H3** predicted that applying the pursuit BDFT model to a touchscreen step task would result in a worse cancellation performance than for the pursuit task. Although different measures to quantify BDFT cancellation performance are used between tasks, it was indeed shown that the step task cancellation was ineffective and in fact increased the effects of BDFT rather than attenuating them. For both the SA and OSFA models, the endpoint variation for HOR was five times higher compared to when the cancellation was turned off, and double for the VER condition. The subjects were easily able to stabilize the hand once they reached the endpoint location. The majority mentioned that the step task was easier than the pursuit task, since they only needed to move their finger between four points on the screen. Once at the endpoint location they quickly learned to apply more pressure on the screen to stabilize their hand motion. Most subjects also rolled or pivoted around their finger to keep it in the same location. That is, once a subject had reached the endpoint, the task was a pure disturbance-rejection task, with a singular focus on reducing the biodynamic feedthrough. The pursuit task on the other hand is a target-following and disturbance-rejection task, meaning the subjects had to make a tradeoff between following the target and minimizing the BDFT from the disturbance. Continuous and point-to-point dragging tasks, as used here, have shown to be markedly different. Lowering G_{BDFT} to compensate for the lower magnitude BDFT experienced for the step task only produced and average BDFT reduction of 12% compared to the when cancellation was off. Evaluating if this performance is acceptable in a drag-and-drop task is an important next step. Overall, the model-based BDFT cancellation was ineffective for the step task and therefore the hypothesis is accepted.

This paper considered a model-based approach to reduce the effect of biodynamic feedthrough arising from turbulence on the human operator. While it was shown that cancellation is possible, adding noise to the deterministic multisine disturbance signal is sure to have a detrimental effects on the success of the cancellation. In addition, the step task tried to simulate a more realistic pilot-screen interaction than the pursuit task. However, the subjects were never aware of the BDFT cancellation taking place, since it was being applied in the software. A future experiment can increase realism by using short dragging tasks where the operator lifts their finger off from the screen between drags. This will give immediate feedback about the successful placement of an object and is also the kind of tasks expected on the future flight deck.[19,20] Finally, since the BDFT model did not achieve effective cancellation for the step task, it shows the inadequacy of a single BDFT model with varying parameters to capture the complex nature of BDFT. Future work can investigate other methods, such as online identification of BDFT dynamics,[43] or use predictive methods based on motion tracking.[44] No matter the solution, the pilot should, by FAA recommendations[45], find her or his touch location predictable and obvious.

VI. Conclusion

This paper presents the result of an experiment performed to investigate the reduction of BDFT on touchscreen dragging tasks by using a model-based approach. Linear BDFT models were identified for all 18 participants in two conditions: sway with horizontal touchscreen inputs and heave with vertical input. Two types of BDFT models were identified, one was a subject-average model and the second a one-size-fits-all solution being the average of all subject-average models. Overall, both models were shown to be able to successfully reduce the amount of motion feedthrough when applied in the same two-dimensional pursuit dragging task used for BDFT model identification. However, the lower cancellation achieved for certain subjects illustrate the danger of model-based cancellation with models based on the average dynamics of people. It was shown that within-subject differences play a role in effective cancellation and that OSFA models can be rendered ineffective, if for example, subjects show less feedthrough than predicted. Using the BDFT models on a precision point-to-point (step) dragging task proved unsuccessful. By using a combination of pressure on the screen and rolling of the fingertip only very low amounts of feedthrough were observed and resulted in the cancellation amplifying rather than attenuating the BDFT. While the study showed that model-based BDFT cancellation can be successful, the mixed results demonstrate that the types of tasks pilots will perform on touchscreens should be carefully analyzed before implementing model-based BDFT cancellation. Using this approach the models should be adaptable to individual human operators and be effective across different touchscreen tasks.

References

[1] Kingsley-Jones, M. *Airbus aims for airliner cockpit-touchscreen first with A350*. FlightGlobal. 2018. URL: `https://www.flightglobal.com/news/articles/airbus-aims-for-airliner-cockpit-touchscreen-first-449481/` (visited on 15/01/2020).

[2] Trimble, S. *Boeing selects Rockwell Collins for 777X touchscreens*. FlightGlobal. 2016. URL: `https://www.flightglobal.com/news/articles/boeing-selects-rockwell-collins-for-777x-touchscreen-429565/` (visited on 15/01/2020).

[3] Watkins, C. B., Nilson, C., Taylor, S., Medin, K. B., Kuljanin, I., and Nguyen, H. B. "Development of touchscreen displays for the gulfstream G500 and G600 symmetry™ flight deck". In: *2018 IEEE/AIAA 37th Digital Avionics Systems Conference (DASC)*. IEEE. 2018, pp. 1–10.

[4] Avsar, H. "Exploring potential benefits and challenges of touch screens on the flight deck". PhD thesis. University of Nottingham, 2017.

[5] Kaminani, S. "Human computer interaction issues with touch screen interfaces in the flight deck". In: *2011 IEEE/AIAA 30th Digital Avionics Systems Conference*. 2011, pp. 4–1.

[6] Dodd, S., Lancaster, J., Miranda, A., Grothe, S., DeMers, B., and Rogers, B. "Touch Screens on the Flight Deck: The Impact of Touch Target Size, Spacing, Touch Technology and Turbulence on Pilot Performance". In: *Proceedings of the Human Factors and Ergonomics Society Annual Meeting* 58.1 (Sept. 2014), pp. 6–10.

[7] Cockburn, A., Gutwin, C., Palanque, P., Deleris, Y., Trask, C., Coveney, A., Yung, M., and MacLean, K. "Turbulent Touch: Touchscreen Input for Cockpit Flight Displays". In: *Proceedings of the 2017 CHI Conference on Human Factors in Computing Systems*. CHI '17. New York, NY, USA: ACM, 2017, pp. 6742–6753.

[8] Venrooij, J. "Measuring, modeling and mitigating biodynamic feedthrough". PhD thesis. Delft University of Technology, 2015.

[9] Mobertz, X., Pool, D. M., van Paassen, M. M., and Mulder, M. "A Cybernetic Analysis of Biodynamic Effects in Touchscreen Operation in Turbulence". In: *2018 AIAA Modeling and Simulation Technologies Conference*. AIAA SciTech Forum. American Institute of Aeronautics and Astronautics, Jan. 2018.

[10] Allen, R. W., Jex, H. R., and Magdaleno, R. E. *Manual control performance and dynamic response during sinusoidal vibration*. Tech. rep. Hawthorne CA: System Technology Inc, 1973.

[11] Mayo, J. R. "The involuntary participation of a human pilot in a helicopter". In: *15th Eur. Rotorcraft Forum*. Amsterdam, The Netherlands, 1989, pp. 81–001.

[12] Masarati, P., Quaranta, G., Bernardini, A., and Guglieri, G. "Voluntary Pilot Action Through Biodynamics for Helicopter Flight Dynamics Simulation". In: *Journal of Guidance, Control, and Dynamics* 38.3 (Jan. 2015), pp. 431–441.

[13] Jex, H. R. "Problems in modeling man-machine control behavior in biodynamic environments". In: *Seventh Annual Conference on Manual Control*. Vol. 281. 1972, p. 3.

[14] Humphreys, H. C., Book, W. J., and Huggins, J. D. "Modeling of biodynamic feedthrough in backhoe operation". In: *Proceedings of the ASME Dynamic Systems and Control Conference 2009, DSCC2009*. PART B. 2010, pp. 969–976.

[15] Banerjee, D., Jordan, L. M., and Rosen, M. J. "Modeling the effects of inertial reactions on occupants of moving power wheelchairs". In: *Proceedings of the Rehabilitation Engineering and Assistive Technology Society of North America Conference (RESNA)*. 1996, pp. 220–222.

[16] Lancaster, J., Mers, B., Rogers, B., Smart, A., and Whitlow, S. "57.3: The Effect of Touch Screen Hand Stability Method on Performance & Subjective Preference in Turbulence". In: *SID Symposium Digest of Technical Papers* 42.1 (2011), pp. 841–844.

[17] Bauersfeld, K. G. "Effects of turbulence and activation method on touchscreen performance in aviation environments". MA thesis. San Jose State University, 1992.

[18] Cockburn, A., Masson, D., Gutwin, C., Palanque, P., Goguey, A., Yung, M., Gris, C., and Trask, C. "Design and evaluation of braced touch for touchscreen input stabilisation". In: *International Journal of Human-Computer Studies* 122 (Feb. 2019), pp. 21–37.

[19] Mertens, M. and Damveld, H. J. "An avionics touch screen-based control display concept". In: *Head-and Helmet-Mounted Displays XVII; and Display Technologies and Applications for Defense, Security, and Avionics VI*. Vol. 8383. International Society for Optics and Photonics, 2012, p. 83830L.

[20] Stuyven, G., Damveld, H. J., and Borst, C. "Concept for an Avionics Multi Touch Flight Deck". In: *SAE International Journal of Aerospace* 5.2012-01-2120 (2012), pp. 164–171.

[21] Alapetite, A., Fogh, R., Zammit-Mangion, D., Zammit, C., Agius, I., Fabbri, M., Pregnolato, M., and Becouarn, L. "Direct tactile manipulation of the flight plan in a modern aircraft cockpit". In: *Proceedings of HCI Aero*. APA, 2012, pp. 2–5.

[22]Gauci, J., Cauchi, N., Theuma, K., Zammit-Mangion, D., and Muscat, A. "Design and evaluation of a touch screen concept for pilot interaction with avionic systems". In: *2015 IEEE/AIAA 34th Digital Avionics Systems Conference (DASC)*. 2015, pp. 2–1.

[23]Gillespie, R. B., Hasser, C., and Tang, P. "Cancellation of feedthrough dynamics using a force-reflecting joystick". In: *Proc. ASME Dynamic Systems and Controls Division*. 1999, pp. 319–326.

[24]Sirouspour, M. R. and Salcudean, S. E. "Suppressing operator-induced oscillations in manual control systems with movable bases". In: *IEEE Transactions on Control Systems Technology* 11.4 (2003), pp. 448–459.

[25]Sövényi, S. and Gillespie, R. B. "Cancellation of Biodynamic Feedthrough in Vehicle Control Tasks". In: *IEEE Transactions on Control Systems Technology* 15.6 (2007), pp. 1018–1029.

[26]Venrooij, J., Mulder, M., van Paassen, M. M., Mulder, M., and Abbink, D. A. "A review of biodynamic feedthrough mitigation techniques". In: *IFAC Proceedings Volumes*. Vol. 43. Elsevier, Jan. 2010, pp. 316–321.

[27]Venrooij, J., Mulder, M., van Paassen, M. M., Mulder, M., and Abbink, D. A. "Relating biodynamic feedthrough to neuromuscular admittance". In: *Conference Proceedings - IEEE International Conference on Systems, Man and Cybernetics*. 2009, pp. 1668–1673.

[28]Damveld, H. J., Abbink, D. A., Mulder, M., Mulder, M., van Paassen, M. M., van der Helm, F. C. T., and Hosman, R. "Identification of the Feedback Components of the Neuromuscular System in a Pitch Control Task". In: *AIAA Modeling and Simulation Technologies Conference*. Reston, Virigina: American Institute of Aeronautics and Astronautics, Aug. 2013.

[29]Venrooij, J., Mulder, M., van Paassen, M. M., Abbink, D. A., Bülthoff, H. H., and Mulder, M. "Cancelling biodynamic feedthrough requires a subject and task dependent approach". In: *2011 IEEE International Conference on Systems, Man, and Cybernetics*. 2011, pp. 1670–1675.

[30]Zaal, P. M. T., Pool, D. M., Bruin, J. D., Mulder, M., and van Paassen, M. M. "Use of pitch and heave motion cues in a pitch control task". In: *Journal of Guidance, Control, and Dynamics* 32.2 (2009), pp. 366–377.

[31]Hourlier, S., Guérard, S., and Servantie, X. "Avionics Touch Screen in Turbulence: Simulator Design and Selected Human–Machine Interface Metrics". In: *Improving Aviation Performance through Applying Engineering Psychology: Advances in Aviation Psychology*. Vol. 3. CRC Press, 2019, pp. 53–75.

[32]van Paassen, M. M. and Mulder, M. "Identification of human control behavior". In: *International encyclopedia of ergonomics and human factors* (2006), pp. 400–407.

[33]Pintelon, R. and Schoukens, J. *System identification: a frequency domain approach*. John Wiley & Sons, 2012.

[34]Berkouwer, W., Stroosma, O., van Paassen, M. M., Mulder, M., and Mulder, B. "Measuring the performance of the SIMONA research simulator's motion system". In: *AIAA Modeling and Simulation Technologies Conference and Exhibit*. 2005, p. 6504.

[35]Vrouwenvelder, S. "Cybernetic investigation of point-to-point touchscreen dragging tasks". unpublished. Unpublished.

[36]Griffin, M. J. "The validation of biodynamic models". In: *Clinical Biomechanics* (2001).

[37]McLeod, R. and Griffin, M. "Review of the effects of translational whole-body vibration on continuous manual control performance". In: *Journal of Sound and Vibration* 133.1 (Aug. 1989), pp. 55–115.

[38]Grabski, G. and Robinson, T. "P.132: Enhancing the Visual Performance of Touch Screen Displays". In: *SID Symposium Digest of Technical Papers* 44.1 (June 2013), pp. 1509–1512.

[39]Prentice, A. M. and Jebb, S. A. "Beyond body mass index". In: *Obesity reviews* 2.3 (2001), pp. 141–147.

[40]Venrooij, J., van Paassen, M. M., Mulder, M., Abbink, D. A., Mulder, M., van der Helm, F. C. T., and Bülthoff, H. H. "A framework for biodynamic feedthrough analysis - Part I: Theoretical foundations". In: *IEEE Transactions on Cybernetics* 44.9 (2014), pp. 1686–1698.

[41]Venrooij, J., Pavel, M. D., Max, M., van der Helm, F. C. T., and H, B. H. "A practical biodynamic feedthrough model for helicopters". In: *CEAS Aeronautical Journal* 4.4 (Dec. 2013), pp. 421–432.

[42]Griffin, M. J. and Whitham, E. "Individual variability and its effect on subjective and biodynamic response to whole-body vibration". In: *Journal of Sound and Vibration* 58.2 (May 1978), pp. 239–250.

[43]Plaetinck, W., Pool, D. M., van Paassen, M. M., and Mulder, M. "Online Identification of Pilot Adaptation to Sudden Degradations in Vehicle Stability". In: *15th IFAC Symposium on Large Scale Complex Systems LSS 2019 Delft, The Netherlands, 26–28 May 2019*. Vol. 51. 34. 2019.

[44]Ahmad, B. I., Langdon, P. M., and Godsill, S. J. "Stabilising Touch Interactions in Cockpits, Aerospace, and Vibrating Environments". In: *Universal Access in Human-Computer Interaction. Methods, Technologies, and Users*. Ed. by M. Antona and C. Stephanidis. Cham: Springer International Publishing, 2018, pp. 133–145.

[45]*Advisory Circular 20-175: Controls for Flight Deck Systems*. Tech. rep. Federal Aviation Administration, 2011.

Part II

Preliminary Report

Note: This part has already been examined under course AE4020 Literature Study

Chapter 2

Preliminary Research Question

Before a final experiment proposal and a main research question is posed a preliminary research question will guide the literature study and data analysis performed in this preliminary report. Here the goal is to explore the topics as relating to the research objective. The keywords of the preliminary research question below has are mitigation, biodynamic feedthrough, flight deck operations and touchscreens. The four sub-questions have been created to answer the preliminary research question based on the keywords.

Preliminary research question:
What are the ways to mitigate biodynamic feedthrough in the context of flight deck operations using touchscreen technology?

Sub-questions

1. What are the properties of touchscreens pertinent to BDFT mitigation?
2. What type of touchscreen task exist and what is the trend for future flight decks?
3. What are the types of mitigation which are possible for BDFT?
4. How can BDFT be modelled to be used in model-based cancellation?

Chapter 3

Touchscreens on the Flight Deck

Touchscreens will soon be part of commercial aviation and bring with them a new way for pilots to interact with the aircraft systems. This chapter explores touchscreens and their introduction to the flight deck. First the advantages and challenges of touchscreens in the cockpit is discussed in Section 3-1. In Section 3-2 some touchscreen properties which are important for the current research are investigated. Different ways of interacting with a touchscreen will be looked at in Section 3-3 and finally in Section 3-4 different touchscreen task used in research and in current aircraft are presented.

3-1 Advantages and Challenges

The introduction of touchscreens on the flight deck brings with them many advantages, but also a new set of challenges. Benefits such as increased situational awareness and decreased workload are cited as a reason for its introduction [29], but many reasons have been proposed. Avsar [17] asked major aerospace companies developing or integrating touchscreens their motivation for replacing hard controls with touchscreens. The respondents said touchscreens are *"easy to learn, have a more natural and intuitive way of interaction, reduce crew workload and training time, perform better than current input devices, declutter/tidy up the flight deck , reduce weight, increase flight efficiency and enhance pilot and passenger safety"* [17]. However, as Rouwhorst et al. [30] found in their their experimental touchscreen study, the benefits of touchscreens are not only inherent to the technology, but depend on its implementation to perform better than current systems. In Table 3-1 major advantages and challenges of using touchscreens on the flight deck are listed. For BDFT arm fatigue and screen response time can be of importance. Fatigue can change the arm dynamics over time and the pilots might interact with the screens in a way to minimize fatigue. Although screen technology has improved, any screen delay can make a model-based mitigation approach less effective.

Table 3-1: Advantages and challenges with introducing touchscreens in the fight deck.

Advantages	Challenges
Situational awareness and workload [30]: Touchscreens have the potential to increase the situational awareness and decrease the workload. Although some research shows no improvement compared to other input devices [20].	**Loss of tactile feedback [21,31]:** Physical controls have different surface textures and auditory feedback which help the pilots choose the right setting. Touchscreen do not have this feature.
Direct manipulation [18, 20, 21]: Touchscreen are direct manipulation devices where the user input is directly translated to the device output. This is seen as a benefit as it is intuitive and does not require the the operator to map between input and output.	**Environment such as turbulence [9, 22–24] and glare [14, 18, 25]:** Turbulence has shown to degrade touchscreen usage and increase workload. Knobs, buttons and physical control have the advantage of providing vibration support for the pilot, minimizing the effect of the vibration. Glare can also be a risk to the flight crew since making the screens difficult to read and operate.
Better use cockpit real estate [18]: A cockpit has limited surface area for input devices and output devices. A touchscreen has the potential to make more efficient use of the available area.	**Head down instead of out [32]:** A danger of using touchscreens is the pilot gazing too much on the screen instead of out of the window or on other critical instruments.
Easy upgrades and customization [18, 33]: Once a touchscreen is installed its display can be updated through software updates instead of costly change in hardware. What information is displayed can change e.g., based on pilot preference.	**Loss of unique location of button/controls [31]:** With hardware buttons in a dark cockpit pilots would often still be able to find the right button based on its location in the cockpit. With a lot of functionality moving the to touchscreen quick access to certain functionalities can be an issue.
Reduction in material an maintenance cost [18]: Touchscreen can replace a large amount of hardware buttons, reducing cost. It also does not need the same maintenance since it has no moving parts.	**Fatigue from outstretched arm [20, 21]:** Depending on the screen location and tasks, there is potential for fatigue since the arm is not supported.
New types of of visualization [18]: Touchscreens can present information in new ways and create new ways of pilot interaction not possible with analog systems.	**Body discomfort [20]:** Since individual controls will be replaced by touchscreens it will have a higher usage time than any individual button or knob. Its location and implementation must therefore be researched to not cause discomfort in its use.
Input and output in same location [21]: The screen input and visual output are in the same location which makes the user more focused and can reduce hand-eye coordination.	**Screen response time [31]:** Touchscreen latency has been cited a potential challenge for the usability for pilots. However for today's touchscreen technology this is not an issue. However, for model-based BDFT cancellation this can still be important.

3-2 Touchscreen Properties

Touchscreens have a latency between a user action and the resulting change in the screen. This lag has been stated to originating from the three main sources: the physical touch sensor, the touch processing software and display itself. A 2012 study found that modern smartphones had a lag between 50-200 ms and that latencies down to 25 ms could decrease performance for dragging tasks [34].

Registering touch can be done in several ways with the two most popular technologies being capacitive and resistive. Other technologies exists such as infrared and surface acoustic touchscreens [17, 35]. Capacative screens sense touch by measuring the change in capacitance when a conducting element such as a finger is in contact with the screen [18]. A resistive touchscreen is activated when pressure from a finger or stylus make two sheets touch registering an X and Y location [35].

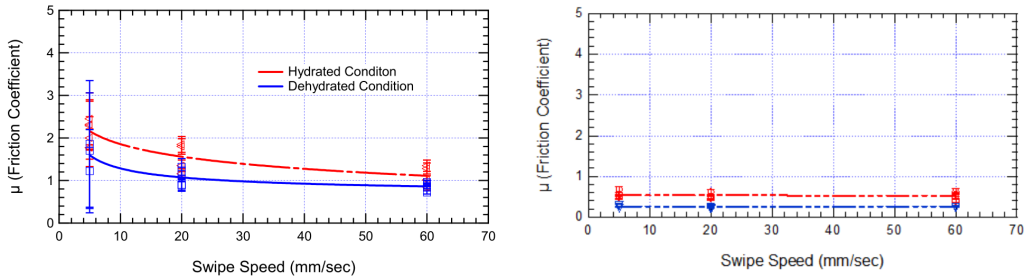

(a) No screen coating **(b)** With low friction coating

Figure 3-1: The kinetic friction coefficient for a hydrated and dehydrated finger as a function of swipe velocity. The coating reduces and keeps the friction coefficient constant over different dragging speeds. The stick-slip at low velocities is also considerably reduced [2].

The only way a human interacts with a touchscreen is through the swiping, dragging or pushing of a finger on the screen. This interaction is analogous to the tires of a car interacting with the road surface. Robinson et al. [2] showed that the kinetic friction coefficient stays constant with increasing normal force at a constant dragging speed, but decreases considerably with increasing velocity. However, with a low friction coating this variability was almost removed entirely together with the stick-slip behaviour which occurred at low dragging speeds shown in Figure 3-1.

3-3 Touchscreen Interaction Methods

Interactions with touchscreens can happen in many ways which can be contrasted to physical control inceptors such as a joystick or control columns. The most common touchscreen interaction methods (gestures) can be grouped into discrete (D) and continuous (C) movements as well as single touch (ST) and multi-touch (MT). This classification is compiled from Google, Microsoft and Apple's design and developer manuals [36–38] and the Touch Gesture Reference Guide [39] and has been used in the thesis work of Mobertz et al. and Berg [9, 10]. Continuous movements are when the finger has prolonged contact with the screen while discrete movements are are quick screen interactions, such as pushing a virtual button. Single touch interaction is defined as only using one finger when interacting with the screen while multi-touch is more than one finger. Table 3-2 shows how the most common gestures can be classified. Single touch dragging tasks have been used for the

remainder of the research. Even though the interaction methods are only described in a qualitative way, an actual implementation could define the gestures based on time, velocity and direction [40]. The companies mentioned often tie their gestures directly to the user-interface design, resulting in a more specific gestures classification.

Table 3-2: Classification of interaction methods with a touchscreen. Single Touch (ST), Multi-touch (MT), Discrete (D) and Continuous (C) [9, 10].

Interaction method	Description	ST	MT	D	C
Tap	Quick touch	•		•	
Double tap	Quick successive touches	•		•	
Hold	Stationary finger position	•		•	
Swipe	Quick dragging movement	•	•	•	
Drag	Prolonged movement	•	•		•
Pinch	Change distance between fingers		•		•
Rotate	Circle fingers around a point		•		•

3-4 Touchscreens Tasks on the Flight Deck

There is a wide variety of possible interaction methods as detailed in Section 3-3. The current research on touchscreens in cockpits have used various tasks for evaluating the effect of turbulence of the flight deck. This research has mainly focused on how much turbulence deteriorates touchscreen use by comparing touchscreens to other more traditional input methods [19, 20], assessing workload and situational awareness using touchscreens [23, 30, 41–43], mitigation of BDFT (see Chapter 4), the effect of screen position and virtual button sizes [19, 23, 27, 43–45]. The following sections looks at which types of tasks have been used in research relating to touchscreens on the flight deck and in a turbulent or vibrating condition.

3-4-1 Discrete Tasks

A popular choice for discrete tasks in these studies comes from ISO 9241-9 which deals with the evaluation of visual displays for office work [19, 22, 43, 46]. The multi-directional tapping test (MDTT) in Figure 3-2 is one of the tasks of the standard [47]. This is a discrete task where the sequence of taps is known to the participant. The experiments are usually evaluated using throughput, a measure based on Fitt's Law to compare different experiment conditions. Thomas [19] used throughput to compare touchscreens to other input devices while Avsar et al. [46] used it to compare different display positions. However, error rates, movement time and end-point position is also used as a performance measure. A task similar to the MDTT was used by Cockburn et al. [44] using mean task time and error rate for its statistical analysis.

Other studies have moved away from the (unrealistic) Fitt's law tasks, but use task time and error rate to assess performance and accuracy. Data entry tasks using a virtual keypad or keyboard try to be more realistic with the task resembling entry of a waypoint or other alphanumeric string into the FMS [23, 41, 44]. Other operational tasks are also used, Bauersfeld [24], in one of the earliest studies on touchscreen use under the influence of turbulence, employed a typical checklist task as used in different phases of flight, while

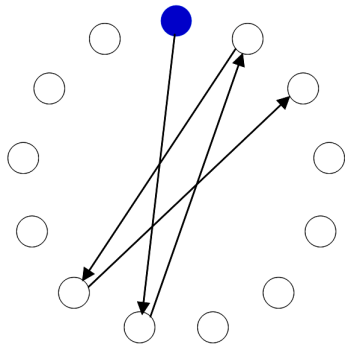

Figure 3-2: The multi-directional tapping test (MDTT) used to assess pointing devices [3]

Lancaster et al. [41] used a menu navigation task. In the latest study by Cockburn et al. [22] they also chose tasks which mimicked a more realistic flight deck scenario by requiring the participants to touch the control-stick between every tap of the MDTT task since normal interactions with the cockpit interfaces usually are short. A second task in the same paper presented an auxiliary power unit (APU) warning while the participants where flying level, requiring the correct response according to normal flight procedures. This consisted of ST and discrete touchscreen actions.

3-4-2 Continuous Tasks

Touchscreen dragging tasks (ST or MT continuous tasks) in a flight deck setting are less researched than discrete tasks. To investigate the effects of turbulence while operating a touchscreen Mobertz et al. used a multisine pursuit dragging tasks [9]. This was used to quantify a tracking error and to use spectral decomposition methods. This is an unrealistic flight deck task for two reasons. The drags lasted much longer than typical dragging tasks with each being 90 seconds. Secondly, prolonged target following tasks are not typically used in a touchscreen flight deck setting. For future research they recommended the use of a more realistic task. To assess hand stabilisation methods Lancaster et al. [41] used a dragging task similar to a map panning along a predefined path. In an other study Alapetite et al. [48] studied the effects of turbulence on touchscreen use were one of the participants had to drag circles into a ring. He found that the dragging task produces more errors than a tapping tasks. This was also found by Coutts et al. [43] when assessing the effect of turbulence on touchscreens when using a slider task and a ghost ball following task. Cockburn et al. [44] came to a similar conclusion, finding dragging tasks (slider and dial) that register touch on lift-off to have high error rates in a no motion condition which was exacerbated with turbulence.

Although most of these dragging tasks are of a generic nature similar motions can be used in more realistic task such as the mentioned map panning, or menu scrolling and flight plan modifications.

3-4-3 Future Tasks

As of mid 2019 touchscreens have not been implemented in commercial aircraft, but will shortly be available in Boeing's 777X [16] and Airbus' A350 aircraft [15]. How these will operate in terms of ST and MT tasks are still not available. Currently Gulfstream has reinvented their cockpits by implementing ten touchscreens in their G500/600 business

jets. These only support ST gestures with drag/scroll, swipe and press-and-hold being supported [14].

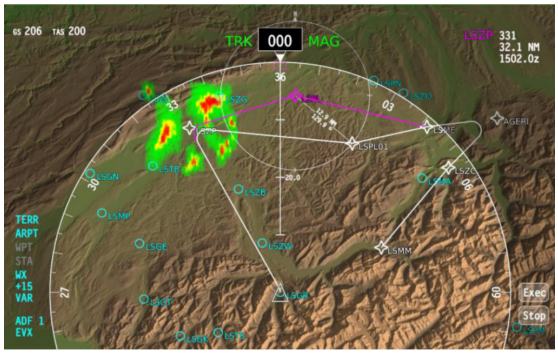

(a) A proposed flight plan manipulation task. The purple line represent the current route while the white the modified route. The change is made by dragging a waypoint to the desires location [18]

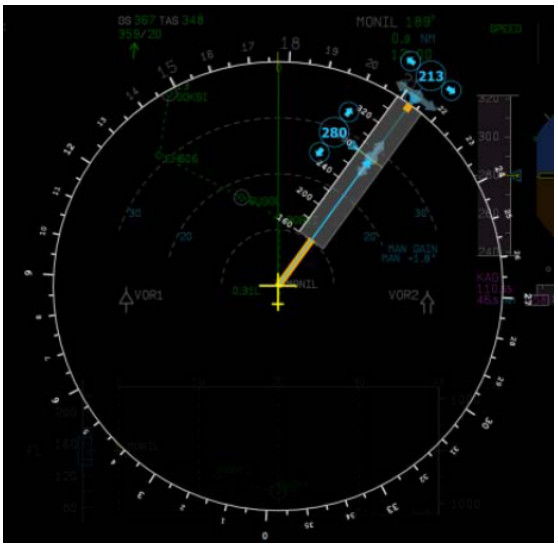

(b) The pilot can change the heading by dragging the dial to the desired location. The aircraft horizontal speed can be set by dragging the dial radially [30].

Figure 3-3: Direct manipulation tasks for future flight deck operations

Some cockpit concepts have been presented which exploit the direct manipulation capabilities of touchscreens. Mertens and Damveld [33] and Stuyven et al. [18] developed an intuitive flight plan modification where pilots could change waypoints with a drag-and-drop operation, a ST continuous task (Figure 3-3a). A waypoint change was also proposed by Alapetite et al., but consisted of ST discrete actions. Another contribution from Rouwhorst et al. [30] used a novel touch interface to change the aircraft's speed, heading, altitude, flight level and vertical speed (Example in Figure 3-3b). And a way to change the runway and selecting an alternate airport. These tasks consisted of both ST and MT, as well as discrete and continuous tasks.

3-5 Chapter Discussion

This chapter has looked at the implementation of touchscreens in the the aviation industry by investigating the their advantages and challenges, properties and tasks. When it comes to model-based mitigating of biodynamic feedthrough (see Chapter 4) several of the studied factors can play a role. The chapter has addressed sub-questions 1 and 2 of the preliminary research question, namely *What are the properties of touchscreens pertinent to BDFT mitigation?* and *What type of touchscreen interaction methods exist and what is the trend for future flight decks?*.

One identified challenge with touchscreens is their latency. Since model-based BDFT cancellation uses the current touch input, a lag can create a unacceptable phase shift resulting in a worse cancellation. It is recommended this effect is looked into.

Another property of touchscreens is the friction between finger and touch surface. Dragging tasks at different speeds can cause non-linear behaviour and especially at low

speeds [2]. Using linear biodynamic feedthrough models might therefore not be adequate. Although low friction coating can be used to remove the variability of the friction coefficient it is not certain manufacturers will do so (e.g., Gulfstream G500/600 [14]). To control this variable it is recommended to use a glove which provides low friction properties as well as the same amount of friction for all participant.

Several types of tasks have been proposed for future application on a touchscreen interface, taking advantage of their direct manipulation capabilities. Especially dragging tasks have the potential to create new ways of interacting with the flight management and navigation [18, 30, 33, 49]. However, these types of tasks have been found to cause large errors in turbulent conditions with their use being advised against [43, 44]. Model-based biodynamic feedthrough mitigation can therefore be a solution to this challenge.

Conclusions:

- Current touchscreen technology has latency associated with their use.
- Friction between finger and touchscreen can be substantial and nonlinear.
- Touchscreen tasks can be classified as discrete and continuous with future user interfaces likely taking advantage of their direct manipulation capabilities.

Recommendations:

- The amount of touchscreen latency should be investigated to quantify the effect it will have on model-based BDFT cancellation.
- The final experiment should use gloves to minimize the nonlinear effects of friction between the finger and touchscreen.
- The use of dragging tasks for model-based BDFT cancellation is recommended since literature has warned against their use in aircraft touchscreen tasks .

Chapter 4

BDFT Mitigation and Modelling

Biodynamic feedthrough (BDFT) caused by turbulence has shown to have adverse effects on touchscreen performance. With the looming arrival of touchscreens on the flight deck it has become important to mitigate this effect. This chapter first looks at the definition of BDFT (Section 4-1) before exploring the different BDFT mitigation techniques (Section 4-2). The model-based mitigation approach will then be further researched by looking at classifications of pilot modelling (Section 4-3), types of BDFT models (Section 4-4) and the variability of human response to vibration (Section 4-5).

4-1 BDFT Definition

The human body is often exposed to accelerating environments such as walking, when using a cellphone, driving a car, biking, or piloting an aircraft. The acceleration can have an impact on the ability to perform a manual control task. There are several effects of vibration on the human body such as visual impairment (blurring of image), neuro-muscular interference (lower signal-to-noise ratio between voluntary and involuntary movements), central effects (interference of the cognitive process) and biodynamic feedthrough (BDFT) [50]. Most definitions of BDFT are limited to a control inceptors, such as sidesticks or control columns, which is controlling the vehicle, making it a closed-loop problem [4, 26, 50]. However, BDFT is also present in open-loop, that is when the operator's control task is not influencing the state of the vehicle [51], which in the context of touchscreens operations in a cockpit environment can be a flight plan modification or panning of a map. A general definition of BDFT can therefore be stated as the following and is illustrated in Figure 4-1.

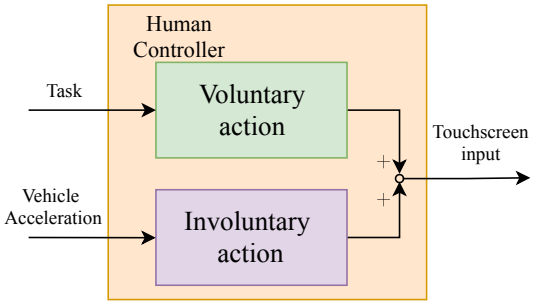

Figure 4-1: Definition of BDFT as an involuntary response to acceleration. Here shown in open-loop, when the touch input does not affect the state of the vehicle. Adapted from [4].

Definition of biodynamic feedthrough:
Biodynamic feedthough is the involuntary limb motion arising from acceleration on the human body.

4-2 BDFT Mitigation

BDFT can be reduced in several ways. Three possible categories to reduce inadvertent touch suggested by a recent Aerospace Recommended Practice (ARP) are by stabilization, touch interactive areas and confirmation [52]. Stabilization means minimizing BDFT by letting the arm/hand rest or support itself on a physical structure in the cockpit. Secondly, by clearly defining specific areas on the display where touch is possible inadvertent touch can be reduced. Lastly, a software solution is adding a confirmation step reducing the risk of accidental selection. The two latter methods do not reduce BDFT, but rather try to lessen the effects it has on the human operator. However, other methods exist hardware and software solutions exist. Below, a non-exhaustive list of possible BDFT mitigation methods from literature is presented:

Neuromuscular Adaption

Human operators have a remarkable ability to change their neuromuscular stiffness to adapt to the tasks and environment. For example, helicopter pilots are instructed to relax their hand (and thus the stiffness of the neuromuscular system) when operating the cyclic [53]. Arm stiffness is controlled through voluntary co-contraction (activation of antagonistic muscle groups) which is slow and energy consuming or through reflexive behaviour which is fast and energy efficient. Both help to resist external force perturbations [54]. However, this leaves the pilot to deal with the BDFT by changing the arms stiffness. The operator must therefore tradeoff between accuracy and performance of the touchscreen tasks [26]. This technique can be used for both discrete and continuous tasks, but tightening of the arm muscles (co-contraction) during longer dragging tasks can be fatiguing.

Bracing/ hand support

By bracing on the frame of the touchscreen or on the screen itself, the effects of BDFT can be lowered. Boeing is introducing its 777X aircraft with five touchscreens which will use the screens bezels for pilots to rest their hands to interact with the screens [16]. Garmin, the first manufacturer to introduce touchscreen in in general aviation aircraft have also recognized bracing as a strategy for their products [28]. The Gulfstram G500/600 aircraft introduced in 2018 have also made use of bezel support for hand stabilization as seen in Figure 4-2b [14].

A study by Cockburn et al. [44] showed that participants would brace on the edge of the screen when completing common touchscreen tasks. Although the effects of braced and un-braced touch were not compared, the authors concluded that bracing helped complete the task. A follow up study directly compared braced and un-braced touch interaction in turbulence. In this study four fingers were rested on the screen while the fifth was used for selection with either single or double-tap gestures shown in Figure 4-2a. The results showed that the braces approach was faster, made fewer errors and was preferred by most participants. This method while more complicated than bezel bracing does have the advantage of the hand not stretching from the edge of the screen which can be an issue for larger screens and especially for continuous tasks [22].

In another study conducted by Lanchester et al. [41], different hand bracing methods were compared, all relying on mechanical bezel features. Although no significant differences were seen between the methods the participants noted that some kind of hand stability is necessary.

Hand bracing, either by using high friction materials, hand rests or modified screen bezels is generally simple to implement and low cost. Aircraft manufacturers are therefore

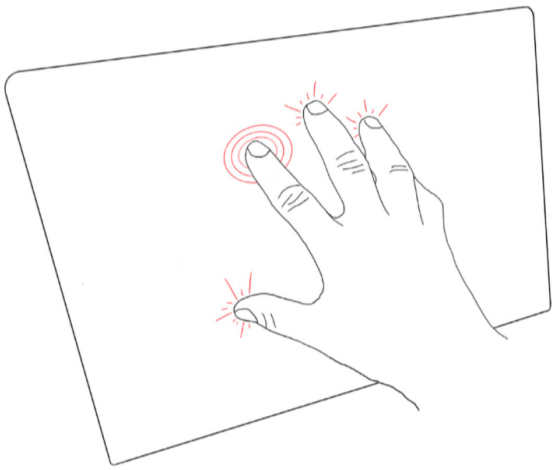

(a) Example of a novel screen bracing method where the index finger is used for selection while the other fingers provide support by resting on the screen [22].

(b) Example of touchscreen hand bracing found on the Gulfstram G500/600 [14]

Figure 4-2: Different methods for touchscreen bracing

likely to prefer this solution.

Touch Technology

There are several touch technologies which are used in commercial products. The two most popular being capacitive and resistive shown in Figure 4-3. Resistive touchscreens detect the finger or stylus location when the two layers touch as a result of applied force on the screen. Conversely, capacitive technology which was popularized with the release of the first iPhone in 2007 can detect a change in its electrostatic field when a conductive material touches it. The resulting change in capacitance is used to detect the fingers location [17]. Because of the pressure needed to activate the resistive screen the possibility of inadvertent touch is reduced. A study by Dodd et al. [23] found that pilots committed more errors using a capacitive touchscreen when compared to resistive. However, with new technology like Apple's force touch [55] capacitive screens can get similar capabilities.

Force activation was also investigated by Cockburn et al. [22] by placing a force sensor on the the participants fingers. While some subjects had good selection performance others were not able to get used to the force threshold. The authors attribute this to the finger sensor implementation.

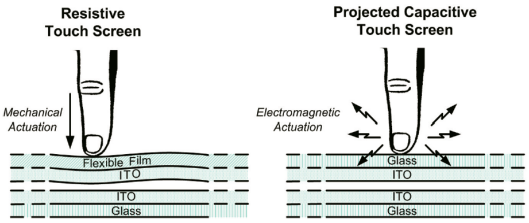

Figure 4-3: The two most popular touch technologies: restive and capacitive [5]

Since both screens technologies are capable of integrating force sensitivity, either one is a possible choice for the mitigation of BDFT. However, both are mostly useful for discrete tasks such as tapping to select menu items. Continuous dragging tasks will not benefit from this feature and the effects of BDFT are not mitigated.

Stencils

A stencil is a material with cut-outs placed as an overlay on a touchscreen to stabilize hand movement. Users can also place their hand on top of the stencil without triggering

the screen and then slide their hand into the stencil cut-out with the edges guiding and stabilizing the movement. This method was tested by Cockburn et al. [44] in a comparative study between touch, trackball and stencil input at none, medium and high vibration levels. In both discrete and continuous tasks, the stencil did not improve performance. Only in high vibration with small targets in a discrete task did the stencil show lower errors. Because only the part with the cut-outs are exposed to the touchscreen, a change in the user interface would also require a new stencil. In addition, continuous dragging tasks would also be limited by this solution since free movement on the screen would not be possible.

Signal Filtering

Using an approach called input filtering the screen input signal can be separated as voluntary and involuntary control. The voluntary control is the deliberate movement of the pilot while the involuntary input is caused by the vibration. Signal filtering assumes that the voluntary and involuntary contributions have a clear frequency separation. This is called the separation assumption [53]. The validity of the assumptions is not clear since voluntary control frequencies might be higher than the cutoff and conversely, BDFT frequencies can be lower than the cutoff. An input filter can therefore risk removing part of the voluntary control or not remove parts of the BDFT below the threshold frequency. Velger et al. [56] created an adaptive filter which changed its cutoff based on the input acceleration. Although this can be a better solution, it is still reliant on the separation assumption. Input filtering would only work for continuous dragging tasks since discrete tapping tasks would not produce enough data for filtering.

Model-Based Cancellation

A model capturing the involuntary motion resulting from vibration on the body and finger can be used to mitigate BDFT. The model outputs the involuntary movement of the finger and by subtracting it from the touchscreen input, consisting of both voluntary and involuntary motion, the feedthrough motion can be cancelled as illustrated in Figure 4-4.

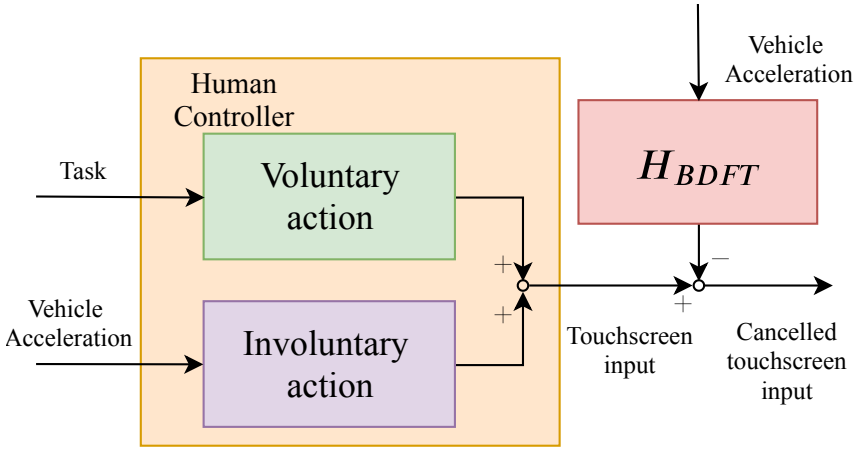

Figure 4-4: A BDFT model needs to accurately describe the involuntary movement of the human arm in the presence of motion disturbance such as turbulence. This modelled signal is then subtracted from the total touchscreen control signal consisting of both voluntary and involuntary contributions.

In literature two types cancellation methods have been used with control inceptors; force cancellation and signal cancellation [53]. Either the model output has been converted to a

torque which was fed back to the inceptor, or the cancellation was done purely in software, without the pilots involvement in the cancellation loop.

In contrast to input filtering, this method does not assume a certain frequency range where BDFT occurs. However, the success of the method rests on the accuracy of the model. BDFT is a complex phenomena dependent on variables such as physical, mental and environmental factors, making the creation of a model a difficult task [26]. This methods can be used either for discrete or continuous tasks. However, since BDFT models can be created in many different ways what type of tasks they are applicable for will vary. The rest of this chapter deals with the modelling of BDFT.

Other Methods

There exists many concepts that could help attenuate BDFT or its effects. One concept uses gesture tracking to predict the screen element the operator intends to interact with shown in Figure 4-5a [57]. Although this has been proposed for discrete tasks, similar predictive mitigation techniques can be implemented for continuous dragging tasks. However, the method is task dependent. A non-precision task such as map panning does not have a determined endpoint making predictions impossible. However a waypoint change with predetermined positions could benefit from this method. A more novel approach suggested in literature consist of a foldable touchscreen display [58]. The folds on the screen (Figure 4-5b) can help to stabilize the finger, but for dragging tasks the display would have to "flatten out" to allow for easy finger movement across the screen.

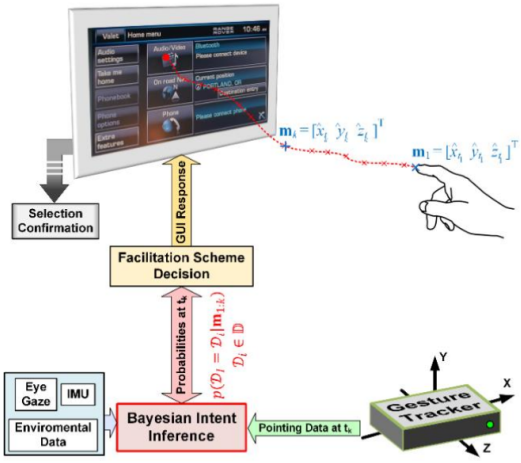

(a) A gesture tracking framework for predicting what on-screen object the operator intends to use [57] .

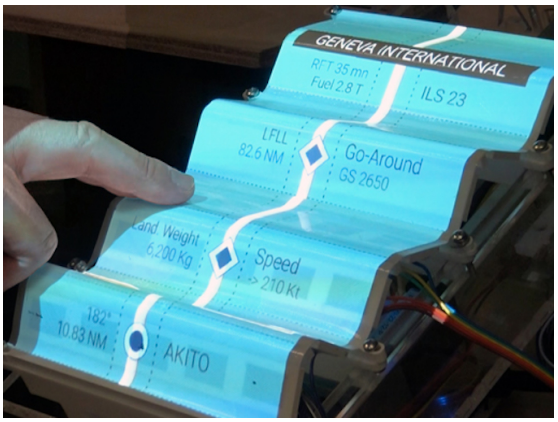

(b) A prototype of a foldable and reconfigurable display creating "valleys" where the finger is less perturbed by vibrations [58].

Figure 4-5: Different methods for touchscreen bracing

4-3 Pilot Modelling

Modelling pilot behaviour has been an important part of aircraft handling qualities requirements and increasingly in fly-by-wire flight control, large flexible airframes and flight simulation [59]. According to Xu et al. [6] pilot models can be classified as seen in Figure 4-6. The types of pilot models are the ones based on control theory, human physiology and

intelligence techniques. In a pilot modelling review paper by Lone and Cooke [59] a different classification of control-theoretic models, biomechanic models and sensory models is used. For the investigation of model-based BDFT mitigation the biodynamic/biomechanic class of models is of interest.

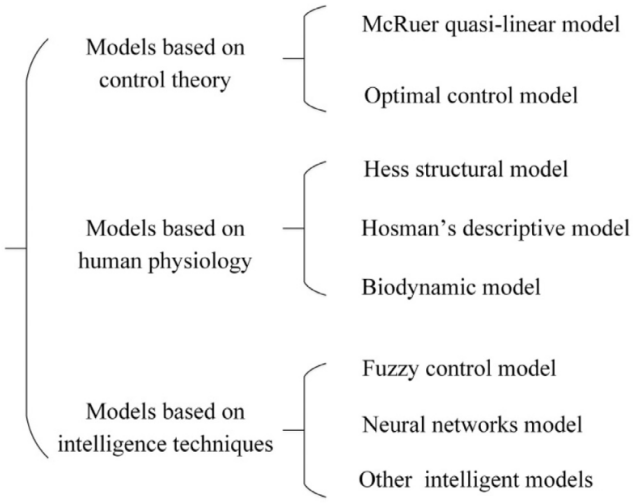

Figure 4-6: Types of pilot models defined by Xu et al. [6]

Different authors group these types of models using different classifications. Mansfield says the most common biodynamic models are lumped-parameter and physical models, with the latter referring to real-life models such as crash test dummies which is not of interest for BDFT modelling [60]. Griffin [61], while also defining physical models (which he calls effect models), also defines mechanistic and quantitative models. Building on this work both Sövényi [62] and Venrooij [26] call the two latter types black-box and physical models (not to be confused with effect models), respectively, which is the terminology used for the remainder of this study. Black-box models only relate the endpoint finger movement to the vibration without taking into account physical principals such as seat dynamics, human dynamics, kinematics and screen interaction. Physical models on the other hand do take all or parts of the knowledge of the system into account when creating a model.

4-4 BDFT Modelling

There is limited research on BDFT modelling with respect to touchscreen use since this is a relatively new research topic. Touchscreens were only made commercially available in 2007 with the launch of the Apple iPhone and has a decade later become ubiquitous in everyday life. The slow introduction of touchscreens on the flight deck has resulted in only a few studies on its use during turbulence. With the majority of the research focusing on the impact on performance or BDFT mitigation through hand bracing, touch technology or stencil use. Only one of these studies has created a BDFT model for touchscreen use under simulated turbulence [9]. This was the MSc thesis work of Mobertz from the Control & Simulation department at the TU Delft and is the work which the current thesis is based on.

On the other hand there is extensive research on the effect of vibration on the human body and biodynamic feedthrough in relation to physical control devices (e.g., [7, 11, 50,

60]). Despite this extensive research, model-based mitigation has only been implemented a handful of times with little follow up research.

As mentioned earlier, in literature there are two main types of models used for BDFT modelling: black-box and physical models. The physical models are based on physical principals of human motion and result in greater insight into the nature of vibration on the human operator and BDFT. On the other hand these models are usually more complex and parameter estimation can be difficult and result in over-fitting. Venrooij states that the increased complexity of physical models *"complicates parametrization, implementation and [their] proper use"* [26].

Black-box models only try to describe an input-output relationship. For BDFT relating to touchscreens the input is vehicle acceleration while the output is finger position [9]. Because black-box models only relate the input to the output they cannot give the same underlying insight as a physical model, but because they only consist of a limited amount of parameters they can more easily be estimated [26]. Griffin [61] points out that these models have no predictive power since they are not based on any physiological mechanism. Using different input signals (such as frequency and magnitude) than what the model was originally created with does not guarantee a valid output.

4-4-1 Example Black-Box BDFT Models

Mobertz et al. [27] in the only paper to date, quantified and modelled BDFT using a touchscreen on a flight deck. The 16 participants were presented with an open-loop pursuit tracking task on two touchscreens. One in a typical PFD position and the second in a position similar to the CDU. A sinusoidal motion disturbance signal was used for each axis which allowed for quantification of the BDFT at each disturbance frequency. This was done by estimating the frequency response function between the disturbance input and screen input. A second-order transfer function (Equation (4.1)) with an additional gain was used as a black-box model with the parameters estimated using a genetic algorithm and steepest decent method. Because of high lag at higher frequencies a time delay term was also added. However, the parameter estimation yielded inconsistent results due to the low magnitude at those frequencies and was therefore not used.

$$\hat{H}_{BDFT}(s) = G_{BDFT} \cdot \frac{1}{m_{BDFT} \cdot s^2 + b_{BDFT} \cdot s + k_{BDFT}} \tag{4.1}$$

A separate model was created for each screen input and disturbance direction, but only when these two axes were aligned was there enough BDFT feedthrough to make a reliable model. The exception being horizontal screen input during surge for the PFD location. A possible explanation being the arm kinematics causing a cross-coupling. The models were validated using variance accounted for (VAF). A VAF of over 70% was achieved for the mentioned conditions when averaged over all participants indicating the potential usefulness of the model in BDFT signal cancellation.

Sövényi & Gillespie [63] did a successful BDFT signal cancellation experiment in a single axis joystick experiment. Two experiments were conducted, one for system identification and a second to evaluate the created model. Both experiments featured the same 12 subjects. The authors used an autoregressive moving average (ARMA) model to fit the data to the model using four poles and four zeros. With the compensator the resonant peaks of the power spectral density decreased significantly and as well as the RMS of the tracking error. This was a closed-loop study since the joystick movement controlled the

position of the moving base. Although this could be possible for touchscreen operations on the flight deck the main concern is the replacement of hardware buttons and knobs with direct manipulation. Direct control of the aircraft or other feedback systems is therefore outside of the scope of this research study.

Mayo [64] created a BDFT model in a helicopter experiment by fitting a second-order transfer function between the vertical acceleration at the seat and the acceleration at the hand operating the collective in an open-loop experiment. BDFT is seen as especially prone to helicopters in the vertical axis [65], for this type of model to be useful for BDFT signal cancellation its model output must be integrated to get the screen position. More importantly there has to be a way to measure the acceleration at the finger. In contrast to physical input devices such as joysticks, there is no easy way to acquire that measurement without numerically differentiating the position input causing any noise to be amplified.

4-4-2 Example Physical Models

Allen et al. [7] created a physical BDFT model in the early seventies with the goal of understanding the bio-mechanical process and *"predict complex vibration"*. Allen created two BDFT models: one for vertical vibration and one for lateral as shown in Figure 4-7. These models use masses, springs and dampers to "lump" the constituent parts of the system together. Although black-box models also can use similar techniques, a lumped parameter model uses knowledge of the human dynamics and kinematics as shown here by Allen.

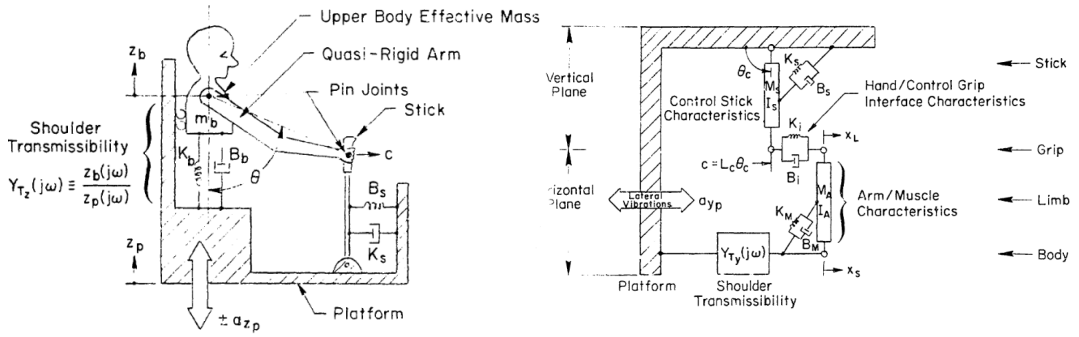

Figure 4-7: The left figure shows the lumped parameter model for the vertical vibration feedthrough. The right figure shows the later vibration feedthrough model [7].

Masarati et al. [4, 66, 67] developed a detailed multibody model of the arm shown in Figure 4-8. The model was used to investigate effect of BDFT on helicopter stability and maneuvering performance. This model creates a muscle activation model which depends on the *"task, the level of attention, workload, training, and other subjective, random or hardly quantifiable, parameters"* [66]. The muscular activation tries to model the two ways muscles operate, either by voluntary co-contraction or reflexive behaviour.

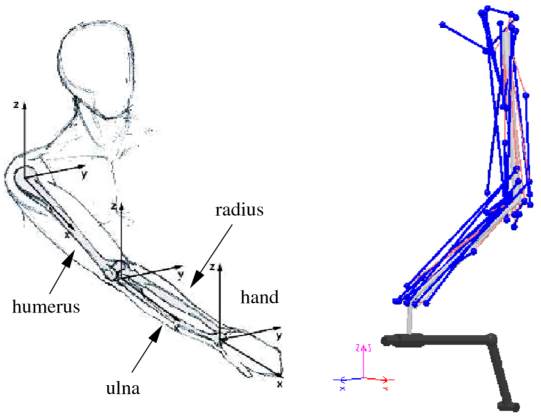

Figure 4-8: A multibody biomechanical model of the arm used to investigate BDFT in helicopters [4].

4-5 Human Variability to Vibration

There is a large variability in human reaction to vibration [68]. Therefore, to draw general conclusions of human reactions to vibration across individuals, statistical methods are used with an appropriate amount of participants. The variability of human response to vibration is categorized in between-subject variability and within-subject variability. The former is the variation of responses between different individuals while the latter is the change in response which can occur over time for one subject [11]. In Table 4-1 the possible sources for these changes are presented. The effect of these variables make BDFT a complex problem.

Table 4-1: Sources of between-subject variability and within-subject variability [11].

Between-subject Variability	Within-subject variability
Body dynamics	Body dynamics
Body dimensions	Body posture
Body posture	Age
Age	Health
Gender	Experience and training
Health	Attitude and motivation
Experience and training	Sensitivity and susceptibility
Attitude and motivation	
Sensitivity and susceptibility	

The variability in human response in manual control tasks has been recognized in several fields. For example, in haptic shared control, where the human and control device cooperate, the presence of neuromuscular adaptability has been acknowledged [69]. In human health and safety research the effect of vibration from industrial sources such as power tools has been extensively researched. This research typically employs frequencies of several hundred Hertz, much higher than that of interest in the current research. However, human variability is also present here. A paper by Concettoni [70] showed the human variability in the transmissibility responses (input acceleration to output acceleration) for the hand when touching a vibrating metal plate. The author pointed out the variability of the resonance frequency between subjects and points out that averaging the subjects re-

sponses can remove peaks seen in individual responses. This is an important consideration for creating a one-size-fits-all (OSFA) model, as the variance of individuals is lost.

4-5-1 Subject Variability in BDFT studies

Sövényi and Gillespie [63] concluded in a BDFT cancellation experiment that significant differences between the participants meant a single BDFT model could not be used, although this was not tested. They cite anecdotal evidence when stating that a model created for one subject can not be used by an other subject. Rather, each identified model was based on each subjects own experiment data. The causes for the variations are not investigated, but are speculated to come from differences in height, weight, posture, physical restraint, different clothing and nominal muscle activation.

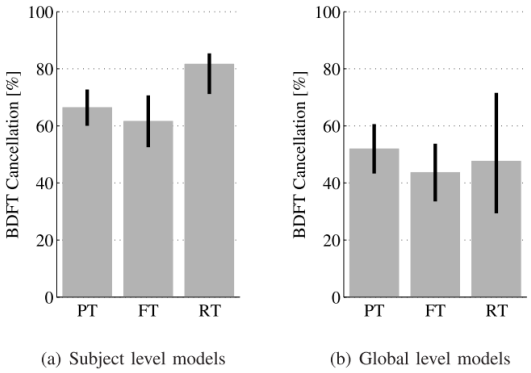

Figure 4-9: In a study by Venrooij subject average models (left) performed better than models based on averages of all subject (right) in an offline BDFT cancellation [8].

Venrooij [26] investigated to what extent individualization was necessary. By averaging over several experiment runs to obtain subject and global level models (averaged over all subjects) the signal cancellation on a per run basis could be quantified offline. As a model he used the Frequency Response Function (FRF) between the motion disturbance input and the stick angle output. The models were created for three tasks types, position, force and relax task with part of the results reproduced in Figure 4-9. This shows that subject level models could cancel between 60% to 80% of the BDFT when applied to run level data. The global level models were less successful and could only cancel between 40% to 50% of the BDFT, which can be attributed to between-subject variability. It is also clear that the subject level models result in smaller variations than the global level models. The authors conclude that BDFT should be both adapted to the subject and the task. While the task itself is not important, the different neuromuscular settings required to perform that task is.

Mayo [64] studied between-subject variability when investigating BDFT in helicopter cyclic operations. He grouped experiment subjects into ectomorphic and mesomorphic body types and fit a separate BDFT model to to each group. The two second-order transfer functions had slight differences in resonant peaks and phase which can indicate the importance of body type under vibration. Higher frequencies also showed increased variability within the group. However, the study was preformed with only six subject, three in each body type category making it hard to draw definitive conclusions. Moreover, Mansfield states that there is little evidence to suggest that anthropometric measures change the vibration response between people [60].

4-6 Chapter Discussion

This chapter has looked at different BDFT mitigation techniques as well as BDFT modelling relevant for model-based mitigation. The following sub-questions of the preliminary

research question has been addressed: *What are the types of mitigation which are possible for BDFT?* and *How can BDFT be modelled to be used in model-based cancellation?*.

Several mitigation techniques exist with the most important ones mentioned in this chapter. The different techniques can be more suitable for discrete or continuous tasks. For example, using a resistive touchscreen will only help prevent inadvertent touch and the performance of discrete tasks. While a model-based approach can work for continuous tasks or discrete tasks, depending on the applicability of the model.

Model-based mitigation presents an opportunity to improve the task performance for dragging tasks which have been dissuaded from use because of their poor performance in turbulence (see Section 3-4-2). Dragging tasks will likely become more common on the flight deck in order to exploit the potential touch interfaces have for direct manipulation (e.g., [18, 30]),

The most difficult part of model-based mitigation is creating an accurate BDFT model. A wide variety of models which can be classified into black-box and physical models. Black-box models only try to model the BDFT without considering prior knowledge of the system. Physical models on the other hand use physiological knowledge to model the BDFT. For the purpose of BDFT mitigation the use of a black-box model is most appropriate. Their straightforward computer implementation and simple system identification is conducive not only for the current research, but also for future use. As shown by Mobertz [9] a simple second order model was able to capture on average 70% of the occurring BDFT. It is therefore recommended to build on this work and use a similarly simple model for the rest of the this thesis.

Ideally the development of a single model would be adequate to describe the different responses of the human controller, that is a one-size-fits-all solution. However, literature shows this might not be possible. Because touchscreen tasks differ from control inceptor tasks, the level of model generalization should be investigated.

A remaining question is how to perform the BDFT cancellation on the touchscreen. Literature showed two methods used with aircraft control inceptor; force cancellation and signal cancellation. For touchscreens three methods of cancellation can be defined:

- Signal cancellation,
- Signal cancellation with feedback,
- Display compensation

With signal cancellation the BDFT model output is subtracted from the screen input signal directly. The human operator receives no haptic, visual or auditory feedback when the cancellation is taking place. The second method cancels the BDFT signal in the same way as the first method, but now gives feedback of the cancellation to the operator. An example implementation is an on screen marker showing the actual position of the registered signal after cancellation. Display compensation involves moving the entire image on the screen proportional to the cancellation signal. The two latter options gives the pilots feedback making them part of the BDFT cancellation loop. The cancellation is still open-loop since the operator is not directly controlling the state of the vehicle. Venrooij et al. state feedback is desirable since the pilot is being made aware of the cancellation [53]. This also is in line with Federal Aviation Administration (FAA) recommendations that controls should be *"predictable and obvious"* [71]. However, how this feedback changes the nature of BDFT is not known.

Conclusions:

- A variety of methods exists for mitigation of BDFT. Model-based cancellation seems promising to improve dragging task performance.
- Black-box models are simple to construct and use, physical models are complex and difficult to identify.
- Variability between and within subjects can cause different responses to vibration complicating BDFT modelling.

Recommendations:

- A black-box model, similar to Mobertz [27] should be used to model BDFT.
- Using signal cancellation with feedback should be investigated.
- Investigation should be made into the necessity of individualizing the BDFT model.

Chapter 5

Offline Model-Based Cancellation

Data collected by Mobertz as part of a MSc thesis work are used in this chapter to perform an offline BDFT cancellation which will guide the proposal of a full experiment. The experiment Mobertz performed is first explained in Section 5-1. Then the objectives of the current data analysis are explained in Section 5-2. The methods for BDFT cancellation are further elaborated in Section 5-3. Then the results of the analysis are presented and discussed in Section 5-4. Finally, in Section 5-5 some differences between experiment participants are examined.

5-1 Source of Data: Experimental Setup and Results

Data collected from an experiment conducted by Mobertz [9] to quantify the effect of BDFT when using a touchscreens have been used in this chapter to perform an offline BDFT model-based cancellation. The pursuit control task is depicted in Figure 5-1. The repeated measures experiment was conducted using the 6-DOF SIMONA research simulator at the TU Delft [72]. A multisine disturbance signal based on 10 frequencies was used to simulate turbulence for the surge, sway and heave axis ($f_{d_{x,y,z}}$). Each of the 16 subjects conducted a 2D pursuit tracking task on a touchscreen with instructions to minimize the horizontal and vertical tracking error (e_x, e_y). The error was defined as the difference between the tracking signals (f_{t_x}, f_{t_y}) and the finger input signal on the touchscreen (u_x, u_y). The tracking signal was also a multisine consisting of three frequencies, each different for the horizontal and vertical screen directions. The multisine signals were created by using Equation (5.1) with signal properties found in Table 5-1.

$$f_{d,t}(t) = \sum_{k=1}^{N_{d,t}} A_{d,t}[k] \sin\left(\omega_{d,t}[k]t + \phi_{d,t}[k]\right) \tag{5.1}$$

Table 5-1: Multisine properties used for the disturbance and pursuit target signal

	Disturbance, $f_{d_{y,z}}$				Target, f_{t_x}				Target, f_{t_y}			
k	n_d	ω_d	A_d	ϕ_d	n_{t_x}	ω_{t_x}	A_{t_x}	ϕ_{t_x}	n_{t_y}	ω_{t_y}	A_{t_y}	ϕ_{t_y}
-	-	rad s^{-1}	m s^{-2}	rad	-	rad s^{-1}	-	rad	-	rad s^{-1}	-	rad
1	5	0.3835	$1.067 \cdot 10^{-1}$	-0.269	3	0.230	0.646	1.445	2	0.153	0.894	0.308
2	11	0.8437	$8.069 \cdot 10^{-2}$	4.016	7	0.537	0.784	0.000	13	0.997	1.562	-0.431
3	23	1.7641	$4.019 \cdot 10^{-2}$	-0.806	19	1.457	1.406	-1.825	17	1.304	1.866	-1.591
4	37	2.8379	$2.048 \cdot 10^{-2}$	4.938								
5	51	3.9117	$1.246 \cdot 10^{-2}$	5.442								
6	71	5.4456	$7.568 \cdot 10^{-2}$	2.274								
7	101	7.7466	$4.735 \cdot 10^{-3}$	1.636								
8	137	10.5078	$3.424 \cdot 10^{-3}$	2.973								
9	171	13.1155	$2.856 \cdot 10^{-3}$	3.429								
10	226	17.3340	$2.416 \cdot 10^{-3}$	3.486								

Two screens where used, one in a position representative of the primary flight display (PFD), in front of the subject. The second screen was placed at the pedestal in a similar position as a control display unit (CDU) in a typical commercial aircraft. Each participant performed eight runs of 90 seconds per condition, of which only the last 81.92 seconds were used (measurement time T_m). The multisine signals were integer multiples of the fundamental frequency $\omega_m = 2\pi/T_m = 0.0767$ rad/s. This prevented leakage of the input signal. For the system identification step only the last 4 runs for a certain condition were used.

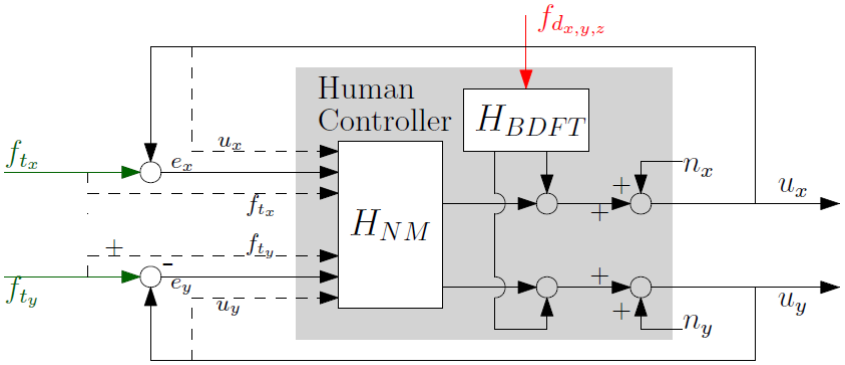

Figure 5-1: The control task as performed by Mobertz [9]. The abstracted version of the human controller consists of the neuromuscular system (H_{NM}) which represents the volitional control defined by the pursuit task. The biodynamic feedthrough (H_{BDFT}) is the involuntary part of the control task affected by the motion disturbance. Together, the voluntary part, involuntary part and the remnant ($n_{x,y}$, nonlinear contribution of the human controller) define the screen input signal ($u_{x,y}$).

Table 5-2: Motion disturbance component f_d in the variance of the screen input $\sigma^2_{u_{x,y}}$ [9].

Screen	Input Direction	Disturbance	$\sigma^2_{u_{f_d}}/\sigma^2_u \cdot 100[\%]$	Possibility of accurate BDFT estimate	Condition
PFD	Horizontal	Surge (X)	0.5	■	C4
PFD	Horizontal	Sway (Y)	1.8	■	C1
PFD	Horizontal	Heave (Z)	0.2	■	-
PFD	Vertical	Surge (X)	1.3	■	C2
PFD	Vertical	Sway (Y)	0.2	■	-
PFD	Vertical	Heave (Z)	0.8	■	C3

The experiment showed that the effects of BDFT were most prominent when the finger input axis and disturbance direction were aligned. As a consequence, only those conditions could reliably be identified, with exception of horizontal input during surge on the PFD as shown in Table 5-2. Identification was only reliable when the motion disturbance component in the variance of the input signal ($\sigma^2_{u_{f_d}}/\sigma^2_u$) was at least 0.5%. The models showed on average a variance accounted for (VAF) of 70%, which Mobertz concluded would make model-based BDFT mitigation a possibility [9].

5-2 Data Analysis Objectives

Having data available from a previous experiment is a great benefit for the current analysis. The results of the offline model-based cancellation in this chapter will help shape the research question and will investigate the feasibility of model-based BDFT mitigation. Moreover, this analysis also quantifies to what extent mitigation is possible. Since the final experiment will be limited to the PFD, only the analysis will be limited to that screen location. Additionally the offline cancellation will only deal with condition C1-C4 as defined on Table 5-2. The goal of the data analysis is the following:

Is model-based cancellation possible?
Mobertz showed that BDFT in conditions with enough feedthrough could be modelled with a mean VAF of 70% and therefore concluded the model had a good possibility of being used for BDFT cancellation. The current analysis therefore answers if model-based signal cancellation is at all possible.

Does higher feedthrough lead to better cancellation?
If cancellation is possible, it is important to ask what makes it more or less successful. Mobertz found that only the experiment conditions where the disturbance input variance was above 0.5% of the total input variance could reliably be modelled. Therefore the amount of motion disturbance feedthrough is investigated to find its effect on cancellation.

Do BDFT models need to be individualized?
Chapter 4 recommended further investigation into the need of individualization of BDFT models. Ideally a single BDFT model can mitigate the involuntary finger movements for all participants. However, because of between-subject and within-subject variability this is not likely. By creating BDFT models with different levels of generality this question can be answered. Models will be made for three levels of generality, for a certain run, a certain subject and for for all subjects. By comparing their cancellation performance the most suitable model can be chosen.

5-3 BDFT Cancellation Method

5-3-1 Model Identification

The multisine input signals have the benefit of a discrete frequency spectrum. The contribution from the disturbance signal and target signal can therefore be separated, and only the effect of the motion disturbance be investigated. The frequency response function (FRF) between the disturbance signal and screen input signal gives a non-parametric estimate of the BDFT dynamics at the disturbance frequencies (Equation (5.2)) by taking the ratio of the cross-correlation density between the motion disturbance and the screen input signal ($S_{f_d,u_{x,y}}(j\omega_d)$) with the auto-correlation density of the motion disturbance ($S_{f_d,f_d}(j\omega_d)$).

$$\hat{H}_{BDFT}(j\omega_d) = \frac{S_{f_d,u_{x,y}}(j\omega_d)}{S_{f_d,f_d}(j\omega_d)} \tag{5.2}$$

By investigating the FRFs it was decided to use a mass-spring-damper system with an additional gain to model the BDFT dynamics, which was also used by Mobertz [9] and shown in Equation (5.3). Because the frequency responses showed a decrease in phase at higher frequencies, a time delay (τ) was also added to better estimate the higher frequency

contributions. Comparisons of cancellations results when using models with a time delay showed they consistently performed better than when this term was left out. The issues related to reliable identification as experienced by Mobertz were not encountered. The model parameters were identified by using MATLABs `fmincon` function with the initial conditions and bounds in Table 5-3 with the cost function (Equation (5.4)) being the sum of the normalized absolute difference between the FRF and the model. The system identification resulted in a model fit defined by the parameters in Equation (5.5).

$$H_{BDFT}(s) = G_{BDFT} \cdot \frac{1}{m_{BDFT} \cdot s^2 + b_{BDFT} \cdot s + k_{BDFT}} e^{-\tau_{BDFT} s} \tag{5.3}$$

$$J(\theta) = \sum \left| \frac{\hat{H}_{BDFT}(j\omega_d) - H_{BDFT}(j\omega_d|\theta)}{\hat{H}_{BDFT}(j\omega_d)} \right| \tag{5.4}$$

$$\theta = \begin{bmatrix} G_{BDFT} & m_{BDFT} & b_{BDFT} & k_{BDFT} & \tau_{BDFT} \end{bmatrix} \tag{5.5}$$

Table 5-3: Limits and initial conditions for the parameter estimation

	G_{BDFT} [-]	m_{BDFT} [kg]	b_{BDFT} $[\frac{kg}{sec}]$	k_{BDFT} $[\frac{kg}{sec^2}]$	τ_{BDFT} [sec]
Lower limit	0.0	0.0	0.0	0.0	0.0
Upper limit	30.0	4.0	12.0	40.0	2.0
Initial condition	15.0	2.0	2.0	30.0	0.1

To explore how the generality of the models influences the cancellation three levels of models are investigated: run, subject and global models (Figure 5-2). Run-specific models are identified from a single run as performed by a subject. Since the subjects performed each experiment condition eight times there are also eight models per condition. By averaging over the eight sets of model parameters we get the subject average model (denoted SA) for a specific condition. Each subject will therefore have one SA model for each of the four conditions C1 to C4. The global model, or one-size-fits-all (denoted OSFA) model, is created by averaging over the parameters of the subject average models for each condition. Therefore, each of the four conditions have only one OSFA model.

Figure 5-2: Example of how different model generalities are connected for a certain experiment condition. Each black box represents a model. Averaging the model parameters of the eight runs results in a subject average (SA) model. Averaging the SA models for all subject results in the one-size-fits-all model (OSFA) for that condition.

5-3-2 Signal Cancellation

With the identified models, the motion disturbance contribution to the screen input ($u_{x,y}$) can be cancelled. This signal has several contributions and can therefore be split into two parts. One part of the input signal can be attributed to the motion disturbance ($u^{f_d}_{x,y}$) while the other part is the residual ($u^{res}_{x,y}$). The residual consist of voluntary CNS contribution as well as the remnant which is the component not linearly correlated with the tracking signal or motion disturbance [26]. The goal of the cancellation is to remove the contribution of the motion disturbance by subtracting the modelled BDFT contribution ($u_{BDFT_{x,y}}$). The cancelled screen input signal and tracking error can therefore be described as follows:

$$u_{x,y_{can}} = u^{f_d}_{x,y} + u^{res}_{x,y} - u_{BDFT_{x,y}} \tag{5.6}$$

$$e_{x,y_{can}} = f_{t_{x,y}} - u_{x,y_{can}} \tag{5.7}$$

5-3-3 BDFT Cancellation Metrics

The method used to asses the amount of cancellation looks at the percentage change of the motion disturbance component in the error variance shown in Equation (5.8). A negative percentage means a reduction in the motion disturbance with a negative 100% being a perfect cancellation. A positive percentage means the motion disturbance component of the error variance has in fact increased. That is, the cancellation is doing more harm than good.

$$\Delta\sigma^2_{e_{f_d}} = \frac{\sigma^2_{e_{f_{d\,can}}} - \sigma^2_{e_{f_d}}}{\sigma^2_{e_{f_d}}} \cdot 100[\%] \tag{5.8}$$

Since the identified BDFT models are linear their output will have the same frequency content as the input, with only the amplitude and phase changed. That means the cancellation will only affect the motion disturbance component in the error variance, leaving the other contributions equal to their value before cancellation.

5-4 Results

5-4-1 BDFT Cancellation

For the four different conditions Tables 5-4 to 5-11 show the percentage change of the motion disturbance component ($\sigma^2_{e_{f_d}}$) in the error variance (σ^2_e). Each of the eight runs per experiment condition have been identified and used to cancel the BDFT of the screen input. It is possible that run-specific models have a low generality which means using them to cancel a previous or subsequent run will yield bad cancellation or even an increase in the disturbance. The tables therefore show each of the eight models cancelling all the other runs. To investigate if a higher feedthrough leads to better cancellation Tables 5-4, 5-6, 5-8 and 5-10, on the left side have been sorted based on the percentage feedthrough observed in the error variance. The sorting was first done for each subject before being averaged across all subjects. For example, the top left corner shows the BDFT model from the run with the highest feedthrough cancelling that same run. The bottom right corner shows the BDFT model created from the run with the least percentage feedthrough cancelling itself. Tables 5-5, 5-7, 5-9 and 5-11 on the right right have been averaged across subject in the order of each experiment run. This can be useful in finding any order effect.

The same color scale is used between the four conditions making comparison between them easier. Since the range of values seen across conditions is notably different, the colors should only be used as a guidance. The minimum value (■) is set to negative 80%, the mid value (□) to negative 60% and the maximum value (■) to positive 20%.

Table 5-4: Percentage change of f_d in σ_e^2 when sorted based on percentage of f_d in error variance across all subjects for condition C1. Disturbance direction: Sway. Input direction: Horizontal.

Model	Run: max $\sigma^2_{e_{f_d}}/\sigma^2_e$ →							min $\sigma^2_{e_{f_d}}/\sigma^2_e$
max $\sigma^2_{e_{f_d}}/\sigma^2_e$	-80.15	-77.98	-78.14	-75.87	-77.06	-76.70	-73.19	-70.42
	-77.30	-79.34	-77.49	-77.12	-76.53	-76.43	-72.80	-69.27
	-75.90	-75.82	-78.48	-72.82	-76.22	-73.95	-70.01	-67.85
	-76.34	-76.89	-76.06	-78.98	-77.01	-76.85	-73.42	-72.51
	-72.62	-71.93	-73.22	-71.64	-76.28	-72.38	-70.22	-67.24
	-76.81	-76.39	-76.01	-75.88	-76.73	-79.32	-76.86	-73.76
	-74.01	-73.23	-73.37	-73.91	-73.95	-75.97	-77.88	-73.41
min $\sigma^2_{e_{f_d}}/\sigma^2_e$	-72.81	-72.14	-72.45	-72.44	-73.15	-74.95	-75.16	-79.32
SA model	-78.33	-78.24	-78.29	-77.91	-78.74	-79.13	-77.37	-75.48
OSFA model	-74.04	-72.49	-72.85	-73.32	-72.82	-74.18	-70.19	-63.71

Table 5-5: Percentage change of f_d in σ_e^2 when sorted based on run order across all subjects for condition C1. Disturbance direction: Sway. Input direction: Horizontal.

	Run 1	Run 2	Run 3	Run 4	Run 5	Run 6	Run 7	Run 8
Model 1	-81.04	-76.88	-74.87	-74.14	-73.77	-73.07	-72.03	-72.33
Model 2	-78.04	-78.90	-76.70	-75.90	-75.66	-74.64	-74.29	-73.68
Model 3	-74.22	-76.72	-79.98	-77.08	-75.76	-76.36	-75.01	-75.02
Model 4	-74.01	-77.93	-77.87	-79.00	-76.43	-76.33	-76.08	-77.17
Model 5	-73.84	-75.03	-76.69	-75.35	-79.50	-78.02	-75.23	-75.53
Model 6	-71.97	-74.03	-75.82	-74.54	-76.76	-80.87	-76.48	-74.93
Model 7	-67.40	-67.05	-69.08	-67.92	-68.79	-70.06	-71.90	-68.75
Model 8	-70.21	-72.74	-74.23	-74.27	-74.06	-74.96	-74.87	-78.56
SA model	-77.21	-78.22	-78.42	-77.93	-78.00	-78.48	-77.52	-77.70
OSFA model	-74.98	-74.46	-72.77	-72.00	-71.30	-67.39	-72.22	-68.49

Table 5-6: Percentage change of f_d in σ_e^2 when sorted based on percentage of f_d in error variance across all subjects for condition C2. Disturbance direction: Surge. Input direction: Vertical.

Model	Run: max $\sigma^2_{e_{f_d}}/\sigma^2_e$ →							min $\sigma^2_{e_{f_d}}/\sigma^2_e$
max $\sigma^2_{e_{f_d}}/\sigma^2_e$	-80.74	-67.43	-66.12	-61.45	-48.28	-39.82	-8.20	-17.80
	-73.85	-79.41	-75.23	-73.93	-70.39	-69.86	-64.41	-47.83
	-69.77	-73.07	-77.67	-71.48	-68.16	-72.05	-64.35	-60.14
	-67.01	-70.58	-69.41	-73.12	-64.18	-65.80	-58.67	-60.79
	-70.59	-73.47	-73.24	-74.50	-78.37	-72.12	-69.56	-63.73
	-67.45	-69.37	-73.33	-69.72	-70.76	-76.38	-72.49	-64.74
	-65.62	-68.13	-69.81	-67.18	-68.50	-69.54	-74.68	-65.05
min $\sigma^2_{e_{f_d}}/\sigma^2_e$	-64.28	-67.81	-69.30	-69.24	-68.53	-68.39	-67.55	-73.45
SA model	-73.61	-76.43	-77.18	-76.44	-74.39	-74.58	-72.03	-65.21
OSFA model	-71.96	-70.78	-69.82	-68.12	-60.36	-59.02	-48.39	-45.34

Table 5-7: Percentage change of f_d in σ_e^2 when sorted based on run order across all subjects for condition C2. Disturbance direction: Surge. Input direction: Vertical.

	Run 1	Run 2	Run 3	Run 4	Run 5	Run 6	Run 7	Run 8
Model 1	-81.77	-63.91	-44.58	-66.94	-50.95	-47.12	-42.46	-22.44
Model 2	-69.36	-83.27	-77.33	-75.26	-77.88	-70.24	-64.04	-70.69
Model 3	-67.31	-78.63	-81.28	-74.57	-75.86	-71.71	-71.91	-74.68
Model 4	-65.10	-71.74	-66.92	-76.05	-69.24	-70.97	-56.77	-71.11
Model 5	-68.09	-74.90	-77.08	-75.87	-80.08	-71.33	-72.95	-75.23
Model 6	-68.62	-73.99	-74.77	-74.56	-74.18	-80.04	-71.38	-78.12
Model 7	-64.98	-71.57	-75.80	-74.55	-75.92	-72.94	-83.50	-75.39
Model 8	-64.93	-67.55	-72.60	-73.26	-71.86	-68.73	-69.20	-83.99
SA model	-73.41	-80.14	-79.72	-79.81	-79.24	-76.85	-74.96	-80.75
OSFA model	-69.16	-71.26	-61.38	-71.03	-66.65	-59.24	-57.58	-59.63

Table 5-8: Percentage change of f_d in σ_e^2 when sorted based on percentage of f_d in error variance across all subjects for condition C3. Disturbance direction: Heave. Input direction: Vertical.

model	Run: max $\sigma^2_{e_{f_d}}/\sigma^2_e$ →							min $\sigma^2_{e_{f_d}}/\sigma^2_e$
max $\sigma^2_{e_{f_d}}/\sigma^2_e$	-91.18	-71.54	-31.52	-36.28	-20.05	20.26	95.98	95.00
	-77.29	-85.50	-68.75	-60.57	-56.37	-41.22	7.36	17.23
	-69.32	-73.93	-79.40	-69.84	-68.30	-66.68	-24.57	-25.02
	-66.46	-70.45	-70.17	-78.57	-72.36	-71.25	-47.21	-37.88
	-67.07	-69.99	-72.15	-72.52	-80.54	-68.81	-43.68	-35.45
	-64.32	-68.12	-67.99	-72.43	-70.14	-77.65	-51.45	-46.84
	-52.76	-55.99	-57.78	-61.19	-57.71	-60.64	-65.97	-53.39
min $\sigma^2_{e_{f_d}}/\sigma^2_e$	-47.37	-53.97	-53.25	-55.94	-55.36	-57.58	-53.15	-60.28
SA model	-69.42	-75.95	-75.05	-76.85	-75.66	-75.57	-48.69	-40.55
OSFA model	-71.44	-65.74	-31.87	-33.63	-19.93	13.30	52.16	81.40

Table 5-9: Percentage change of f_d in σ_e^2 when sorted based on run order across all subjects for condition C3. Disturbance direction: Heave. Input direction: Vertical.

	Run 1	Run 2	Run 3	Run 4	Run 5	Run 6	Run 7	Run 8
Model 1	-88.16	-40.16	10.95	-15.81	65.25	15.71	3.48	27.95
Model 2	-66.54	-78.49	-47.22	-69.22	-28.74	-57.31	-61.29	-28.69
Model 3	-63.47	-61.48	-73.53	-69.63	-59.34	-68.81	-66.20	-51.79
Model 4	-62.23	-68.09	-61.89	-78.34	-46.89	-68.70	-65.29	-46.45
Model 5	-57.79	-56.82	-55.69	-62.73	-70.80	-58.96	-55.91	-46.38
Model 6	-58.43	-51.46	-63.96	-65.27	-53.95	-81.25	-62.67	-41.57
Model 7	-63.97	-62.39	-42.74	-67.72	-48.95	-61.90	-74.90	-45.23
Model 8	-56.30	-50.50	-49.64	-48.04	-32.80	-45.64	-43.92	-73.62
SA model	-67.85	-70.67	-62.74	-75.68	-60.89	-71.34	-69.52	-59.03
OSFA model	-71.52	-25.16	-3.86	-11.92	43.21	-4.57	6.52	-8.43

Run Level Models

Tables 5-5, 5-7, 5-9 and 5-11 show that for the run level models the diagonal has the highest cancellation, always above 70% and with certain conditions reaching close to 90%. That is, a run has better cancellation from its own model than any other model. This is

Table 5-10: Percentage change of f_d in σ_e^2 when sorted based on percentage of f_d in error variance across all subjects for condition C4. Disturbance direction: Surge. Input direction: Horizontal.

Model	Run: max $\sigma^2_{e_{f_d}}/\sigma^2_e$ →						min $\sigma^2_{e_{f_d}}/\sigma^2_e$
max $\sigma^2_{e_{f_d}}/\sigma^2_e$	-77.26	-72.74	-71.67	-64.97	-65.34	-61.88	-60.90	-26.95
	-72.83	-77.18	-74.26	-67.54	-65.30	-63.02	-63.16	-28.10
	-69.31	-70.58	-77.32	-68.47	-64.97	-61.36	-62.26	-25.70
	-68.93	-69.71	-71.86	-71.09	-64.61	-66.01	-65.87	-39.67
	-65.11	-63.07	-66.28	-63.94	-70.44	-59.99	-60.67	-39.07
	-62.56	-61.53	-64.77	-59.59	-63.28	-68.50	-61.61	-50.07
	-64.74	-66.60	-67.33	-66.23	-63.95	-63.64	-73.34	-41.35
min $\sigma^2_{e_{f_d}}/\sigma^2_e$	-58.38	-60.14	-57.44	-54.81	-60.60	-57.44	-56.31	-63.36
SA model	-71.97	-70.59	-71.63	-66.20	-68.44	-67.23	-66.88	-45.20
OSFA model	-68.60	-65.90	-62.26	-55.17	-52.57	-52.13	-44.86	-20.37

Table 5-11: Percentage change of f_d in σ_e^2 when sorted based on run order across all subjects for condition C4. Disturbance direction: Surge. Input direction: Horizontal.

	Run 1	Run 2	Run 3	Run 4	Run 5	Run 6	Run 7	Run 8
Model 1	-71.80	-61.71	-61.31	-55.66	-66.81	-53.43	-58.27	-56.64
Model 2	-35.82	-76.95	-70.73	-69.49	-71.86	-71.02	-68.43	-69.15
Model 3	-36.13	-71.72	-77.01	-70.64	-75.08	-68.03	-69.41	-70.55
Model 4	-49.97	-67.02	-66.75	-73.92	-71.67	-64.66	-67.48	-68.03
Model 5	-54.36	-69.96	-69.95	-68.66	-81.88	-70.85	-69.76	-72.63
Model 6	-40.04	-65.83	-66.56	-63.31	-72.20	-79.92	-68.03	-70.66
Model 7	-43.93	-66.64	-70.60	-69.98	-74.27	-68.24	-78.12	-73.22
Model 8	-43.73	-66.02	-61.56	-65.50	-69.00	-71.88	-66.65	-75.04
SA model	-51.93	-73.71	-71.70	-71.91	-75.64	-71.65	-72.34	-72.27
OSFA model	-39.81	-59.08	-65.20	-57.73	-67.46	-46.68	-58.08	-54.17

seen across conditions, but the size of the effect differs. Condition C1 with the highest feedthrough, has only a small difference between the diagonal entries and the other model and run combinations with the majority having between 70-80% cancellation. There is a higher variability for the lower feedthrough conditions, C2-C4. Having a high feedthrough therefore seems to produce high and consistent cancellation across runs. However, other reason such as beneficial human dynamics in the sway direction might have produced this result. Other conditions with similarly high feedthrough should be investigated to have more confidence that its a reason for high and consistent cancellation.

The tables also show that the first run typically has worse cancellation than other runs. This effect is stronger with the conditions having the lowest feedthrough. The first run of any condition is typically used by the participants to get used to the task and find and adjust their strategy. This training effect can explain why other run models are less effective at cancelling the first run and why the model from run one is ineffective at cancelling the subsequent runs.

When sorted based on proportion of feedthrough in the error variance shown in Tables 5-4, 5-6, 5-8 and 5-10 some interesting patterns emerge. The cancellation of the diagonal for all conditions, except C1, is decreasing towards the lower right suggesting that a higher feedthrough run results in better cancellation when a model is cancelling its own run. The low variability of the C1 condition, probably caused by a high feedthrough can be the reason this effect is not observed.

The tables also reveal that high feedthrough models are not effective in cancelling the lower feedthrough runs seen by light green and red colors in the upper right corners, this is especially visible in conditions C2 and C3, but also observable in the other conditions. On the other hand, lower feedthrough models are more successful in cancelling higher feedthrough runs seen in the lower left corner. Having a darker green color around the diagonal shows that similar feedthrough runs cancel each the best. There is some evidence suggesting this, especially in conditions C2 and C3.

The C3 condition seems to have poorer performance than C4 in the runs with lower feedthrough. However, the model identification of several runs could not be estimated reliably because of insufficient feedthrough and is therefore believed to cause the lower performance.

In conclusion, the results show that the amount of feedthrough in a run does have an impact on cancellation using run-specific models, but with varying success.

Subject Average Models

Of the three model generalities the subject average models have the best performance across the different conditions. The sorted tables have been used for this analysis since they control for the amount of feedthrough. For the C1, C2 and C3 condition the SA models consistently have the second highest cancellation. For the lower feedthrough runs (run 7-8) of C3 the SA model performs worse, but still above the average. For C4 there is a bigger variability in terms of ranking, but the SA model still has high performance in terms of percentage cancellation. The C1 condition is able to cancel between 75%-80% of the feedthrough, while the C2 condition between 65%-77%. The C3 and C4 conditions cancel between 40%-77% and 45%-72%, respectively. A benefit of the SA models over a run-specific model are their robustness. The variability in an operator's performance means a run model might have a hit and miss cancellation performance. Because the SA model is based on the average of the operator's dynamics, atypical runs can still be effectively cancelled. In general a subject average model is able to have a high performance despite within-subject variability.

One-Size-Fits-All Models

The performance of a OSFA model varies more across conditions than the SA model. For the C1 conditions the OSFA model has a high performance, just below the SA model. Conditions C2-C4 show that only the higher feedthrough runs still have a good performance, suggesting that the between-subject variability is too large to be captured by the model.

5-4-2 Error Analysis

The cancellation results show that a reduction of BDFT is possible. They reveal that the tracking error can be reduced when applying model-based signal cancellation. These results are important to indicate if BDFT cancellation is possible, but they do not capture the final goal: to reduce the BDFT at any given point in time. In fact, the cancelled error signal can be higher than the original signal, meaning the tracking error is amplified instead of attenuated. If model-based cancellation is to be used for precision task such as changing waypoints, a larger error at the wrong moment in time is likely to leave the BDFT cancellation ineffective. The tracking tasks performed by Mobertz did not give the operator feedback on their performance during a run. The error amplification therefore has no effect on the operator strategy when cancellation is turned on.

If the distance between the two tracking errors is small the impact might be negligible. By combining Equation (5.6) and Equation (5.7) the relationship between the cancelled and original tracking error becomes apparent (Equation (5.9)). The distance between them equals the BDFT model output. A certain model will therefore have a constant difference between the tracking errors irrespective of the run being cancelled.

$$u_{BDFT_{x,y}} = e_{x,y_{can}} - e_{x,y} \tag{5.9}$$

In Figure 5-3 the tracking error for a typical subject is compared before and after cancellation using the subject average model. The error is often smaller after cancellation as expected, but sometimes also larger.

The models with higher motion disturbance feedthrough have on average a larger signal amplitude than models with lower feedthrough. The example in Figure 5-4 compares for a typical subject the disturbances component of the input signal with the modelled signal for

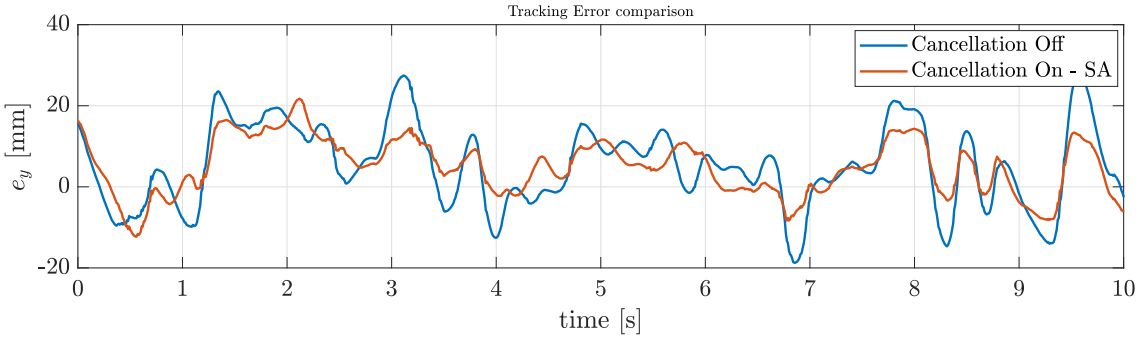

Figure 5-3: Comparing e_x and $e_{x_{can}}$ for typical run and subject using the SA model.

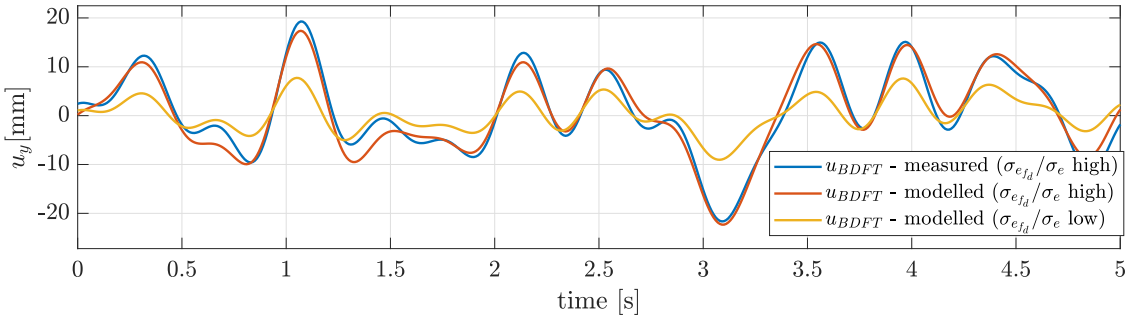

Figure 5-4: Comparing e_x and $e_{x_{can}}$ for typical run and subject using the SA model.

a high and low feedthrough run. The smaller amplitude of the low feedthrough model also means the tracking error amplification will be lower. Moreover, the reason cancellation results were low feedthrough models (bottom left of tables) cancelled high feedthrough runs (left table columns) better than the converse situation can now be explained. The lower amplitude signal of the low feedthrough models will cancel higher amplitude signal without a large error. One can therefore conclude that similar amount of feedthrough will lead to a better cancellation, assuming a good system identification.

5-5 Individual Performance

Human manual control tasks shows both between-subject variability and within-subject variability as discussed in Chapter 4 of the literature review. The previous section also showed that the SA models on average had better BDFT cancellation than the OSFA models. The within-subject differences were small enough to make the SA models effective while the between-subject differences were large enough to make the OSFA cancellation ineffective for most experiment conditions. Another way to look at these differences is by looking at the decomposition of the tracking error into contributions from the target signal, disturbance signal and remnant. The following section will use examples from subjects to highlight broad differences seen in the data.

The examples in Figure 5-5a and Figure 5-5b show the specter of variation in performance that was observed between subject. The figures show the tracking error variance (σ_e^2) for two different subjects for the C1 condition. Both showing the percentage and absolute breakdown on the left and right, respectively. The top row shows the measurements before cancellation and for reference the bottom row shows the error variance after BDFT cancellation has been applied using the SA model.

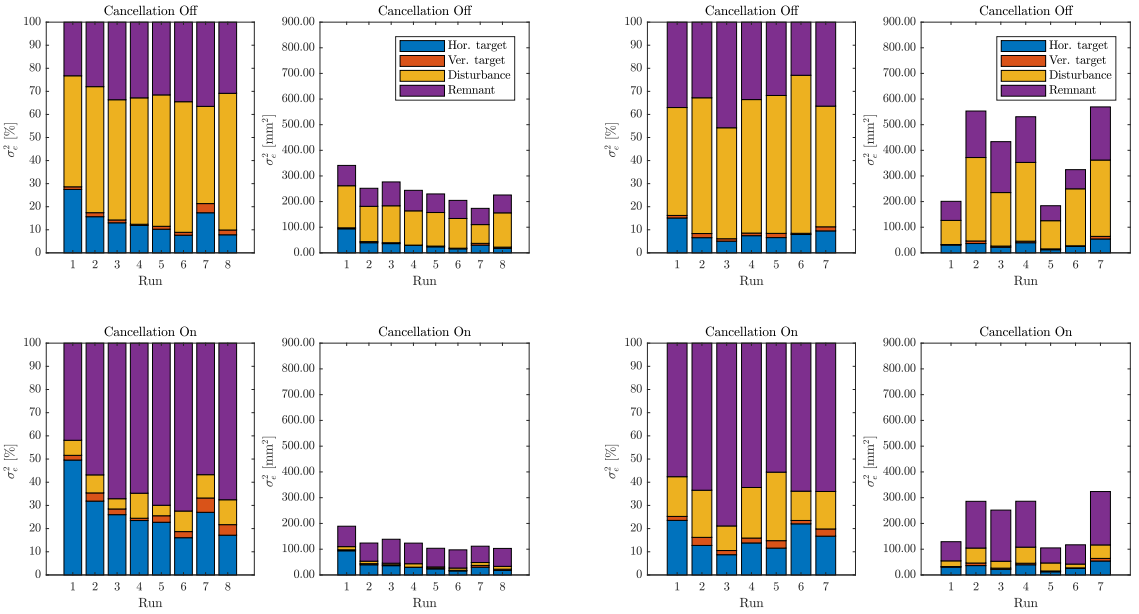

(a) Condition C1 subject 9 **(b)** Condition C1 subject 11

Figure 5-5: The error variance between subjects can vary greatly. The left side shows a subject producing a low error and showing ability to improve. The person on the right has a high error and is not getting better at the task.

Subject 9 shows a consistent performance over all runs and a clear ability to improve task performance. He is also able to decrease both his target error, arising from lag between target and finger position [27], and also decrease the biodynamic feedthrough from the motion disturbance. The value of the error variance is also average for the subjects in the C1 condition. On the other hand, subject 11 has the most inconsistent performance and highest error variance seen by any subject in the C1 condition and therefore shows the extreme of the variability that can be expected. Although the two subjects have similar percentage contributions from the decomposed error signals, their performance is not similar.

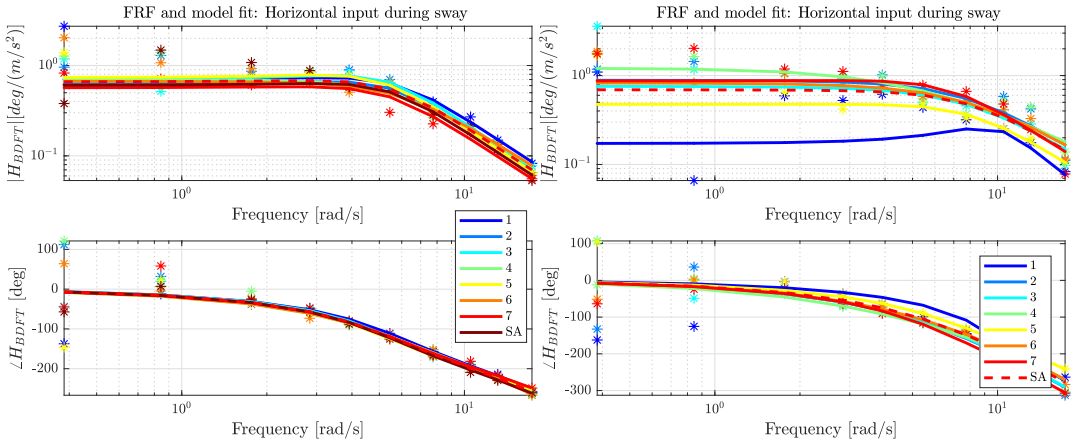

(a) Condition C1 subject 9 **(b)** Condition C1 subject 11

Figure 5-6: Bode plot showing the system identification results for two subject.

The error variance of the cancelled tracking signal on the bottom row of Figure 5-5 demonstrate that both subjects can have effective cancellation of the biodynamic feedthrough, indicating that an individuals task performance does not necessarily have an effect on BDFT cancellation. However, if the dynamics of the participants can not be be fully captured by the assumed model, the result will be a model ineffective in BDFT cancellation. In Figure 5-6 the results of the system identification is shown for the same two subjects. The larger variation of subject 11 in Figure 5-6b becomes clear. Moreover his first run does not correspond well to the model structure resulting in a bad system identification.

5-6 Conclusions & Recommendations

Using data from a previous touchscreen BDFT experiment [9], an offline analysis was performed to evaluate the feasibility of biodynamic feedthrough cancellation for a continuous dragging task. The cancellation used a simple linear mass-spring-damper-system with an additional gain and delay. It was shown that cancellation was possible for models based on a specific run, subject average models (SA) and global models (OSFA). The SA models showed a better cancellation for all four experiment conditions and was more robust than the run models, while the OSFA models were only effective for the C1 condition which has the highest amount of motion disturbance feedthrough, and for runs with high feedthrough. The goals of the data analysis were the following:

- Is BDFT cancellation possible?
- Does higher feedthrough lead to better cancellation?
- Does cancellation need to individualized?

Next to showing that cancellation is in fact possible, the data also revealed what can make it more successful. In general the experiment conditions with the highest feedthrough also had the highest and more consistent cancellation. This low variability can explain why the OSFA model was efficient in cancelling only the C1 condition, but if the low variability is due to the high feedthrough is an open question.

The tracking error analysis showed that even when cancellation is applied the tracking error can sometimes be higher than when cancellation is off. If this matters depends on the application. Non-precision tasks such as map panning will not be affected, but precision tasks such as waypoint modifications it might. If the operator lets go of the target at the wrong moment the new waypoint position might be further away from the goal than if cancellation was off.

Conclusions:

- High feedthrough run models are not effective in cancelling low feedthrough runs.
- Low feedthrough models are better at cancelling high feedthrough runs.
- Subject average models shows high and consistent cancellation.
- One-size-fits-all models show good cancellation for conditions with low subject variability, but is not adequate for most conditions.

Recommendations:

- Future research should investigate the effect of error amplification after cancellation.
- A subject average model should be used for the remainder of this work.

Chapter 6

Pilot Experiment: Online Model-Based BDFT Cancellation

Model-based BDFT cancellation has been shown to work in experiments with physical control inceptors in both online [63, 73, 74] as well as offline experiments [8]. Moreover, Mobertz [9] showed that BDFT-models can be identified for a continuous touchscreen task using a multisine disturbance input resembling turbulence. The offline analysis of Chapter 5 also concluded that model-based signal cancellation is possible and effective for continuous dragging tasks using touchscreens, and is therefore worth pursuing in a an online experiment. To improve realism Mobertz recommended applying a more realistic turbulence profile as experienced by airliners and to use shorter dragging task which are more commonly used with touchscreens. The literature research in Chapter 3 showed that such tasks can be waypoint dragging, or tasks related to direct manipulation used in future cockpit concepts. To narrow down the focus of the research this pilot experiment therefore assessed the possibility of BDFT mitigation using a more realistic step dragging tasks.

First in Section 6-1 the setup of the experiment is explained. The results are presented in Section 6-2 in three parts. First the results of the system identification is shown followed by the results of a multisine BDFT cancellation and finally a step task cancellation.

6-1 Experiment Setup

The pilot experiment consisted of three parts and was performed by only one subject (the author of this report) in the SIMONA 6-DOF motion simulator at the Control & Simulation department at the TU Delft. The first part was the system identification step. This was the same experiment as performed by Mobertz in [9] and summarized in Section 5-1. However, the multisine disturbance signal was only applied in the heave axis (Z). Furthermore, only four runs were performed compared to the eight used by Mobertz. After the completion of the runs, a break of around 30 minutes allowed for the identification of the a subject average (SA) BDFT model as recommended in Chapter 5 using the same parametric model. The model represented the BDFT for the vertical screen input caused by the heave acceleration.

Step two and three evaluated the use of the identified model by doing an online BDFT cancellation using the method presented in Section 5-3-2. For the first evaluation the same experiment conditions as the system identification step was used. This was done with no feedback to the participant who could therefore not assess the effectiveness of the cancellation.

The second evaluation changed the multisine target signal to a step task. The step had four possible locations on the screen as presented in Figure 6-1. The left figure shows the distances between the step locations while the right figure is how the participant would see the task. Each step lasted two seconds. The goal of the participant was to track

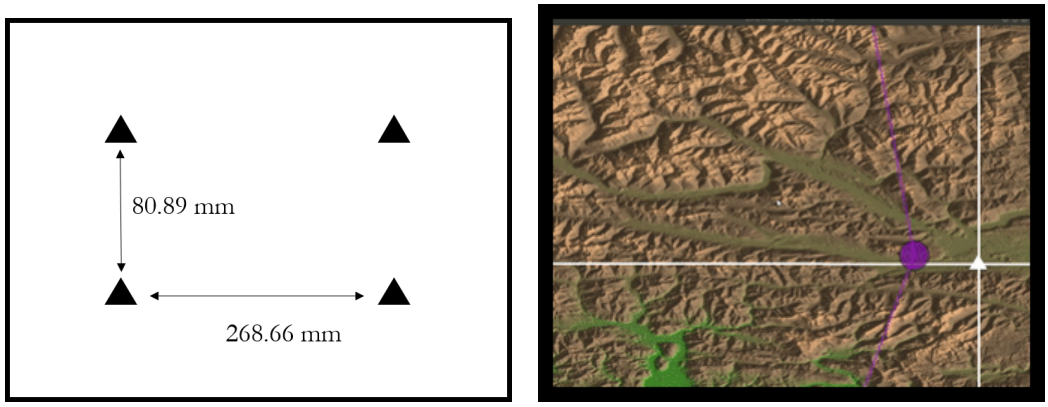

Figure 6-1: Left: the dimensions of the step tasks used in the pilot experiment. Right: display as seen by the participant. The purple circle follows the finger position while the white triangle represents the step signal.

the step signal always having contact with the screen. That meant a dragging action in either horizontal, vertical or diagonal direction. Once the location of the step was reached the finger would would keep that position until a new step change occurred. Again, the participant did not get any feedback about how successful the cancellation was. The horizontal and vertical target signal amplitudes of the multisine and step tasks were 80% of the presented value such that they would fit on the screen.

6-2 Results

This section will present the results of the three parts of the pilot experiment. First the system identification, then the BDFT cancellation with the multisine task and step task, respectively.

6-2-1 System Identification

The result of the system identification is shown in Figure 6-2 for each run as well as the subject average run. The variance accounted for (VAF) of the fitted BDFT model is presented in Table 6-1. VAF is a measure of the decrease in the variance between the measured and modelled signal. A VAF of 100% means the modelled BDFT signal perfectly replicates the measured BDFT. The high values mean the mass-spring-damper system is able to model the biodynamic feedthrough to a high degree of accuracy which is necessary for BDFT cancellation.

Table 6-1: Variance accounted for (VAF) for the identified models of each run.

	Run 1	Run 2	Run 3	Run 4
VAF [%]	86.60	94.57	94.97	95.01

6-2-2 Evaluation 1: Multi-sine Target Signal

Figure 6-3 shows the decomposition of the error variance (σ_e^2) before (top) and after (bottom) the BDFT cancellation. It is clear the part of the error variance originating from

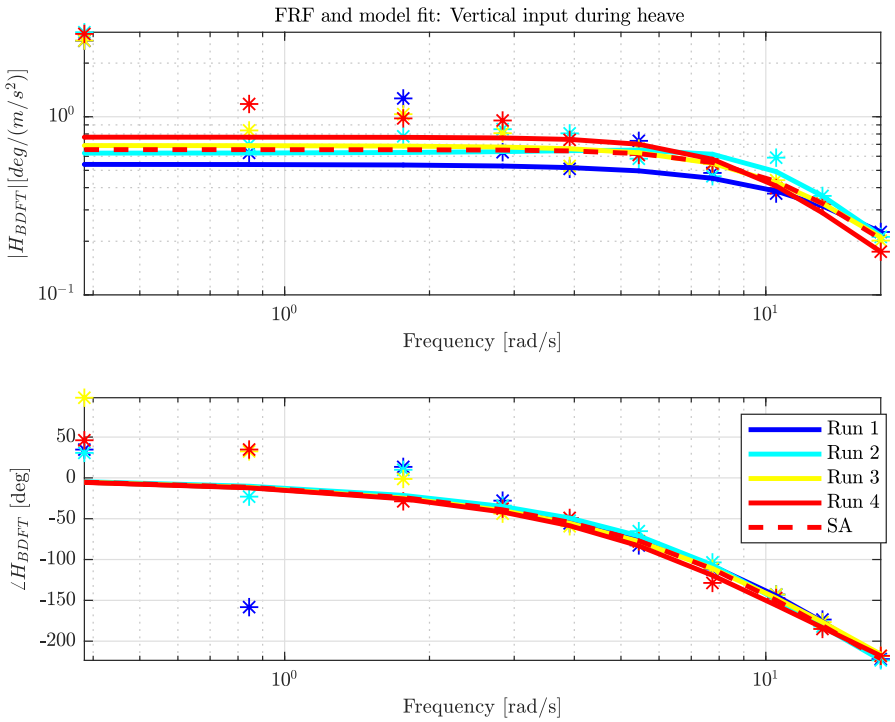

Figure 6-2: The frequency response function (FRF) and model fit of the four runs and their of the system identification step. The subject average (SA) is also shown.

Table 6-2: Identified BDFT model parameters. For reference the parameters for a model without a delay is shown on the bottom.

	G_{BDFT} [-]	m_{BDFT} [kg]	b_{BDFT} $[\frac{kg}{sec}]$	k_{BDFT} $[\frac{kg}{sec^2}]$	τ_{BDFT} [sec]
Run 1	15.46	0.17	3.73	28.61	0.11
Run 2	17.95	0.29	3.46	28.73	0.09
Run 3	19.13	0.27	4.25	27.76	0.09
Run 4	20.84	0.38	4.63	27.14	0.08
Subject Average	18.34	0.28	4.02	28.06	0.09
Run 1	15.75	0.66	3.89	27.44	-
Run 2	20.10	0.63	5.28	27.15	-
Run 3	17.84	0.64	4.82	24.76	-
Run 4	23.12	0.79	5.23	25.56	-
Subject Average	19.20	0.68	4.81	26.23	-

the disturbance signal has been strongly attenuated. Over 90% on average for the four runs. The PSD of the of the vertical screen input signal is depicted in Figure 6-4 for each of the four runs. The blue line showing before cancellation and orange after cancellation. The power is significantly lower at the disturbance frequencies after cancellation indicating that the BDFT models ability to be used for cancellation.

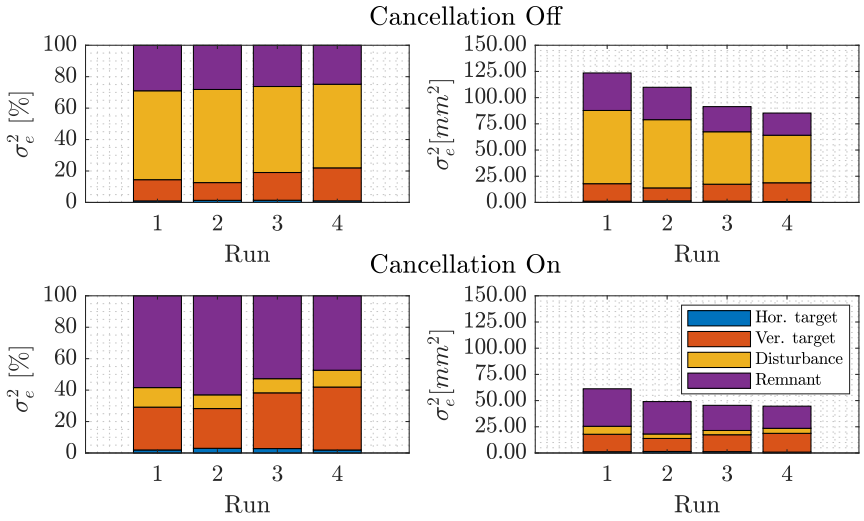

Figure 6-3: Error variance (σ_e^2) decomposition before and after cancellation for the multisine target signal in absolute and percentage terms.

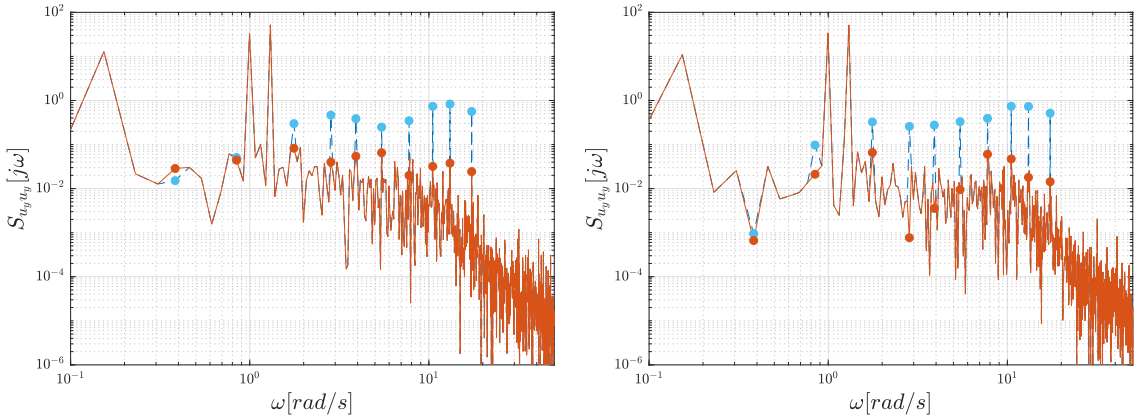

(a) PSD of run 1

(b) PSD of run 2

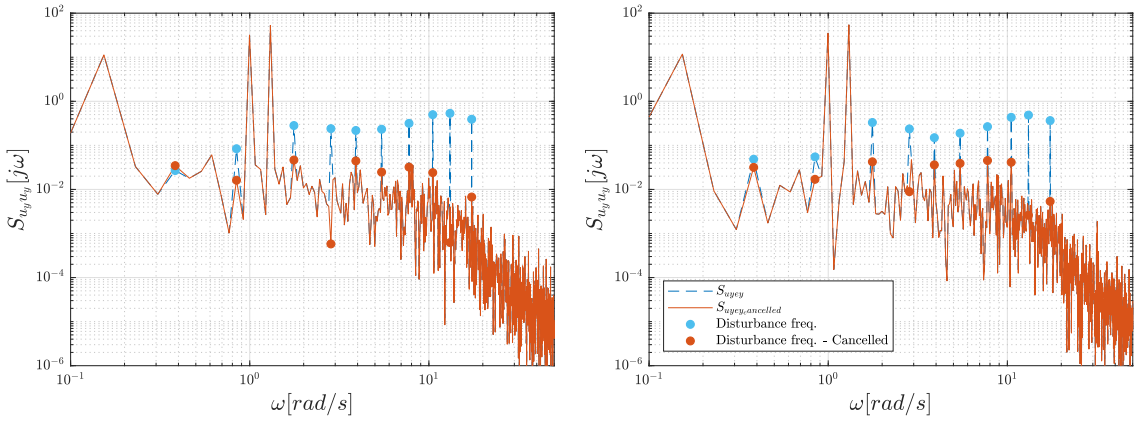

(c) PSD of run 3

(d) PSD of run 4

Figure 6-4: PSD of the vertical input signal (u_y) before and after cancellation with the multisine target signal.

6-2-3 Evaluation 2: Step Target Signal

The PSD of the vertical screen input signal for before and after cancellation is shown in Figure 6-7. A difficulty arises when interpreting these plots. The step target signal no longer has power at distinct frequencies. The target signal is therefore contributing power at our disturbance frequencies.

The screen input signal at the disturbance frequencies can no longer be fully attributed to the disturbance signal. With this limitation in mind there is still an attenuation of feedthrough power at the disturbance frequencies. Furthermore, the BDFT has most of its power at the higher frequencies, with the lower frequencies almost absent of any feedthrough. In a precision dragging task such as a flightplan modification only the endpoint of the task matters. The feedthrough experienced during the dragging task towards the endpoint does not influence the performance of the task, which is to place a waypoint at a specific location. It is therefore interesting to look at the effectiveness of the BDFT cancellation at the endpoint. It was empirically found that the last 0.6 seconds of the 2 seconds steps were performed at the endpoint location before a new step was begun. The blue areas in the example time trace in Figure 6-6 show the portion of the steps which were used for the analysis. The input data was then split into the four endpoint locations and compared before and after cancellation for the vertical input signal as seen in Figure 6-5.

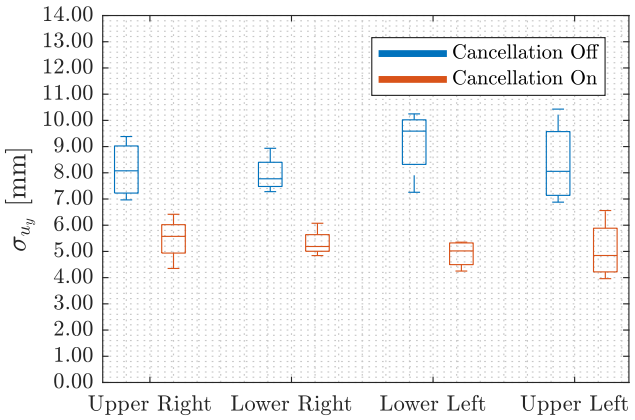

Figure 6-5: Standard deviation of vertical screen input for the four runs with BDFT cancellation on/off. Evaluated for the four endpoint locations.

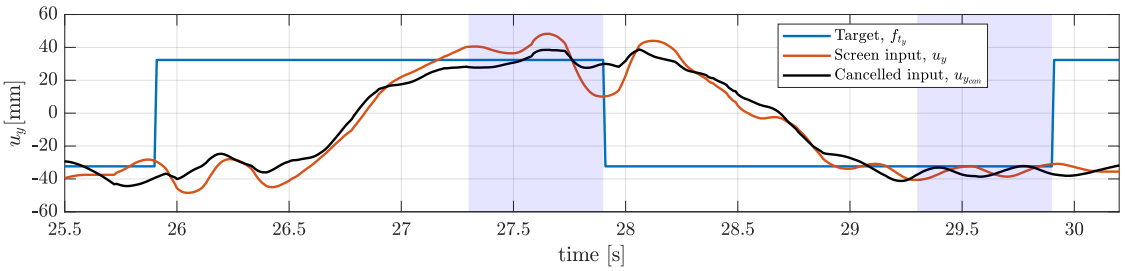

Figure 6-6: Example time trace of the vertical step target signal (f_{t_y}), screen input (u_y) and cancelled input ($u_{y_{can}}$). The shaded areas show the part of each step which was used for the endpoint analysis.

The boxplot shows the variation of the screen input across the four runs. For all endpoint locations the cancelled standard deviation of the input signal is significantly lower than the when cancellation is off. The mean relative change across all four screen locations is 38%. This means lifting the hand from the screen would on average result in more success with the cancellation on.

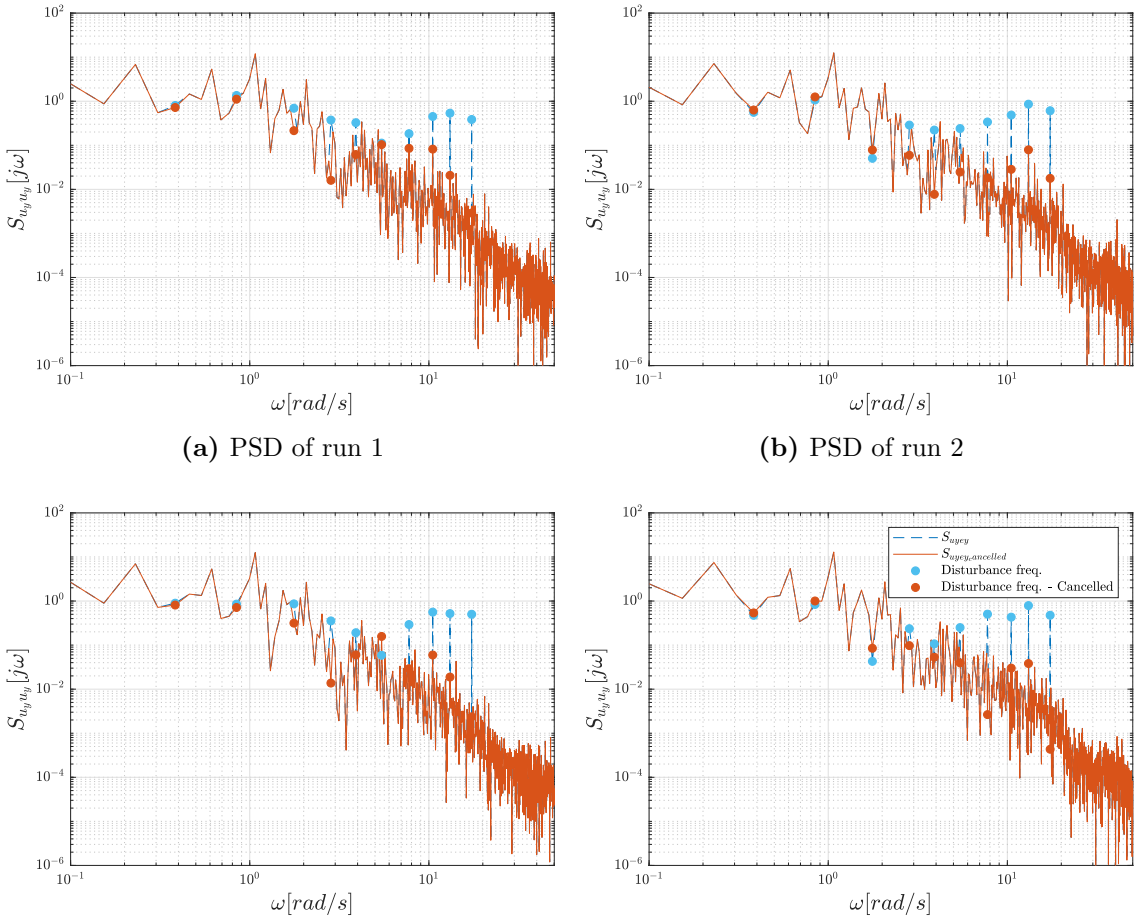

(a) PSD of run 1

(b) PSD of run 2

(c) PSD of run 3

(d) PSD of run 4

Figure 6-7: PSD of the vertical input signal (u_y) before and after cancellation with the step target signal.

6-3 Conclusions and Recommendations

This chapter presented a pilot experiment with the goal of performing online BDFT cancellation by using both a multisine and step target signal with a subject average BDFT model. The cancellation was successful when the identified model was used on the same multisine task it was identified from, with an average reduction of 90% in the error variance due to the disturbance signal ($\sigma^2_{e_{f_d}}$). The PSDs for each run also show decreased power at the disturbance frequencies. The step tasks also showed a decrease in power at the disturbance frequencies. However, BDFT was only observed in the highest frequencies. Moreover, the step target signal has power at the disturbance frequencies, the PSDs of the step task should therefore only be used in a qualitative way. Below are some conclusions and recommendations based on the pilot experiment.

Conclusions:

- Online BDFT signal cancellation is feasible.
- A 38% relative decrease of the standard deviation of the screen input for the step task was observed. An identified model of a multisine dragging task can therefore successfully be used on a step task.
- BDFT is only present at higher frequencies for a step task.

Recommendations:

- The operator is not aware the signal cancellation is happening. It is therefore recommended to test the use of operator feedback by an on screen marker showing the registered position after cancellation.
- Friction between the finger and screen has shown to vary with screen velocity, especially at low dragging speeds [2]. It is recommended to keep using a glove to minimize these effects. Future research should look into how friction influences model-based BDFT cancellation.
- With each step signal lasting two second only limited data could be collected for the endpoint cancellation performance. It is therefore recommended to increase each the step duration.
- The four touchscreen endpoints for the step signal were placed in a rectangular pattern. Rather, the steps should be placed in a square pattern to make horizontal and vertical movements equal distance movements.

Chapter 7

Research Proposal

Based on the literature study and an offline and online BDFT cancellation analysis, a full experiment is proposed to be carried out on the SIMONA Research Simulator (SRS) 6-DOF motion simulator at the TU Delft.

7-1 Research Question

It was shown in Chapter 5 that offline BDFT cancellation is possible for a multisine dragging task and that a subject average model had the best cancellation performance. In Chapter 6 an online BDFT cancellation pilot experiment showed the possibility to extend the use of the model on a step task which is a more realistic precision task. These results lead to the following research question.

> To what extent can biodynamic feedthrough be mitigated using a model-based approach whilst performing a step dragging task on a touchscreen display located at a typical flight deck PFD position?

7-2 Experiment Design

7-2-1 Independent Variables

A multisine disturbance signal will be used, resembling turbulence. With the motion disturbance being varied between surge, sway, heave as well as a no motion condition. Mobertz showed that the motion disturbance axis has a large influence on the amount of feedthrough [9] which makes it interesting to compare the different axes with each other, even though realistic turbulence mainly occurs in the heave and sway axis [75, 76]. The investigation of any cross-coupling effects due to multi-axis motion is outside the scope of this investigation. The motion disturbance will therefore only be applied to a single axis.

7-2-2 Control Variables

In the literature review in Chapter 3 it was shown that touchscreens have nonlinear friction properties between finger and screen, especially at low dragging speeds. Researching the effects of friction between the finger and touch surface is beyond the scope of this experiment. To control for this effect, participants will use gloves which will help to keep consistent friction properties. The gloves will also alleviate the effects of finger fatigue.

Because the operator's movement on the touchscreen does not influence the state of the vehicle, the disturbance signal will therefore be equal for all conditions and for all

participants. The multisine target signal and the step target signal will also stay constant. However, the target signal will still be mirrored either along the horizontal or vertical axis (four combinations) to make sure the participants can not anticipate the signals movements. The frequencies, amplitudes and phases of the disturbance and target signal (for the system identification phase) are presented in are the same as presented in Chapter 5. The step target signal will have four endpoint locations with a distance of 180 mm between them. The step will randomly jump to one of the three other possible locations after 3 seconds.

In Chapter 4 it was recommended to investigate the use of signal cancellation with feedback. In Figure 7-2 the purple target will instead of showing the current finger location rather show the screen input after BDFT cancellation. This will give feedback to the operator about the effect of the cancellation, but it is uncertain if this will change the strategy of the operator or have an effect on the BDFT. It is therefore recommended to perform a small test to determine if this feedback should be included in the experiment.

7-2-3 Dependent variables

To asses how effectiveness of the BDFT mitigation the finger input on the touch surface will be collected. The output of the touchscreen is the finger position in the horizontal (u_x) and vertical direction (u_y). In addition, the model-based cancellation will be producing two new variables: $u_{x_{can}}$ and $u_{y_{can}}$ which will be logged while the experiment is taking place. Comparisons between no cancellation and model-based cancellation can be made based on these variables. Specifically the following dependent variables will be useful:

BDFT model parameters: For effective BDFT cancellation it is required to have a successful system identification. The parameters define the dynamics BDFT model.

PSD of input signal: The power spectral densities of both the original and cancelled screen input signal can be used to estimate the feedthrough caused by the motion disturbance. However, the step target signal will have power at frequencies which overlap with the motion disturbance, frequency decomposition methods can therefore not be used.

Standard deviation ($\sigma_{u_{x,y}}$, $\sigma_{u_{x,y},can}$) : Because of the limitations of spectral methods with a step task the standard deviation of the input signal will be a measure of the feedthrough. A lower standard deviation for the cancelled signal will mean the BDFT cancellation is attenuating the input signal.

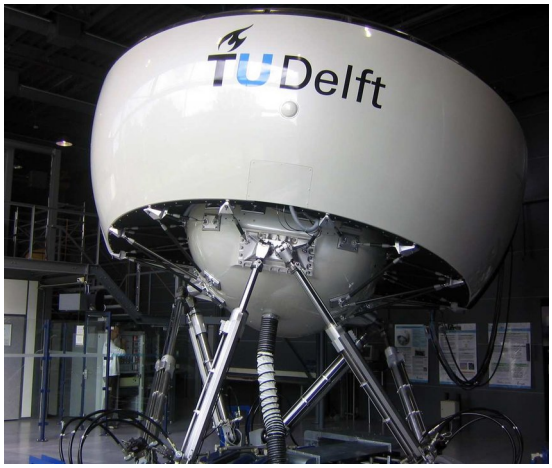

Figure 7-1: The SIMONA Research Simulator (SRS)

7-2-4 Participants and Procedure

The experiment will have a within-subject design, meaning all participants will perform each experiment condition. A experiment briefing will be given before the experiment begins. The briefing will explain

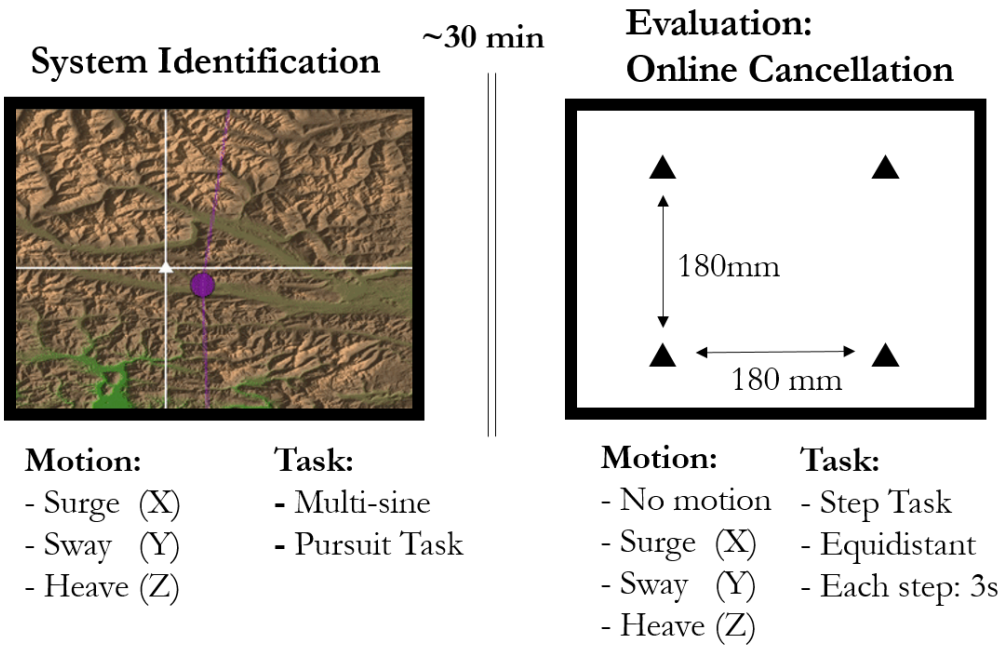

Figure 7-2: The experiment procedure. A first experiment is done to identify the BDFT dynamics. A 30 minutes break is taken for the identification to take place before model is used in the evaluation experiment

the purpose, the task, experiment procedure and the participants rights. The participant will then take a seat in the SRS Figure 7-1, a 6-DOF motion simulator. Through a headset there will be communication between the SRS and the control room. The experiment will start with the system identification task shown in Figure 7-2 with each condition consisting of 8 runs. After the three motion conditions, surge, sway and heave (24 runs total) the experiment will take a break of around 30 minutes while the system identification is taking place on a separate computer Using MATLAB. The second part of the experiment consist of evaluating the identified BDFT model by cancelling the feedthrough. Here an additional "no motion" condition is added. Each condition will again have 8 runs totalling 32 runs for part two of the experiment. Overall, 56 runs will be performed per subject. For both phases of the experiment the tasks will last 90 seconds.

The experiment has one independent variable with 4 conditions: no motion, surge, sway and heave motion conditions. A total of 16 participants will therefore be recruited which is a multiple of the amount of experiment conditions.

Chapter 8

Conclusions Preliminary Report

The involuntary body motion caused by turbulence, called biodynamic feedthrough, has shown to adversely effects the use of touchscreens and has therefore been a major concern for implementation in commercial airliners. Literature showed that continuous tasks involving longer interactions such as dragging and pinching are likely to be used in future aircraft touchscreen tasks. At the same time these tasks have been discouraged from flight deck use because of their susceptibility to turbulence. The use of model-based mitigation was therefore applied to these tasks in an offline and online analysis. To take the first step to investigate the feasibility of model-based mitigation a mass-spring-damper BDFT model was used, similar to Mobertz [27]. These models are simple with only a few parameters and are easy to use for system identification.

In Chapter 5, an offline BDFT cancellation showed the successful reduction of BDFT using the proposed BDFT model for a multisine dragging task. The results also showed that between-subject variability was significant for for certain combinations of simulator motion direction and screen cancellation direction. To test the applicability of the same model on a more realistic touchscreen task Chapter 6 looked at the online cancellation of a point-to-point (step) task. The finding showed that the model could successfully be used with a 38% reduction in standard deviation of the screen input at the endpoint of the dragging task.

The BDFT model has been used for BDFT mitigation on a multisine dragging task as well as on a step task. However, since the pilot experiment was only performed with one subject, a final experiment was proposed to further test the transferability of BDFT cancellation across different tasks. The experiment will consist of two parts. One where the participants will do a multisine dragging task as performed by Mobertz [27]. A subject average BDFT model will be identified before the second part begins. Here the subject will do a step task with online BDFT cancellation. There will be motion in all transitional axes as well as a no motion condition functioning as a baseline. Literature showed that it is desirable for the operator to be aware that the cancellation is taking place. A simulator test will be conducted before the experiment to determine if BDFT cancellation with operator feedback will alter the effectiveness of BDFT cancellation.

Bibliography

[1] N. Heath, "Inside the Touchscreen Cockpit of the Future." https://www.techrepublic.com/pictures/inside-the-touchscreen-cockpit-of-the-future/3/, 2012.

[2] T. Robinson, G. Grabski, J. Green, M. Jacobson, C. Byrne, and D. Harper, "P-171: Physical Touch Aspects of the Touch Interface for Flight Deck Applications," *SID Symposium Digest of Technical Papers*, vol. 45, pp. 1618–1621, 6 2014.

[3] "ISO 9241-400:2007, Ergonomics of human — system interaction — Part 400: Principles and requirements for physical input devices," 2007.

[4] P. Masarati, G. Quaranta, A. Bernardini, and G. Guglieri, "Voluntary Pilot Action Through Biodynamics for Helicopter Flight Dynamics Simulation," *Journal of Guidance, Control, and Dynamics*, vol. 38, pp. 431–441, 1 2015.

[5] H. Benake, "HB Blog 112: Resistive VS Capacitive Touchscreen.." http://harshalbenake.blogspot.com/2016/06/hb-blog-112-resistive-vs-capacitive.html, 2016.

[6] S. Xu, W. Tan, A. V. Efremov, L. Sun, and X. Qu, "Review of control models for human pilot behavior," *Annual Reviews in Control*, vol. 44, pp. 274–291, 2017.

[7] R. W. Allen, H. R. Jex, and R. E. Magdaleno, "Manual control performance and dynamic response during sinusoidal vibration," tech. rep., System Technology Inc, Hawthorne CA, 1973.

[8] J. Venrooij, M. Mulder, M. M. v. Paassen, D. A. Abbink, H. H. Bülthoff, and M. Mulder, "Cancelling biodynamic feedthrough requires a subject and task dependent approach," in *2011 IEEE International Conference on Systems, Man, and Cybernetics*, pp. 1670–1675, 2011.

[9] X. Mobertz, D. M. Pool, M. van Paassen, and M. Mulder, "A Cybernetic Analysis of Biodynamic Effects in Touchscreen Operation in Turbulence," in *2018 AIAA Modeling and Simulation Technologies Conference*, AIAA SciTech Forum, American Institute of Aeronautics and Astronautics, 1 2018.

[10] R. V. D. Berg, "Investigating the Effects of Turbulence and Spatial Gesture Thresholds on Multi-Touch Interaction," Master's thesis, Delft Univeristy of Technology, 2014.

[11] M. J. Griffin, *Handbook of Human Vibration*. Academic Press, 1990.

[12] C. Spitzer, U. Ferrell, and T. Ferrell, eds., *Digital Avionics Handbook*. Boca Raton: CRC press, 3rd ed., 2015.

[13] D. Harris, *Human Performance on the Flight Deck*. London: CRC Press, 1st ed., 2011.

[14] C. B. Watkins, C. Nilson, S. Taylor, K. B. Medin, I. Kuljanin, and H. B. Nguyen, "Development of touchscreen displays for the gulfstream G500 and G600 Symmetry^{TM} flight deck," in *AIAA/IEEE Digital Avionics Systems Conference - Proceedings*, vol. 2018-Septe, Institute of Electrical and Electronics Engineers Inc., 12 2018.

[15] M. Kingsley-Jones, "Airbus aims for airliner cockpit-touchscreen first with A350." https://www.flightglobal.com/news/articles/airbus-aims-for-airliner-cockpit-touchscreen-first-449481/, 2018.

[16] S. Trimble, "Boeing selects Rockwell Collins for 777X touchscreens." https://www.flightglobal.com/news/articles/boeing-selects-rockwell-collins-for-777x-touchscreen-429565/, 9 2016.

[17] H. Avsar, *Exploring potential benefits and challenges of touch screens on the flight deck*. PhD thesis, University of Nottingham, 2017.

[18] G. Stuyven, H. Damveld, and C. Borst, "Concept for an Avionics Multi Touch Flight Deck," *SAE International Journal of Aerospace*, vol. 5, no. 2012-01-2120, pp. 164–171, 2012.

[19] P. R. Thomas, "Performance, characteristics, and error rates of cursor control devices for aircraft cockpit interaction," *International Journal of Human-Computer Studies*, vol. 109, pp. 41–53, 1 2018.

[20] N. A. Stanton, C. Harvey, K. L. Plant, and L. Bolton, "To twist, roll, stroke or poke? A study of input devices for menu navigation in the cockpit," *Ergonomics*, vol. 56, pp. 590–611, 4 2013.

[21] S. Kaminani, "Human computer interaction issues with touch screen interfaces in the flight deck," in *2011 IEEE/AIAA 30th Digital Avionics Systems Conference*, pp. 4–1, 2011.

[22] A. Cockburn, D. Masson, C. Gutwin, P. Palanque, A. Goguey, M. Yung, C. Gris, and C. Trask, "Design and evaluation of braced touch for touchscreen input stabilisation," *International Journal of Human-Computer Studies*, vol. 122, pp. 21–37, 2 2019.

[23] S. Dodd, J. Lancaster, A. Miranda, S. Grothe, B. DeMers, and B. Rogers, "Touch Screens on the Flight Deck: The Impact of Touch Target Size, Spacing, Touch Technology and Turbulence on Pilot Performance," *Proceedings of the Human Factors and Ergonomics Society Annual Meeting*, vol. 58, pp. 6–10, 9 2014.

[24] K. G. Bauersfeld, *Effects of turbulence and activation method on touchscreen performance in aviation environments*. PhD thesis, San Jose State University, 1992.

[25] G. Grabski and T. Robinson, "P.132: Enhancing the Visual Performance of Touch Screen Displays," *SID Symposium Digest of Technical Papers*, vol. 44, pp. 1509–1512, 6 2013.

[26] J. Venrooij, *Measuring, modeling and mitigating biodynamic feedthrough*. PhD thesis, Delft University of Technology, 2015.

[27] X. Mobertz, "A Cybernetic Analysis of Biodynamic Effects in Touchscreen Operation in Turbulence," Master's thesis, Delft University of Technology, 2018.

[28] C. Adams, "Human Factors in Avionics Design." https://www.aviationtoday.com/2013/11/01/human-factors-in-avionics-design/, 2013.

[29] N. Clark, "Touch Screens Are Tested for Piloting Passenger Jets." https://www.nytimes.com/2013/07/06/technology/passenger-jets-testing-touch-screen-technology.html, 7 2013.

[30] W. Rouwhorst, R. Verhoeven, M. Suijkerbuijk, T. Bos, A. Maij, M. Vermaat, and R. Arents, "Use of touch screen display applications for aircraft flight control," in *2017 IEEE/AIAA 36th Digital Avionics Systems Conference (DASC)*, pp. 1–10, IEEE, 9 2017.

[31] A. Degani, E. A. Palmer, and K. G. Bauersfeld, ""Soft" Controls for Hard Displays: Still a Challenge," *Proceedings of the Human Factors and Ergonomics Society Annual Meeting*, vol. 36, pp. 52–56, 7 1992.

[32] S. Pauchet, C. Letondal, J.-L. Vinot, M. Causse, M. Cousy, V. Becquet, and G. Crouzet, "GazeForm: Dynamic Gaze-adaptive Touch Surface for Eyes-free Interaction in Airliner Cockpits," in *Proceedings of the 2018 on Designing Interactive Systems Conference 2018*, pp. 1193–1205, 2018.

[33] M. Mertens and H. J. Damveld, "An avionics touch screen-based control display concept," in *Head-and Helmet-Mounted Displays XVII; and Display Technologies and Applications for Defense, Security, and Avionics VI*, vol. 8383, p. 83830L, International Society for Optics and Photonics, 2012.

[34] A. Ng, J. Lepinski, D. Wigdor, S. Sanders, and P. Dietz, "Designing for Low-latency Direct-touch Input," in *Proceedings of the 25th Annual ACM Symposium on User Interface Software and Technology*, UIST '12, (New York, NY, USA), pp. 453–464, ACM, 2012.

[35] A. Dhir, *The Digital Consumer Technology Handbook*. Elsevier, 1st ed., 2004.

[36] Google, "Gestures." https://material.io/design/interaction/gestures.html#types-of-gestures, 2019.

[37] Apple, "Human Interface Guidelines - Gestures." https://developer.apple.com/design/human-interface-guidelines/ios/user-interaction/gestures/, 2019.

[38] Microsoft, "Touch interactions." https://docs.microsoft.com/en-us/windows/uwp/design/input/touch-interactions, 2019.

[39] L. Wroblewski, "Touch Gesture Reference Guide." https://static.lukew.com/TouchGestureGuide.pdf, 2010.

[40] E. Petit and C. Maldivi, "Unifying gestures and direct manipulation in touchscreen interfaces," 2013.

[41] J. Lancaster, B. Mers, B. Rogers, A. Smart, and S. Whitlow, "57.3: The Effect of Touch Screen Hand Stability Method on Performance & Subjective Preference in Turbulence," *SID Symposium Digest of Technical Papers*, vol. 42, no. 1, pp. 841–844, 2011.

[42] N. Goode, M. G. Lenné, and P. Salmon, "The impact of on-road motion on BMS touch screen device operation," *Ergonomics*, vol. 55, pp. 986–996, 9 2012.

[43] L. V. Coutts, K. L. Plant, M. Smith, L. Bolton, K. J. Parnell, J. Arnold, and N. A. Stanton, "Future technology on the flight deck: assessing the use of touchscreens in vibration environments," *Ergonomics*, pp. 1–19, 11 2019.

[44] A. Cockburn, C. Gutwin, P. Palanque, Y. Deleris, C. Trask, A. Coveney, M. Yung, and K. MacLean, "Turbulent Touch: Touchscreen Input for Cockpit Flight Displays," in *Proceedings of the 2017 CHI Conference on Human Factors in Computing Systems*, CHI '17, (New York, NY, USA), pp. 6742–6753, ACM, 2017.

[45] H.-J. Kim and B. J Martin, "Biodynamic Characteristics of Upper Limb Reaching Movements of the Seated Human Under Whole-Body Vibration," *Journal of applied biomechanics*, vol. 29, pp. 12–22, 2 2013.

[46] H. Avsar, J. E. Fischer, and T. Rodden, "Future Flight Decks: Impact of +Gz on Touchscreen Usability," in *Proceedings of the International Conference on Human-Computer Interaction in Aerospace*, HCI-Aero '16, (New York, NY, USA), pp. 3:1–3:8, ACM, 2016.

[47] R. W. Soukoreff and I. S. MacKenzie, "Towards a standard for pointing device evaluation, perspectives on 27 years of Fitts' law research in HCI," *International Journal of Human-Computer Studies*, vol. 61, pp. 751–789, 12 2004.

[48] A. Alapetite, E. Møllenbach, A. Stockmarr, and K. Minakata, "A Rollercoaster to Model Touch Interactions during Turbulence," *Advances in Human-Computer Interaction*, vol. 2018, pp. 1–16, 2018.

[49] A. Alapetite, R. Fogh, D. Zammit-Mangion, C. Zammit, I. Agius, M. Fabbri, M. Pregnolato, and L. Becouarn, "Direct tactile manipulation of the flight plan in a modern aircraft cockpit," in *Proceedings of HCI Aero*, pp. 2–5, APA, 2012.

[50] R. McLeod and M. Griffin, "Review of the effects of translational whole-body vibration on continuous manual control performance," *Journal of Sound and Vibration*, vol. 133, pp. 55–115, 8 1989.

[51] J. Venrooij, M. M. Van Paassen, M. Mulder, D. A. Abbink, M. Mulder, F. C. van der Helm, and H. H. Bülthoff, "A framework for biodynamic feedthrough analysis - Part I: Theoretical foundations," *IEEE Transactions on Cybernetics*, vol. 44, no. 9, pp. 1686–1698, 2014.

[52] , *Touch Interactive Display Systems: Human Factors Considerations, System Design and Performance Guidelines*, feb 2019.

[53] J. Venrooij, M. Mulder, M. M. van Paassen, M. Mulder, and D. A. Abbink, "A review of biodynamic feedthrough mitigation techniques," in *IFAC Proceedings Volumes*, vol. 43, pp. 316–321, Elsevier, 1 2010.

[54] H. Damveld, D. Abbink, M. Mulder, M. Mulder, M. R. Van Paassen, F. C. van der Helm, and R. Hosman, "Identification of the Feedback Components of the Neuromuscular System in a Pitch Control Task," in *AIAA Modeling and Simulation Technologies Conference*, (Reston, Virigina), American Institute of Aeronautics and Astronautics, 8 2013.

[55] Apple, "Force Touch." https://developer.apple.com/macos/force-touch/, 2019.

[56] M. Velger, A. Grunwald, and S. Merhav, "Adaptive filtering of biodynamic stick feedthrough in manipulation tasks on board moving platforms," *Journal of Guidance, Control, and Dynamics*, vol. 11, no. 2, pp. 153–158, 1988.

[57] B. I. Ahmad, P. M. Langdon, and S. J. Godsill, "Stabilising Touch Interactions in Cockpits, Aerospace, and Vibrating Environments," in *Universal Access in Human-Computer Interaction. Methods, Technologies, and Users* (M. Antona and C. Stephanidis, eds.), (Cham), pp. 133–145, Springer International Publishing, 2018.

[58] S. Pauchet, J.-L. Vinot, C. Letondal, A. Lemort, C. Lavenir, T. Lecomte, S. Rey, V. Becquet, and G. Crouzet, "Multi-plié: a Linear Foldable and Flattenable Interactive Display to Support Efficiency, Safety and Collaboration," 2019.

[59] M. Lone and A. Cooke, "Review of pilot models used in aircraft flight dynamics," *Aerospace Science and Technology*, vol. 34, no. 1, pp. 55–74, 2014.

[60] N. J. Mansfield, *Human Response To Vibration*. Boca Raton: CRC Press, 2004.

[61] M. J. Griffin, "The validation of biodynamic models," *Clinical Biomechanics*, 2001.

[62] S. Sövényi, *Model-based cancellation of biodynamic feedthrough with a motorized manual control interface*. PhD thesis, University of Michigan, 2005.

[63] S. Sövényi and R. B. Gillespie, "Cancellation of Biodynamic Feedthrough in Vehicle Control Tasks," *IEEE Transactions on Control Systems Technology*, vol. 15, no. 6, pp. 1018–1029, 2007.

[64] J. R. Mayo, "The involuntary participation of a human pilot in a helicopter," in *15th Eur. Rotorcraft Forum*, (Amsterdam, The Netherlands), pp. 81–001, 1989.

[65] M. D. Pavel, M. Jump, B. Dang-Vu, P. Masarati, M. Gennaretti, A. Ionita, L. Zaichik, H. Smaili, G. Quaranta, D. Yilmaz, M. Jones, J. Serafini, and J. Malecki, "Adverse rotorcraft pilot couplings—past, present and future challenges," *Progress in Aerospace Sciences*, vol. 62, pp. 1 – 51, 2013.

[66] P. Masarati and G. Quaranta, "Bioaeroservoelastic Analysis of Involuntary Rotorcraft-Pilot Interaction," *Journal of Computational and Nonlinear Dynamics*, vol. 9, p. 031009, 2 2014.

[67] P. Masarati, G. Quaranta, and A. Zanoni, "Dependence of helicopter pilots' biodynamic feedthrough on upper limbs' muscular activation patterns," *Proceedings of the Institution of Mechanical Engineers, Part K: Journal of Multi-body Dynamics*, vol. 227, pp. 344–362, 12 2013.

[68] M. Griffin and E. Whitham, "Individual variability and its effect on subjective and biodynamic response to whole-body vibration," *Journal of Sound and Vibration*, vol. 58, no. 2, pp. 239 – 250, 1978.

[69] D. Abbink, "Neuromuscular Analysis as a Guideline in designing Shared Control," in *Advances in Haptics* (M. Hosseini, ed.), p. Ch. 27, Rijeka: IntechOpen, 2010.

[70] E. Concettoni and M. Griffin, "The apparent mass and mechanical impedance of the hand and the transmission of vibration to the fingers, hand, and arm," *Journal of Sound and Vibration*, vol. 325, no. 3, pp. 664–678, 2009.

[71] "Advisory Circular 20-175: Controls for Flight Deck Systems," tech. rep., Federal Aviation Administration, 2011.

[72] O. Stroosma, M. M. R. van Paassen, and M. Mulder, "Using the SIMONA Research Simulator for Human-machine Interaction Research," in *AIAA Modeling and Simulation Technologies Conference and Exhibit*.

[73] M. R. Sirouspour and S. E. Salcudean, "Suppressing operator-induced oscillations in manual control systems with movable bases," *IEEE Transactions on Control Systems Technology*, vol. 11, no. 4, pp. 448–459, 2003.

[74] R. B. Gillespie, C. Hasser, and P. Tang, "Cancellation of feedthrough dynamics using a force-reflecting joystick," in *Proc. ASME Dynamic Systems and Controls Division*, pp. 319–326, 1999.

[75] J. A. Mulder and J. C. Van der Vaart, "Aircraft responses to atmospheric turbulence," tech. rep., Delft University of Technology, Faculty of Aerospace Engineering, Delft, The Netherlands, 1998.

[76] S. Hourlier, S. Guérard, and X. Servantie, "Avionics Touch Screen in Turbulence: Simulator Design and Selected Human–Machine Interface Metrics," in *Improving Aviation Performance through Applying Engineering Psychology: Advances in Aviation Psychology*, vol. 3, pp. 53–75, CRC Press, 2019.

Part III

Appendicies

Appendix A

Individual BDFT Cancellation Results

This appendix shows the results per subject of the BDFT cancellation performed in Chapter 5 of the preliminary report. Each table is order based on the order the run was performed in.

A-1 Disturbance: Sway (Y), Screen input: Horizontal

Table A-1: Subject 1: Percentage change of f_d in σ_e^2 when sorted based on run order. Motion disturbance: Sway. Screen direction: Horizontal.

	Run 1	Run 2	Run 3	Run 4	Run 5	Run 6	Run 7	Run 8
Model 1	-96.71	-92.51	-92.92	-95.37	-95.45	-94.22	-82.97	-94.89
Model 2	-94.03	-92.40	-89.10	-88.67	-92.79	-93.05	-92.69	-83.75
Model 3	-97.28	-86.70	-87.40	-80.95	-81.65	-88.04	-87.42	-93.38
Model 4	-91.74	-89.16	-88.70	-89.17	-83.19	-83.45	-88.64	-88.50
Model 5	-93.11	-90.66	-83.60	-90.07	-89.92	-90.88	-90.70	-93.03
Model 6	-92.56	-92.58	-90.76	-86.10	-90.05	-88.18	-89.74	-89.29
Model 7	-92.47	-95.48	-95.50	-92.81	-88.49	-91.94	-89.72	-93.05
Model 8	-92.78	-92.08	-92.33	-92.71	-85.92	-75.89	-87.54	-86.85
SA model	-95.95	-93.14	-88.94	-89.46	-92.96	-92.32	-95.01	-91.59
OSFA model	-80.04	-76.35	-60.92	-67.13	-75.19	-73.57	-75.68	-78.59

Table A-2: Subject 2: Percentage change of f_d in σ_e^2 when sorted based on run order. Motion disturbance: Sway. Screen direction: Horizontal.

	Run 1	Run 2	Run 3	Run 4	Run 5	Run 6	Run 7	Run 8
Model 1	-92.03	-77.24	-19.73	-84.91	-88.59	-86.32	-87.86	-88.72
Model 2	-87.87	-85.01	-76.97	-14.92	-83.31	-86.49	-87.80	-83.97
Model 3	-93.13	-86.17	-90.57	-91.44	-12.88	-91.33	-86.49	-87.45
Model 4	-89.96	-89.15	-88.89	-87.94	-85.30	-11.44	-88.36	-88.33
Model 5	-93.07	-91.12	-92.54	-91.51	-94.03	-85.35	-15.60	-91.55
Model 6	-94.63	-89.12	-90.95	-94.53	-88.81	-90.75	-93.59	-11.71
Model 7	-14.94	-90.69	-84.52	-87.27	-91.21	-84.88	-86.75	-91.03
Model 8	-96.30	-9.56	-94.24	-85.56	-88.33	-94.11	-85.02	-88.09
SA model	-87.31	-87.71	-87.70	-89.86	-92.25	-91.14	-87.05	-88.27
OSFA model	-89.78	-87.69	-88.34	-89.68	-91.55	-89.17	-86.08	-86.15

Table A-3: Subject 3: Percentage change of f_d in σ_e^2 when sorted based on run order. Motion disturbance: Sway. Screen direction: Horizontal.

	Run 1	Run 2	Run 3	Run 4	Run 5	Run 6	Run 7	Run 8
Model 1	-94.30	-71.60	-84.69	-86.14	-78.69	-88.19	-89.41	-91.89
Model 2	-85.95	-86.37	-72.39	-79.21	-77.46	-76.97	-86.67	-79.69
Model 3	-91.08	-91.93	-90.93	-74.00	-89.00	-89.07	-81.89	-85.78
Model 4	-88.98	-78.91	-86.43	-85.69	-76.87	-80.71	-77.94	-80.41
Model 5	-87.94	-84.21	-77.67	-83.53	-75.94	-84.46	-86.82	-81.60
Model 6	-86.13	-82.05	-83.19	-85.59	-86.29	-85.35	-76.92	-84.98
Model 7	-86.35	-82.56	-84.52	-81.46	-80.39	-83.46	-77.02	-79.66
Model 8	-84.43	-77.70	-68.54	-83.87	-79.71	-63.58	-73.44	-63.59
SA model	-88.52	-83.51	-90.46	-85.04	-87.24	-86.75	-86.16	-78.55
OSFA model	-88.30	-75.50	-82.39	-72.69	-57.59	-77.90	-61.88	-38.71

Table A-4: Subject 4: Percentage change of f_d in σ_e^2 when sorted based on run order. Motion disturbance: Sway. Screen direction: Horizontal.

	Run 1	Run 2	Run 3	Run 4	Run 5	Run 6	Run 7	Run 8
Model 1	-86.88	-79.65	-59.79	-71.76	-51.23	-86.41	-75.18	-85.47
Model 2	-88.16	-86.88	-77.05	-63.18	-66.31	-39.11	-86.15	-78.70
Model 3	-93.13	-87.07	-84.33	-93.91	-92.25	-93.95	-87.95	-90.26
Model 4	-88.62	-83.64	-86.89	-85.78	-86.65	-75.76	-81.64	-67.17
Model 5	-94.18	-80.80	-82.45	-74.99	-74.04	-87.51	-84.46	-91.79
Model 6	-93.60	-90.99	-85.24	-88.38	-80.66	-77.93	-90.96	-90.42
Model 7	-94.79	-92.55	-86.61	-86.62	-92.20	-83.59	-79.00	-91.70
Model 8	-94.13	-87.47	-91.05	-82.35	-90.82	-88.98	-87.40	-84.68
SA model	-82.03	-81.13	-94.59	-88.04	-86.64	-90.55	-91.80	-92.95
OSFA model	-84.96	-80.81	-89.98	-86.61	-84.35	-86.70	-85.57	-88.60

Table A-5: Subject 5: Percentage change of f_d in σ_e^2 when sorted based on run order. Motion disturbance: Sway. Screen direction: Horizontal.

	Run 1	Run 2	Run 3	Run 4	Run 5	Run 6	Run 7	Run 8
Model 1	-89.97	-80.57	-77.43	-62.39	-77.05	-68.90	-76.35	-78.38
Model 2	-74.95	-84.07	-71.35	-71.67	-86.69	-88.72	-80.88	-81.33
Model 3	-86.44	-67.79	-80.94	-80.78	-80.84	-75.65	-77.82	-84.83
Model 4	-83.06	-80.60	-49.86	-68.53	-72.67	-74.21	-72.78	-70.24
Model 5	-86.25	-78.32	-76.15	-68.32	-79.61	-69.04	-68.68	-84.25
Model 6	-88.17	-85.88	-81.05	-76.66	-63.66	-74.03	-65.89	-67.58
Model 7	-77.25	-67.19	-69.00	-81.61	-79.36	-51.50	-72.11	-78.26
Model 8	-83.65	-79.02	-52.50	-58.29	-75.10	-76.92	-49.84	-71.69
SA model	-82.39	-84.34	-86.52	-78.22	-79.90	-78.91	-78.70	-76.40
OSFA model	-88.26	-82.88	-84.59	-73.11	-77.87	-73.84	-75.90	-76.61

Table A-6: Subject 6: Percentage change of f_d in σ_e^2 when sorted based on run order. Motion disturbance: Sway. Screen direction: Horizontal.

	Run 1	Run 2	Run 3	Run 4	Run 5	Run 6	Run 7	Run 8
Model 1	-89.40	-78.34	-42.19	-68.24	-89.34	-84.03	-85.57	-86.97
Model 2	-93.82	-85.63	-88.92	-44.47	-86.37	-92.17	-92.42	-93.60
Model 3	-93.39	-93.46	-84.92	-87.36	-51.61	-87.29	-92.73	-91.23
Model 4	-92.04	-91.70	-91.49	-82.71	-86.62	-53.16	-88.23	-90.42
Model 5	-92.11	-90.20	-92.53	-92.53	-84.11	-85.33	-41.57	-86.55
Model 6	-93.42	-87.25	-90.52	-91.09	-90.16	-75.59	-86.57	-49.59
Model 7	-53.85	-93.01	-82.98	-89.00	-88.68	-87.58	-70.94	-86.57
Model 8	-91.36	-42.79	-91.28	-85.93	-90.38	-92.14	-91.61	-76.80
SA model	-86.22	-92.60	-91.59	-91.72	-90.17	-89.05	-87.19	-89.47
OSFA model	-85.14	-91.17	-88.94	-89.13	-87.92	-86.46	-85.15	-89.54

Table A-7: Subject 7: Percentage change of f_d in σ_e^2 when sorted based on run order. Motion disturbance: Sway. Screen direction: Horizontal.

	Run 1	Run 2	Run 3	Run 4	Run 5	Run 6	Run 7	Run 8
Model 1	-88.63	-91.38	-85.51	-89.33	-90.37	-90.51	-92.65	-93.36
Model 2	-90.82	-88.80	-89.83	-86.02	-88.66	-89.67	-88.36	-87.67
Model 3	-86.42	-84.00	-77.24	-80.42	-74.08	-78.66	-80.02	-79.28
Model 4	-90.04	-88.04	-90.69	-87.51	-90.45	-85.29	-87.13	-88.04
Model 5	-85.80	-80.60	-84.27	-86.54	-83.72	-83.84	-80.67	-85.64
Model 6	-87.67	-86.42	-79.69	-78.97	-85.14	-84.99	-83.82	-82.03
Model 7	-81.94	-84.07	-84.36	-83.07	-84.78	-86.87	-83.20	-85.53
Model 8	-90.89	-87.90	-87.74	-88.18	-89.36	-84.95	-89.93	-88.62
SA model	-91.97	-90.67	-81.53	-90.12	-85.77	-85.51	-85.77	-90.13
OSFA model	-92.03	-90.04	-81.70	-89.43	-86.69	-88.07	-86.28	-89.52

Table A-8: Subject 8: Percentage change of f_d in σ_e^2 when sorted based on run order. Motion disturbance: Sway. Screen direction: Horizontal.

	Run 1	Run 2	Run 3	Run 4	Run 5	Run 6	Run 7	Run 8
Model 1	-92.58	-76.35	-90.78	-81.25	-93.30	-88.99	-92.50	-93.73
Model 2	-93.21	-93.04	-80.16	-92.23	-82.64	-92.10	-90.60	-92.41
Model 3	-87.77	-86.32	-85.38	-72.70	-83.11	-77.65	-88.96	-84.91
Model 4	-83.83	-84.68	-83.46	-81.74	-70.52	-79.94	-73.68	-86.56
Model 5	-93.62	-88.57	-91.93	-91.83	-90.85	-75.65	-88.68	-80.84
Model 6	-89.12	-81.38	-81.69	-85.62	-76.75	-84.27	-82.34	-83.10
Model 7	-90.28	-81.23	-86.01	-86.85	-87.79	-88.50	-90.06	-79.71
Model 8	-79.97	-81.03	-81.89	-81.86	-85.02	-84.27	-78.07	-81.41
SA model	-90.97	-92.00	-85.65	-82.76	-89.96	-86.43	-88.86	-84.84
OSFA model	-93.37	-92.85	-86.59	-84.55	-91.86	-75.54	-87.79	-78.70

Table A-9: Subject 9: Percentage change of f_d in σ_e^2 when sorted based on run order. Motion disturbance: Sway. Screen direction: Horizontal.

	Run 1	Run 2	Run 3	Run 4	Run 5	Run 6	Run 7	Run 8
Model 1	-95.46	-89.11	-85.87	-90.44	-93.59	-91.47	-94.62	-92.23
Model 2	-92.89	-92.63	-90.95	-87.90	-90.93	-93.38	-91.69	-93.77
Model 3	-98.05	-95.72	-95.47	-93.66	-89.63	-93.00	-97.53	-93.84
Model 4	-89.02	-89.81	-89.69	-88.57	-88.34	-86.01	-88.23	-90.32
Model 5	-97.77	-95.24	-97.05	-95.94	-94.03	-94.83	-91.49	-94.35
Model 6	-92.80	-89.98	-93.05	-89.72	-92.09	-90.17	-91.08	-89.39
Model 7	-91.13	-86.09	-77.33	-85.72	-72.72	-84.35	-71.73	-87.61
Model 8	-90.41	-87.47	-90.50	-92.85	-91.32	-91.37	-90.86	-88.30
SA model	-92.51	-92.99	-95.75	-90.01	-96.41	-92.54	-84.66	-91.72
OSFA model	-83.87	-83.88	-84.42	-81.49	-84.75	-86.74	-86.13	-80.16

Table A-10: Subject 10: Percentage change of f_d in σ_e^2 when sorted based on run order. Motion disturbance: Sway. Screen direction: Horizontal.

	Run 1	Run 2	Run 3	Run 4	Run 5	Run 6	Run 7	Run 8
Model 1	-87.18	-81.40	-80.13	-71.44	-80.72	-84.08	-83.02	-86.42
Model 2	-89.29	-89.79	-83.16	-79.38	-71.35	-82.49	-87.45	-83.89
Model 3	-82.65	-83.27	-83.23	-81.71	-79.75	-74.42	-80.91	-83.53
Model 4	-91.54	-88.08	-90.94	-91.60	-88.72	-84.08	-78.34	-88.17
Model 5	-84.98	-83.40	-81.97	-79.02	-80.34	-84.87	-79.68	-79.01
Model 6	-91.37	-84.84	-76.77	-82.20	-64.25	-63.27	-84.87	-84.08
Model 7	-84.32	-77.72	-83.96	-84.51	-84.84	-83.76	-85.19	-84.62
Model 8	-90.69	-83.44	-83.59	-91.01	-89.37	-85.95	-82.93	-84.63
SA model	-83.47	-85.04	-83.23	-89.67	-83.78	-82.26	-85.63	-88.68
OSFA model	-72.80	-80.68	-55.47	-70.69	-41.02	40.35	-54.27	-42.40

Table A-11: Subject 11: Percentage change of f_d in σ_e^2 when sorted based on run order. Motion disturbance: Sway. Screen direction: Horizontal.

	Run 1	Run 2	Run 3	Run 4	Run 5	Run 6	Run 7
Model 1	-67.99	-20.99	-64.80	-90.36	-27.18	-65.17	-39.99
Model 2	-85.33	-45.46	-78.05	-83.95	-63.16	-82.61	-82.48
Model 3	-88.22	-86.67	-49.64	-78.93	-86.68	-69.25	-83.79
Model 4	-84.45	-79.22	-80.61	-45.86	-69.79	-83.35	-64.08
Model 5	-93.68	-32.33	-55.94	-33.60	-66.06	-9.47	-65.74
Model 6	-95.11	-78.70	-90.12	-90.81	-90.01	-54.86	-77.97
Model 7	-90.56	-82.58	-58.89	-85.33	-86.26	-89.99	-36.05
SA model	-76.48	-82.14	-87.20	-79.68	-71.76	-93.35	-82.42
OSFA model	-91.71	-62.29	-71.81	-61.23	-86.12	-75.98	-65.33

Table A-12: Subject 12: Percentage change of f_d in σ_e^2 when sorted based on run order. Motion disturbance: Sway. Screen direction: Horizontal.

	Run 1	Run 2	Run 3	Run 4	Run 5	Run 6	Run 7	Run 8
Model 1	-92.86	-92.00	-93.73	-87.34	-90.17	-92.91	-90.70	-91.36
Model 2	-85.93	-83.33	-83.07	-84.89	-83.65	-84.60	-85.03	-84.88
Model 3	-93.16	-93.10	-90.12	-89.51	-91.92	-90.56	-91.20	-92.35
Model 4	-92.42	-91.94	-91.46	-91.04	-90.48	-91.96	-89.50	-91.18
Model 5	-91.74	-92.32	-90.68	-92.53	-91.68	-91.48	-92.88	-90.19
Model 6	-91.24	-91.24	-90.57	-90.92	-92.62	-88.47	-88.56	-90.33
Model 7	-95.55	-93.22	-94.73	-95.38	-94.26	-95.29	-94.46	-94.29
Model 8	-92.35	-93.00	-88.89	-91.29	-92.59	-90.19	-90.91	-92.66
SA model	-92.36	-85.09	-92.19	-92.09	-92.51	-91.11	-95.49	-92.46
OSFA model	-92.69	-85.06	-93.92	-90.48	-91.42	-90.99	-94.01	-89.50

Table A-13: Subject 13: Percentage change of f_d in σ_e^2 when sorted based on run order. Motion disturbance: Sway. Screen direction: Horizontal.

	Run 1	Run 2	Run 3	Run 4	Run 5	Run 6	Run 7	Run 8
Model 1	-90.81	-68.73	-88.79	-89.17	-85.38	-88.63	-88.42	-87.27
Model 2	-93.65	-91.46	-73.58	-91.62	-91.73	-93.45	-92.65	-93.25
Model 3	-88.41	-86.90	-87.24	-66.71	-86.62	-86.39	-85.98	-86.34
Model 4	-93.99	-92.07	-92.59	-93.56	-77.77	-90.36	-92.03	-90.74
Model 5	-86.67	-85.32	-86.44	-86.68	-84.54	-67.33	-85.29	-85.23
Model 6	-90.93	-90.12	-88.77	-90.37	-90.43	-89.23	-70.18	-90.78
Model 7	-88.52	-88.02	-86.06	-85.19	-87.34	-86.53	-86.93	-64.60
Model 8	-76.70	-83.59	-86.30	-84.69	-88.87	-86.18	-87.04	-88.16
SA model	-88.67	-92.65	-86.80	-93.34	-85.77	-90.44	-86.86	-88.29
OSFA model	-79.55	-86.63	-83.88	-77.09	-80.85	-82.44	-82.34	-66.15

Table A-14: Subject 14: Percentage change of f_d in σ_e^2 when sorted based on run order. Motion disturbance: Sway. Screen direction: Horizontal.

	Run 1	Run 2	Run 3	Run 4	Run 5	Run 6	Run 7	Run 8
Model 1	-96.25	-82.47	-85.74	-82.89	-87.77	-86.44	-92.55	-95.10
Model 2	-96.00	-92.55	-89.51	-91.11	-90.06	-92.72	-93.08	-95.37
Model 3	-94.34	-93.88	-88.64	-92.12	-90.64	-91.96	-90.44	-94.39
Model 4	-92.50	-90.73	-89.82	-82.57	-90.77	-89.35	-90.91	-89.37
Model 5	-91.43	-89.06	-87.12	-88.93	-81.10	-90.97	-92.07	-91.34
Model 6	-96.57	-94.86	-93.35	-88.75	-90.35	-79.45	-96.31	-96.21
Model 7	-94.99	-94.89	-93.49	-90.80	-87.05	-90.07	-80.18	-94.82
Model 8	-93.07	-91.61	-92.79	-89.90	-89.98	-86.33	-88.53	-79.56
SA model	-91.08	-95.11	-94.10	-91.67	-91.45	-94.53	-93.27	-91.17
OSFA model	-82.14	-86.58	-83.25	-82.92	-87.88	-91.20	-90.64	-85.68

Table A-15: Subject 15: Percentage change of f_d in σ_e^2 when sorted based on run order. Motion disturbance: Sway. Screen direction: Horizontal.

	Run 1	Run 2	Run 3	Run 4	Run 5	Run 6	Run 7
Model 1	-89.09	-73.38	-78.75	-72.81	-72.80	-83.13	-83.62
Model 2	-79.15	-82.20	-69.38	-74.39	-70.28	-69.00	-78.61
Model 3	-92.00	-88.00	-77.94	-87.90	-91.12	-86.37	-87.18
Model 4	-90.15	-88.81	-87.25	-72.20	-90.13	-91.13	-86.58
Model 5	-91.16	-89.47	-88.30	-86.48	-63.99	-88.15	-91.00
Model 6	-91.66	-87.75	-86.24	-91.48	-87.23	-76.96	-86.12
Model 7	-89.35	-90.02	-87.07	-88.78	-87.01	-79.50	-55.81
SA model	-80.81	-76.52	-90.85	-90.64	-89.96	-89.80	-87.42
OSFA model	-74.84	-69.83	-88.78	-90.83	-86.72	-87.31	-89.67

Table A-16: Subject 16: Percentage change of f_d in σ_e^2 when sorted based on run order. Motion disturbance: Sway. Screen direction: Horizontal.

	Run 1	Run 2	Run 3	Run 4	Run 5	Run 6	Run 7	Run 8
Model 1	-92.04	-42.85	-75.16	-79.19	-66.84	-41.51	-40.52	-68.03
Model 2	-88.12	-71.12	-87.67	-85.48	-87.19	-89.21	-88.90	-88.53
Model 3	-90.94	-82.58	-68.16	-91.27	-83.70	-84.38	-88.98	-89.88
Model 4	-91.77	-91.99	-86.31	-66.89	-91.56	-85.91	-86.03	-89.60
Model 5	-94.18	-89.32	-89.68	-88.29	-80.69	-90.12	-90.57	-92.46
Model 6	-96.61	-94.05	-84.44	-84.69	-91.77	-88.83	-85.80	-94.74
Model 7	-83.74	-83.96	-79.79	-70.91	-70.90	-78.95	-77.47	-72.10
Model 8	-91.48	-85.96	-86.13	-89.31	-87.77	-89.95	-83.26	-71.59
SA model	-69.04	-89.59	-87.84	-89.59	-93.17	-94.97	-81.80	-88.83
OSFA model	-78.24	-85.98	-85.22	-85.47	-92.51	-96.41	-83.58	-87.83

A-2 Disturbance: Surge (X), Screen input: Vertical

Table A-17: Subject 1: Percentage change of f_d in σ_e^2 when sorted based on run order. Motion disturbance: Surge. Screen direction: Vertical.

	Run 1	Run 2	Run 3	Run 4	Run 5	Run 6	Run 7	Run 8
Model 1	-86.97	-21.79	-45.06	-31.37	-48.10	-46.25	-35.71	-57.48
Model 2	-79.97	-20.04	-31.33	-70.54	-47.86	-75.21	-64.10	-62.71
Model 3	-55.63	-33.12	215.35	-27.47	-45.57	-39.32	-51.94	-36.47
Model 4	-48.37	-44.37	-59.40	18.38	-22.76	-49.36	-33.97	-55.26
Model 5	-87.06	-68.39	-81.15	-85.46	62.51	-35.78	-87.24	-57.60
Model 6	-60.66	-51.43	-61.73	-54.50	-43.53	282.44	-43.96	-56.35
Model 7	-70.48	-52.31	-66.12	-61.88	-59.25	-70.12	62.70	-33.71
Model 8	-53.40	-33.38	-70.83	-8.46	-50.83	-38.79	12.78	677.08
SA model	-48.94	-73.64	-43.78	-56.77	-82.87	-61.38	-69.77	-38.38
OSFA model	-69.86	-54.17	54.78	-31.90	-22.40	44.45	-24.56	184.71

Table A-18: Subject 2: Percentage change of f_d in σ_e^2 when sorted based on run order. Motion disturbance: Surge. Screen direction: Vertical.

	Run 1	Run 2	Run 3	Run 4	Run 5	Run 6	Run 7	Run 8
Model 1	-90.92	-79.91	-73.41	-83.46	-90.32	-85.33	-79.12	-86.22
Model 2	-90.03	-83.68	-87.47	-81.55	-88.29	-87.62	-83.86	-88.54
Model 3	-94.33	-88.81	-82.51	-92.91	-92.03	-91.98	-89.50	-87.87
Model 4	-92.12	-89.30	-85.39	-83.52	-90.12	-88.78	-91.03	-90.69
Model 5	-92.02	-91.37	-88.34	-87.23	-86.56	-89.63	-87.32	-90.90
Model 6	-94.47	-92.21	-92.58	-92.50	-89.45	-84.66	-93.92	-91.53
Model 7	-94.68	-92.57	-89.57	-90.60	-92.78	-85.07	-80.57	-93.42
Model 8	-92.65	-93.26	-91.39	-86.76	-87.29	-91.61	-84.44	-77.36
SA model	-86.76	-89.24	-92.04	-91.36	-91.73	-94.12	-91.84	-90.03
OSFA model	-86.94	-81.29	-78.94	-81.41	-83.97	-84.23	-78.31	-76.09

Table A-19: Subject 3: Percentage change of f_d in σ_e^2 when sorted based on run order. Motion disturbance: Surge. Screen direction: Vertical.

	Run 1	Run 2	Run 3	Run 4	Run 5	Run 6	Run 7	Run 8
Model 1	-72.25	-61.25	-68.35	-70.06	-70.64	-74.71	-75.31	-75.18
Model 2	-80.62	-77.58	-64.53	-72.83	-75.29	-75.49	-79.70	-81.13
Model 3	-78.89	-78.94	-76.80	-64.39	-72.73	-72.23	-72.99	-78.07
Model 4	-89.51	-88.06	-87.74	-83.18	-78.42	-80.91	-88.30	-88.71
Model 5	-74.44	-74.14	-72.85	-72.34	-67.43	-64.25	-65.65	-74.46
Model 6	-90.68	-90.61	-88.59	-87.26	-85.95	-80.91	-77.77	-78.25
Model 7	-87.13	-69.17	-70.54	-79.12	-74.22	-78.52	-81.40	-85.40
Model 8	-84.13	-82.31	-68.27	-69.43	-75.20	-68.94	-72.97	-75.47
SA model	-73.89	-78.87	-77.59	-88.79	-73.22	-87.66	-83.17	-79.22
OSFA model	-56.49	-61.21	-59.81	-65.13	-53.65	-67.95	-28.43	-26.84

Table A-20: Subject 4: Percentage change of f_d in σ_e^2 when sorted based on run order. Motion disturbance: Surge. Screen direction: Vertical.

	Run 1	Run 2	Run 3	Run 4	Run 5	Run 6	Run 7	Run 8
Model 1	-74.24	-63.71	-56.49	-70.90	-32.30	-47.99	-62.97	-61.56
Model 2	-94.77	-75.01	-71.07	-60.69	-83.47	-50.52	-89.70	-78.04
Model 3	-76.79	-88.84	-72.47	-72.18	-60.81	-80.19	-51.22	-84.45
Model 4	-93.59	-77.54	-87.41	-65.97	-68.40	-62.43	-81.84	-59.66
Model 5	-54.17	-89.46	-79.38	-90.99	-71.20	-72.52	-62.05	-82.50
Model 6	-88.65	-47.46	-70.83	-72.38	-68.24	-76.59	-71.60	-71.06
Model 7	-81.59	-51.84	-25.71	61.07	-44.03	68.17	-63.61	-61.46
Model 8	-77.39	-74.48	-85.50	-58.91	-77.69	-77.19	-66.35	-69.92
SA model	-69.50	-84.06	-82.26	-83.14	-84.23	-81.81	-49.05	-84.34
OSFA model	-73.38	-78.70	-76.38	-73.98	-76.91	-81.63	-66.64	-77.79

Table A-21: Subject 5: Percentage change of f_d in σ_e^2 when sorted based on run order. Motion disturbance: Surge. Screen direction: Vertical.

	Run 1	Run 2	Run 3	Run 4	Run 5	Run 6	Run 7	Run 8
Model 1	-83.38	-59.73	-46.19	-43.66	-63.69	-79.99	-56.45	-69.47
Model 2	-70.92	-70.79	-70.40	-68.64	-62.36	-63.49	-71.88	-62.82
Model 3	-69.06	-70.69	-60.56	-75.99	-76.98	-71.67	-64.28	-61.52
Model 4	-83.89	-58.40	-68.89	-78.92	-69.87	-73.50	-68.84	-58.61
Model 5	-49.20	-82.81	-47.44	-58.23	-78.77	-57.74	-60.92	-55.75
Model 6	-54.89	-45.54	-77.75	-45.83	-53.51	-73.49	-54.64	-55.90
Model 7	-82.98	-73.74	-62.88	-64.45	-67.36	-70.72	-60.82	-76.76
Model 8	-76.56	-78.07	-71.36	-65.01	-64.59	-69.59	-71.91	-62.69
SA model	-65.71	-71.27	-72.98	-71.36	-58.68	-54.39	-74.19	-74.73
OSFA model	-50.86	-62.18	-67.80	-75.87	-62.31	-60.46	-71.09	-69.83

Table A-22: Subject 6: Percentage change of f_d in σ_e^2 when sorted based on run order. Motion disturbance: Surge. Screen direction: Vertical.

	Run 1	Run 2	Run 3	Run 4	Run 5	Run 6	Run 7	Run 8
Model 1	-84.54	-61.71	-44.08	-69.06	-53.48	-68.07	-46.60	-51.80
Model 2	-70.72	2.55	-37.83	-66.48	-72.87	-75.26	-56.18	-67.57
Model 3	-80.13	-72.78	103.15	-21.52	-68.39	-58.72	-74.02	-17.42
Model 4	-80.02	-53.46	-51.24	-52.57	-69.58	-56.66	-64.75	-57.81
Model 5	-73.28	-8.30	-64.16	-70.05	89.55	-9.89	-63.95	-54.65
Model 6	-70.51	-59.65	-66.66	-52.12	-57.14	-62.48	-59.97	-51.62
Model 7	-54.54	-9.49	-44.21	18.46	-41.59	-37.17	165.76	-14.24
Model 8	-84.31	-58.28	-64.33	-57.16	-75.82	-50.60	-51.37	-54.05
SA model	-66.35	-72.68	-61.39	-71.27	-51.89	-69.53	-24.14	-72.31
OSFA model	-78.81	-36.22	25.63	-73.94	27.44	-69.33	71.95	-73.74

Table A-23: Subject 7: Percentage change of f_d in σ_e^2 when sorted based on run order. Motion disturbance: Surge. Screen direction: Vertical.

	Run 1	Run 2	Run 3	Run 4	Run 5	Run 6	Run 7	Run 8
Model 1	-80.40	-51.50	-72.58	-75.13	-73.94	-60.03	-66.98	-68.77
Model 2	-90.26	-79.12	-87.67	-77.29	-79.13	-83.29	-87.72	-87.48
Model 3	-91.04	-86.45	-83.55	-81.80	-82.49	-79.66	-88.31	-88.98
Model 4	-84.97	-84.33	-81.88	-72.06	-81.30	-73.30	-70.06	-79.82
Model 5	-88.25	-90.41	-90.25	-84.97	-80.79	-83.75	-82.31	-77.31
Model 6	-83.03	-82.72	-75.47	-77.78	-76.00	-79.74	-71.15	-86.17
Model 7	-82.92	-79.93	-82.53	-75.83	-78.49	-76.87	-80.68	-69.80
Model 8	-80.04	-72.39	-70.97	-75.81	-80.95	-79.99	-78.18	-69.57
SA model	-73.76	-88.26	-88.90	-81.53	-87.90	-82.17	-81.98	-78.73
OSFA model	-78.06	-80.65	-87.00	-76.66	-85.78	-80.35	-81.42	-71.91

Table A-24: Subject 8: Percentage change of f_d in σ_e^2 when sorted based on run order. Motion disturbance: Surge. Screen direction: Vertical.

	Run 1	Run 2	Run 3	Run 4	Run 5	Run 6	Run 7	Run 8
Model 1	-95.05	-91.77	-85.80	-94.44	-89.91	-94.15	-90.00	-88.02
Model 2	-82.19	-78.69	-81.99	-76.81	-81.96	-82.00	-79.68	-80.32
Model 3	-94.44	-92.00	-90.26	-92.82	-93.30	-91.23	-93.19	-92.73
Model 4	-90.88	-88.11	-86.23	-90.22	-89.16	-84.80	-90.20	-87.95
Model 5	-91.05	-88.15	-90.38	-90.63	-85.79	-90.40	-88.11	-88.51
Model 6	-88.94	-89.87	-87.28	-88.48	-90.09	-85.80	-89.38	-84.83
Model 7	-94.36	-88.12	-92.04	-90.51	-93.92	-90.43	-86.95	-91.53
Model 8	-92.52	-90.11	-90.98	-92.18	-90.97	-92.09	-90.85	-89.09
SA model	-93.02	-81.94	-93.79	-90.06	-90.39	-89.62	-92.05	-92.51
OSFA model	-93.38	-79.31	-88.34	-88.49	-85.12	-85.51	-85.82	-89.15

Table A-25: Subject 9: Percentage change of f_d in σ_e^2 when sorted based on run order. Motion disturbance: Surge. Screen direction: Vertical.

	Run 1	Run 2	Run 3	Run 4	Run 5	Run 6	Run 7	Run 8
Model 1	-69.59	-40.40	-49.20	-50.59	-53.74	-46.72	-65.31	-61.11
Model 2	-85.63	-78.31	-54.59	-50.39	-55.45	-78.64	-46.45	-76.18
Model 3	-76.72	-79.85	-76.56	-65.45	-46.11	-50.10	-78.36	-43.35
Model 4	-37.71	-58.38	-59.76	-57.84	-24.59	-39.89	-42.82	-51.04
Model 5	-79.69	-38.27	-67.36	-74.23	-70.65	-71.98	-42.74	-42.72
Model 6	-36.46	11.89	-31.82	-41.97	-19.04	-25.94	44.05	-25.78
Model 7	-54.37	-48.32	-32.93	-42.40	-51.28	-52.02	-58.43	3.13
Model 8	-81.89	-35.94	-39.12	-81.63	-33.86	-63.37	-73.19	-65.59
SA model	-63.77	-73.86	-71.50	-48.56	-66.31	-15.68	-38.42	-69.45
OSFA model	-31.80	-51.75	-57.22	-19.02	-73.18	86.68	6.24	-85.52

Table A-26: Subject 10: Percentage change of f_d in σ_e^2 when sorted based on run order. Motion disturbance: Surge. Screen direction: Vertical.

	Run 1	Run 2	Run 3	Run 4	Run 5	Run 6	Run 7	Run 8
Model 1	-80.16	-80.25	-82.56	-73.81	-79.71	-81.69	-77.28	-83.81
Model 2	-87.86	-82.17	-85.01	-87.40	-78.91	-84.37	-86.49	-83.60
Model 3	-80.05	-75.76	-70.16	-73.85	-77.67	-72.34	-71.57	-78.80
Model 4	-91.69	-91.91	-89.25	-82.27	-86.44	-91.37	-84.74	-85.10
Model 5	-88.55	-82.91	-72.00	-82.98	-80.01	-86.66	-85.18	-82.67
Model 6	-86.55	-83.26	-84.28	-75.30	-77.84	-76.04	-84.42	-83.74
Model 7	-89.48	-85.06	-86.91	-89.00	-84.05	-87.36	-82.58	-87.48
Model 8	-90.92	-91.51	-87.51	-90.76	-90.54	-82.35	-89.65	-86.21
SA model	-82.39	-87.01	-76.87	-90.02	-85.24	-83.79	-88.97	-91.43
OSFA model	-80.04	-82.80	-74.94	-86.35	-82.18	-83.65	-85.56	-88.62

Table A-27: Subject 11: Percentage change of f_d in σ_e^2 when sorted based on run order. Motion disturbance: Surge. Screen direction: Vertical.

	Run 1	Run 2	Run 3	Run 4	Run 5	Run 6	Run 7	Run 8
Model 1	-89.38	-62.78	-52.55	-62.05	-54.38	-64.18	-68.89	-63.97
Model 2	-86.45	-10.50	-85.75	-83.45	-84.91	-83.03	-86.04	-85.39
Model 3	-88.91	-87.65	-32.88	-87.21	-82.32	-85.02	-82.03	-87.86
Model 4	-80.43	-79.01	-77.23	-21.59	-81.27	-76.53	-75.65	-77.66
Model 5	-87.47	-85.04	-80.29	-84.45	28.75	-85.70	-87.34	-85.24
Model 6	-91.21	-87.59	-87.45	-85.52	-88.57	-3.53	-87.68	-85.06
Model 7	-91.41	-84.94	-90.94	-85.51	-77.53	-84.51	58.44	-85.10
Model 8	-90.16	-85.08	-85.11	-86.01	-88.88	-87.72	-86.19	-17.91
SA model	-63.62	-86.50	-87.92	-79.26	-85.36	-87.98	-86.15	-87.88
OSFA model	-48.52	-81.71	-79.65	-74.62	-86.97	-82.93	-90.50	-83.58

Table A-28: Subject 12: Percentage change of f_d in σ_e^2 when sorted based on run order. Motion disturbance: Surge. Screen direction: Vertical.

	Run 1	Run 2	Run 3	Run 4	Run 5	Run 6	Run 7	Run 8
Model 1	-89.17	-89.62	-88.35	-85.78	-85.40	-80.78	-88.65	-71.94
Model 2	-77.61	-85.87	-89.20	-88.06	-83.48	-86.12	-82.54	-86.74
Model 3	-88.22	-67.50	-83.16	-83.77	-81.77	-74.83	-77.20	-73.29
Model 4	-88.23	-83.10	-81.28	-87.70	-90.25	-90.48	-86.99	-90.70
Model 5	-89.94	-86.28	-86.24	-78.54	-87.93	-91.18	-91.30	-87.57
Model 6	-95.18	-91.74	-85.02	-81.46	-77.27	-82.54	-91.52	-92.54
Model 7	-92.88	-88.08	-90.53	-86.31	-88.13	-77.80	-87.09	-91.67
Model 8	-96.59	-94.17	-90.93	-93.39	-89.35	-91.32	-84.49	-92.34
SA model	-87.62	-88.54	-81.69	-90.95	-90.77	-90.37	-91.39	-95.59
OSFA model	-84.57	-86.17	-82.85	-86.18	-87.08	-83.42	-89.51	-90.68

Table A-29: Subject 13: Percentage change of f_d in σ_e^2 when sorted based on run order. Motion disturbance: Surge. Screen direction: Vertical.

	Run 1	Run 2	Run 3	Run 4	Run 5	Run 6	Run 7	Run 8
Model 1	-56.78	-48.47	-57.68	-54.81	-56.86	-55.92	-56.30	-56.86
Model 2	-88.80	-84.82	-72.54	-74.56	-79.77	-86.10	-72.24	-83.49
Model 3	-84.78	-84.22	-85.53	-75.44	-85.13	-84.13	-85.94	-85.32
Model 4	-89.56	-79.34	-76.07	-78.31	-68.99	-86.09	-77.25	-79.74
Model 5	-73.83	-68.22	-68.50	-72.70	-73.05	-65.23	-68.33	-71.28
Model 6	-84.61	-83.79	-68.08	-73.24	-79.30	-84.39	-78.71	-67.02
Model 7	-90.30	-77.66	-79.90	-90.41	-80.00	-79.12	-78.57	-69.10
Model 8	-81.72	-74.37	-88.33	-88.17	-75.89	-78.69	-83.77	-88.32
SA model	-58.23	-85.80	-88.23	-85.24	-75.06	-81.94	-85.36	-87.56
OSFA model	-55.81	-81.65	-83.39	-81.63	-71.57	-79.03	-79.27	-83.71

Table A-30: Subject 14: Percentage change of f_d in σ_e^2 when sorted based on run order. Motion disturbance: Surge. Screen direction: Vertical.

	Run 1	Run 2	Run 3	Run 4	Run 5	Run 6	Run 7	Run 8
Model 1	-85.51	-78.95	-83.52	-83.04	-85.81	-3.24	-57.54	-60.61
Model 2	-77.01	-47.54	-5.88	-33.85	-53.70	-24.98	-4.68	-65.15
Model 3	-68.99	-70.05	-86.47	-83.19	-86.48	-88.45	-86.11	-3.05
Model 4	-2.38	-54.58	-54.30	-80.05	-86.66	-83.67	-80.10	-85.59
Model 5	-84.01	-4.00	-65.64	-56.86	-79.51	-84.06	-83.67	-79.88
Model 6	-88.37	-88.76	-3.54	-66.15	-67.34	-88.13	-84.45	-88.21
Model 7	-93.12	-89.93	-92.20	-3.26	-62.74	-66.69	-86.73	-92.60
Model 8	-88.66	-86.37	-83.51	-86.07	-3.04	-64.82	-60.64	-80.81
SA model	-80.51	-50.21	-86.84	-78.52	-77.87	-85.83	-84.05	-81.49
OSFA model	-66.07	-64.26	-79.32	-66.15	-71.59	-75.87	-75.69	-75.78

Table A-31: Subject 15: Percentage change of f_d in σ_e^2 when sorted based on run order. Motion disturbance: Surge. Screen direction: Vertical.

	Run 1	Run 2	Run 3	Run 4	Run 5	Run 6	Run 7	Run 8	Run 9
Model 1	-88.01	-79.15	-82.97	-87.93	-88.83	-87.83	-70.62	-88.89	-74.54
Model 2	-80.01	-61.53	-19.13	-67.65	-47.06	-60.87	-43.31	-68.20	-58.60
Model 3	-92.39	-73.93	-84.38	-87.52	-88.08	-90.94	-89.22	-92.84	-73.37
Model 4	-61.24	-78.33	-62.92	-69.60	-75.76	-76.13	-78.70	-77.02	-79.01
Model 5	-91.41	-64.77	-87.65	-65.32	-77.34	-91.84	-83.08	-90.20	-86.37
Model 6	-90.59	-88.76	-66.98	-86.80	-72.36	-80.77	-88.27	-85.25	-90.53
Model 7	-92.75	-89.88	-91.35	-64.72	-89.44	-69.72	-80.97	-90.95	-86.61
Model 8	-89.76	-88.79	-87.43	-88.17	-68.97	-88.78	-74.00	-78.60	-86.24
Model 9	-88.09	-81.50	-85.53	-82.00	-86.63	-63.51	-83.51	-63.75	-72.65
SA model	-88.71	-62.60	-92.18	-78.08	-86.75	-86.59	-88.49	-88.75	-82.94
OSFA model	-86.45	-74.28	-87.91	-74.41	-80.09	-82.80	-83.76	-86.03	-77.16

Table A-32: Subject 16: Percentage change of f_d in σ_e^2 when sorted based on run order. Motion disturbance: Surge. Screen direction: Vertical.

	Run 1	Run 2	Run 3	Run 4	Run 5	Run 6	Run 7	Run 8
Model 1	-92.42	-82.72	-73.02	-83.32	-67.07	-79.61	-79.25	-70.52
Model 2	-86.95	-70.93	-71.39	-73.99	-65.26	-86.43	-85.44	-83.45
Model 3	-88.76	-83.17	-73.91	-73.83	-83.07	-67.52	-87.69	-89.39
Model 4	-83.34	-82.81	-78.21	-69.22	-67.78	-75.65	-62.59	-79.89
Model 5	-93.57	-87.95	-87.04	-87.12	-75.78	-80.82	-83.88	-72.15
Model 6	-70.05	-67.38	-65.71	-67.00	-58.72	-68.00	-75.00	-69.48
Model 7	-91.06	-68.04	-77.93	-82.29	-85.83	-62.49	-72.03	-74.85
Model 8	-79.27	-77.55	-72.82	-74.36	-71.03	-72.73	-63.01	-70.61
SA model	-85.62	-81.95	-85.53	-79.25	-87.63	-73.74	-82.30	-78.53
OSFA model	-85.62	-81.58	-85.15	-78.71	-87.95	-74.59	-82.44	-79.49

A-3 Disturbance: Heave (Z), Screen input: Vertical

Table A-33: Subject 1: Percentage change of f_d in σ_e^2 when sorted based on run order. Motion disturbance: Heave. Screen direction: Vertical.

	Run 1	Run 2	Run 3	Run 4	Run 5	Run 6	Run 7	Run 8
Model 1	-88.65	-45.84	-5.55	27.78	12.54	11.95	0.87	0.45
Model 2	-1.09	258.06	181.51	13.50	30.71	-6.88	-0.06	0.48
Model 3	-0.38	-1.27	164.08	112.84	3.98	1.98	12.05	13.98
Model 4	-8.39	-1.50	0.26	453.41	230.57	15.80	59.26	12.16
Model 5	-9.20	5.84	-0.90	-0.46	623.63	347.55	18.99	50.06
Model 6	-50.42	15.75	27.19	-0.75	-5.55	280.07	241.71	14.81
Model 7	1.99	115.60	34.95	36.41	0.13	-1.60	484.90	303.49
Model 8	-69.67	-11.86	40.04	12.19	10.75	-0.02	0.46	-39.93
SA model	31.88	23.33	11.15	16.29	4.79	16.20	72.43	9.80
OSFA model	-68.81	401.30	279.90	676.33	889.98	472.04	877.49	-40.24

Table A-34: Subject 2: Percentage change of f_d in σ_e^2 when sorted based on run order. Motion disturbance: Heave. Screen direction: Vertical.

	Run 1	Run 2	Run 3	Run 4	Run 5	Run 6	Run 7	Run 8
Model 1	-91.73	-77.27	-89.49	-87.29	-87.66	-89.33	-88.87	-82.20
Model 2	-98.37	-93.52	-74.95	-92.75	-85.66	-87.29	-93.32	-92.90
Model 3	-93.93	-85.33	-89.75	-83.67	-93.78	-90.73	-91.44	-93.90
Model 4	-96.13	-95.93	-93.26	-92.39	-82.16	-95.78	-90.66	-92.34
Model 5	-95.42	-94.25	-94.19	-77.42	-88.94	-87.87	-94.61	-93.96
Model 6	-95.45	-95.16	-92.42	-92.47	-69.70	-89.00	-89.64	-93.05
Model 7	-96.43	-94.09	-94.92	-96.38	-96.28	-85.52	-93.07	-86.44
Model 8	-89.37	-78.48	-86.98	-84.96	-77.39	-78.46	-37.33	-65.30
SA model	-89.67	-91.49	-93.46	-94.83	-94.71	-94.20	-96.33	-80.77
OSFA model	-71.87	-67.40	-73.04	-73.45	-80.27	-81.81	-77.28	-75.91

Table A-35: Subject 3: Percentage change of f_d in σ_e^2 when sorted based on run order. Motion disturbance: Heave. Screen direction: Vertical.

	Run 1	Run 2	Run 3	Run 4	Run 5	Run 6	Run 7	Run 8
Model 1	-91.58	-84.17	-88.34	-87.39	-77.72	-81.69	-86.04	-91.98
Model 2	-93.10	-89.71	-84.88	-87.70	-88.68	-75.76	-78.79	-84.29
Model 3	-83.85	-82.93	-79.03	-83.84	-85.99	-85.78	-71.91	-78.50
Model 4	-84.26	-89.19	-87.37	-86.04	-87.61	-91.06	-89.43	-76.12
Model 5	-79.81	-76.32	-76.87	-67.31	-72.39	-58.80	-72.47	-65.04
Model 6	-94.59	-77.59	-83.19	-89.55	-93.80	-89.18	-92.69	-93.25
Model 7	-82.22	-84.70	-59.14	-70.92	-77.82	-76.58	-69.54	-85.76
Model 8	-95.77	-92.13	-95.38	-70.54	-78.71	-86.73	-89.83	-82.08
SA model	-89.53	-88.89	-85.47	-90.38	-77.31	-92.81	-78.54	-89.28
OSFA model	-78.14	-76.37	-73.09	-77.80	-74.10	-80.43	-64.34	-74.36

Table A-36: Subject 4: Percentage change of f_d in σ_e^2 when sorted based on run order. Motion disturbance: Heave. Screen direction: Vertical.

	Run 1	Run 2	Run 3	Run 4	Run 5	Run 6	Run 7	Run 8
Model 1	-92.70	-29.21	-52.46	-22.62	-53.55	-42.84	-54.06	-68.02
Model 2	-82.60	-62.90	-43.38	-71.65	-35.39	-69.59	-62.68	-71.20
Model 3	-68.23	-64.45	32.23	-39.81	-67.38	-40.23	-65.95	-57.12
Model 4	-69.45	-78.09	-84.61	-34.58	-42.57	-78.68	-41.77	-75.84
Model 5	-73.78	-56.00	-75.02	-67.99	38.29	-40.21	-69.42	-42.08
Model 6	-43.57	-41.91	-17.54	-37.82	22.37	323.07	0.48	-18.17
Model 7	-77.52	-46.05	-66.77	-70.57	-71.68	-71.04	31.96	-43.40
Model 8	-44.34	-69.40	-41.29	-64.72	-65.38	-66.78	-68.38	13.22
SA model	-57.72	-75.86	-67.96	-81.35	-70.83	-15.10	-75.89	-71.34
OSFA model	-76.11	-67.04	-17.67	-56.28	-14.00	107.06	-15.55	-30.72

Table A-37: Subject 5: Percentage change of f_d in σ_e^2 when sorted based on run order. Motion disturbance: Heave. Screen direction: Vertical.

	Run 1	Run 2	Run 3	Run 4	Run 5	Run 6	Run 7	Run 8
Model 1	-91.49	-82.31	-88.86	-54.01	-79.83	-79.40	-79.28	-90.38
Model 2	-87.55	-85.91	-82.98	-87.08	-67.13	-79.16	-85.87	-85.28
Model 3	-96.44	-90.53	-87.05	-88.54	-90.04	-90.66	-92.53	-94.47
Model 4	-95.34	-95.71	-90.39	-87.00	-86.92	-89.95	-89.09	-91.19
Model 5	-91.63	-84.15	-88.48	-87.19	-85.46	-82.32	-85.76	-83.60
Model 6	-87.41	-80.34	-75.27	-80.00	-70.52	-67.05	-70.67	-69.27
Model 7	-89.91	-76.30	-84.70	-91.53	-91.50	-90.26	-87.86	-87.09
Model 8	-92.31	-86.02	-53.62	-74.86	-77.10	-80.94	-85.30	-83.20
SA model	-86.01	-87.49	-94.83	-94.18	-89.26	-76.69	-91.98	-85.63
OSFA model	-67.60	-66.54	-70.23	-68.11	-66.49	-54.87	-69.41	-81.63

Table A-38: Subject 6: Percentage change of f_d in σ_e^2 when sorted based on run order. Motion disturbance: Heave. Screen direction: Vertical.

	Run 1	Run 2	Run 3	Run 4	Run 5	Run 6	Run 7	Run 8
Model 1	-89.15	-39.41	-28.20	-30.28	-11.62	-48.85	-45.53	-36.39
Model 2	-54.04	20.10	-55.34	-43.07	-50.97	-20.44	-64.10	-62.68
Model 3	-54.47	-45.88	-10.52	-44.69	-32.29	-38.85	-14.61	-51.43
Model 4	-60.02	-38.17	-36.52	66.92	-45.92	-41.29	-39.93	-23.25
Model 5	-37.00	-29.20	-10.90	-26.49	445.04	-38.43	-49.63	-41.35
Model 6	-46.69	-17.51	-64.95	-42.85	-37.23	17.25	-43.12	-37.39
Model 7	-31.42	-32.99	-21.90	-18.32	-26.42	-29.15	221.85	-32.50
Model 8	-76.22	-67.00	-61.99	-38.94	-67.82	-66.33	-63.14	143.83
SA model	-50.52	-66.22	-55.74	-46.34	-17.18	-49.80	-22.45	-74.22
OSFA model	-76.29	-24.53	-41.42	30.08	283.08	-11.15	124.83	70.39

Table A-39: Subject 7: Percentage change of f_d in σ_e^2 when sorted based on run order. Motion disturbance: Heave. Screen direction: Vertical.

	Run 1	Run 2	Run 3	Run 4	Run 5	Run 6	Run 7	Run 8
Model 1	-60.61	-62.09	-66.02	-55.58	-58.39	-60.90	-55.05	-55.39
Model 2	-94.63	-68.98	-87.48	-85.35	-94.35	-94.14	-92.23	-93.81
Model 3	-93.52	-93.08	-65.53	-85.94	-81.20	-92.94	-92.89	-88.94
Model 4	-94.53	-92.57	-93.38	-72.39	-86.28	-88.00	-93.60	-92.65
Model 5	-97.11	-94.40	-94.88	-95.65	-72.86	-93.05	-87.44	-96.86
Model 6	-92.65	-92.29	-90.96	-90.37	-91.64	-68.67	-87.20	-83.36
Model 7	-93.17	-78.25	-79.52	-87.65	-76.07	-80.43	-81.46	-79.71
Model 8	-91.73	-84.71	-84.00	-87.40	-83.41	-81.78	-82.57	-77.81
SA model	-63.70	-92.83	-89.91	-93.68	-95.86	-91.33	-88.55	-88.77
OSFA model	-54.68	-73.96	-69.93	-79.63	-77.61	-75.10	-78.49	-70.92

Table A-40: Subject 8: Percentage change of f_d in σ_e^2 when sorted based on run order. Motion disturbance: Heave. Screen direction: Vertical.

	Run 1	Run 2	Run 3	Run 4	Run 5	Run 6	Run 7	Run 8
Model 1	-94.73	-4.68	-85.70	-77.14	-8.49	-92.11	-71.51	-91.28
Model 2	-89.07	-86.58	-3.93	-76.94	-71.77	-7.50	-82.80	-63.55
Model 3	-82.65	-13.12	-29.58	-7.42	-76.65	-77.41	-9.80	-54.83
Model 4	-85.43	-71.17	-81.32	-85.22	-4.85	-83.04	-75.98	-8.76
Model 5	-17.70	217.07	2.90	452.53	363.92	-9.99	110.95	72.97
Model 6	-87.28	-7.24	-77.47	-81.03	-66.49	-69.17	-6.02	-86.84
Model 7	-86.28	-81.64	-8.83	-83.00	-78.24	-71.19	-76.50	-5.72
Model 8	-8.88	74.76	45.39	6.85	193.76	-7.38	368.19	298.63
SA model	-78.85	-68.13	-80.14	-77.17	48.60	-80.57	-81.68	21.58
OSFA model	-81.49	-69.12	-63.08	-76.63	118.45	-73.58	-76.00	90.99

Table A-41: Subject 9: Percentage change of f_d in σ_e^2 when sorted based on run order. Motion disturbance: Heave. Screen direction: Vertical..

	Run 1	Run 2	Run 3	Run 4	Run 5	Run 6	Run 7	Run 8
Model 1	-91.23	-27.02	-70.56	-36.11	-39.41	-36.39	0.70	-62.27
Model 2	-64.39	-63.89	-30.94	-65.28	-39.31	-44.60	-38.68	0.95
Model 3	-2.72	247.96	866.73	23.30	355.24	61.31	78.63	44.89
Model 4	-58.89	-3.85	-35.14	71.89	-51.85	-45.50	-52.64	-56.84
Model 5	-72.63	-57.98	-6.32	-12.94	149.88	-56.81	-24.31	-49.92
Model 6	-71.44	-54.58	-71.31	-6.08	-22.42	305.36	-62.92	25.45
Model 7	-88.58	-51.54	-52.59	-49.53	-2.47	-71.63	-76.55	-41.26
Model 8	-47.50	134.93	-34.64	-30.62	-42.16	-6.30	72.75	544.35
SA model	-54.06	-56.47	147.65	-67.59	-60.26	-57.71	-72.64	0.98
OSFA model	-83.44	-73.02	595.51	29.50	94.62	147.99	-73.37	336.59

Table A-42: Subject 10: Percentage change of f_d in σ_e^2 when sorted based on run order. Motion disturbance: Heave. Screen direction: Vertical.

	Run 1	Run 2	Run 3	Run 4	Run 5	Run 6	Run 7	Run 8
Model 1	-89.36	-70.55	-70.30	-78.32	-71.99	-80.91	-79.16	-80.71
Model 2	-93.14	-80.62	-86.34	-87.36	-87.64	-83.70	-92.16	-91.37
Model 3	-88.13	-87.38	-75.18	-85.34	-84.45	-84.50	-83.32	-88.29
Model 4	-91.71	-90.97	-89.59	-82.23	-84.52	-84.78	-85.03	-82.73
Model 5	-86.87	-82.11	-80.95	-81.38	-73.02	-81.61	-81.14	-87.72
Model 6	-91.61	-89.37	-84.95	-83.43	-85.49	-77.31	-83.68	-83.79
Model 7	-95.59	-82.91	-89.42	-90.16	-91.56	-86.28	-45.57	-94.77
Model 8	-94.29	-93.72	-82.01	-88.10	-88.72	-90.34	-85.61	-46.37
SA model	-79.88	-92.19	-88.76	-90.28	-85.36	-88.60	-90.91	-90.03
OSFA model	-75.53	-83.55	-71.08	-79.02	-57.84	-62.92	-61.01	-59.27

Table A-43: Subject 11: Percentage change of f_d in σ_e^2 when sorted based on run order. Motion disturbance: Heave. Screen direction: Vertical.

	Run 1	Run 2	Run 3	Run 4	Run 5	Run 6	Run 7	Run 8
Model 1	-91.45	-52.71	-50.90	-41.98	-10.51	-34.78	-52.85	-45.87
Model 2	-64.50	50.35	-56.47	-68.43	-61.04	-18.90	-48.61	-70.87
Model 3	-67.61	-52.19	14.80	-53.89	-65.24	-61.66	-18.45	-34.04
Model 4	-61.24	-56.84	-32.27	84.87	-48.20	-60.40	-47.85	-16.16
Model 5	-19.01	-12.86	4.08	6.08	370.58	52.48	-12.50	-23.88
Model 6	-67.67	-23.98	-39.46	-65.01	-36.38	160.10	-35.67	-67.11
Model 7	-79.49	-73.99	-25.67	-54.94	-76.07	-54.58	126.04	-52.78
Model 8	-81.19	-70.97	-61.42	-17.66	-41.28	-75.31	-57.71	7.07
SA model	-55.44	-70.49	-64.59	-61.85	-3.14	-60.58	-77.75	-73.75
OSFA model	-72.96	-28.63	-23.84	-30.08	148.88	37.86	1.39	-46.48

Table A-44: Subject 12: Percentage change of f_d in σ_e^2 when sorted based on run order. Motion disturbance: Heave. Screen direction: Vertical.

	Run 1	Run 2	Run 3	Run 4	Run 5	Run 6	Run 7	Run 8
Model 1	-86.39	-42.92	-63.34	-68.78	-86.39	-70.88	-85.59	-73.39
Model 2	-82.82	-45.91	-63.06	-79.35	-82.94	-45.91	-81.35	-70.69
Model 3	-92.49	-83.94	-83.09	-52.09	-73.83	-79.73	-83.09	-80.88
Model 4	-90.83	-77.19	-90.86	-54.70	-69.26	-88.15	-90.33	-54.70
Model 5	-86.39	-70.88	-85.59	-73.39	-86.39	-42.92	-63.34	-68.78
Model 6	-92.06	-30.84	-87.24	-70.74	-89.78	-30.84	-72.25	-87.09
Model 7	-85.69	-86.08	-35.71	-85.76	-60.28	-84.27	-35.71	-70.49
Model 8	-70.35	-73.21	-67.21	38.76	-64.53	-5.82	-60.00	38.76
SA model	-75.40	-82.03	-85.32	-90.73	-75.40	-87.44	-83.31	-55.52
OSFA model	-66.24	-56.40	-70.87	-69.45	-66.24	-55.44	-59.87	-24.01

Table A-45: Subject 13: Percentage change of f_d in σ_e^2 when sorted based on run order. Motion disturbance: Heave. Screen direction: Vertical.

	Run 1	Run 2	Run 3	Run 4	Run 5	Run 6	Run 7	Run 8
Model 1	-90.59	-77.20	-68.57	-77.65	-81.42	-70.22	-68.88	-56.21
Model 2	-80.02	-68.66	-68.50	-55.45	-76.96	-72.04	-74.90	-70.30
Model 3	-80.65	-54.19	-71.75	-73.14	-57.38	-79.78	-80.08	-77.67
Model 4	-93.83	-90.76	-77.37	-78.78	-76.54	-57.80	-91.85	-86.73
Model 5	-88.92	-86.12	-86.37	-68.64	-86.40	-80.56	-65.35	-89.26
Model 6	-93.98	-91.17	-91.79	-90.39	-70.83	-86.35	-81.87	-65.68
Model 7	-66.91	-75.80	-80.88	-63.73	-76.91	-51.22	-70.41	-79.63
Model 8	-80.77	-66.44	-80.83	-84.34	-74.55	-80.67	-64.41	-73.68
SA model	-81.65	-76.49	-80.40	-88.59	-89.06	-91.90	-80.54	-84.63
OSFA model	-67.04	-68.88	-73.23	-79.80	-77.02	-80.05	-73.00	-78.58

Table A-46: Subject 14: Percentage change of f_d in σ_e^2 when sorted based on run order. Motion disturbance: Heave. Screen direction: Vertical.

	Run 1	Run 2	Run 3	Run 4	Run 5	Run 6	Run 7	Run 8
Model 1	-72.08	-47.93	-79.35	-76.31	-78.69	-71.95	-78.92	-37.47
Model 2	-71.04	-13.23	-69.34	21.18	180.50	2.30	-20.71	67.57
Model 3	-87.18	-36.88	-73.62	-47.60	-85.01	-90.55	-83.00	-76.82
Model 4	-80.08	-63.01	-45.54	-69.33	-60.10	-73.47	-36.65	-77.07
Model 5	-77.98	-73.25	-76.35	-39.61	-70.88	-50.31	-78.23	-69.19
Model 6	-90.33	-80.29	-73.95	-85.36	-35.28	-70.45	-45.50	-82.56
Model 7	-84.58	-82.48	-84.21	-77.86	-83.86	-37.54	-73.13	-50.88
Model 8	-71.27	20.59	183.53	-1.98	-31.91	72.01	-63.04	-4.34
SA model	-76.16	-12.32	-80.25	-76.16	-76.48	-77.70	-80.62	-10.36
OSFA model	-63.82	153.82	-71.86	-42.98	-56.41	-69.65	-72.71	125.00

Table A-47: Subject 15: Percentage change of f_d in σ_e^2 when sorted based on run order. Motion disturbance: Heave. Screen direction: Vertical.

	Run 1	Run 2	Run 3	Run 4	Run 5	Run 6	Run 7	Run 8
Model 1	-91.66	-61.64	-38.46	-73.61	-78.62	-76.91	-83.62	-91.87
Model 2	-95.68	-92.46	-65.20	-40.87	-74.62	-84.44	-82.28	-87.89
Model 3	-85.04	-81.16	-77.75	-69.28	-44.41	-73.12	-80.47	-79.12
Model 4	-90.14	-83.36	-73.45	-73.43	-71.14	-43.69	-80.87	-87.50
Model 5	-87.94	-85.93	-82.55	-75.00	-74.70	-69.48	-38.59	-76.14
Model 6	-91.16	-68.13	-76.20	-79.07	-47.11	-60.99	-72.36	-57.41
Model 7	-54.03	-54.18	-32.74	-42.12	-43.31	25.88	21.66	-68.99
Model 8	-72.01	-56.51	-64.55	-47.83	-55.68	-61.61	-14.17	-15.12
SA model	-80.10	-84.26	-83.24	-84.67	-83.04	-83.29	-53.55	-66.97
OSFA model	-71.15	-75.81	-74.02	-71.35	-73.02	-72.55	-41.92	-55.26

Table A-48: Subject 16: Percentage change of f_d in σ_e^2 when sorted based on run order. Motion disturbance: Heave. Screen direction: Vertical.

	Run 1	Run 2	Run 3	Run 4	Run 5	Run 6	Run 7	Run 8
Model 1	-93.07	-90.46	-90.09	-88.24	-91.32	-63.40	-85.46	-91.36
Model 2	-91.29	-89.84	-87.92	-90.39	-87.33	-87.35	-75.51	-88.28
Model 3	-91.37	-88.49	-85.02	-85.80	-85.20	-81.46	-82.52	-74.97
Model 4	-92.58	-80.60	-84.15	-78.55	-74.52	-86.28	-86.84	-73.61
Model 5	-94.21	-38.13	-82.91	-86.41	-91.91	-93.04	-83.41	-77.45
Model 6	-94.39	-86.05	-84.38	-86.28	-92.32	-90.44	-85.88	-93.11
Model 7	-94.16	-92.70	-87.69	-83.80	-87.81	-92.99	-90.83	-87.43
Model 8	-82.28	-82.13	-78.95	-80.53	-67.57	-84.37	-84.16	-82.27
SA model	-91.65	-91.31	-88.35	-83.62	-87.85	-92.06	-93.04	-84.32
OSFA model	-80.75	-80.48	-82.51	-66.35	-82.90	-75.47	-77.18	-76.62

A-4 Disturbance: Surge (X), Screen input: Horizontal

Table A-49: Subject 1: Percentage change of f_d in σ_e^2 when sorted based on run order. Motion disturbance: Surge. Screen direction: Horizontal.

	Run 1	Run 2	Run 3	Run 4	Run 5	Run 6	Run 7	Run 8
Model 1	-85.25	-83.68	-83.30	-69.21	-83.79	-80.70	-63.93	-64.27
Model 2	-90.86	-79.51	-86.34	-78.29	-90.18	-76.16	-68.46	-90.44
Model 3	-82.81	-82.63	-71.97	-78.56	-70.75	-82.86	-69.05	-61.67
Model 4	-79.70	-85.73	-88.70	-86.39	-90.91	-87.61	-87.57	-85.65
Model 5	-84.26	-81.02	-60.66	-65.94	-81.74	-81.50	-83.67	-66.17
Model 6	-89.21	-74.74	-64.85	-88.68	-83.57	-76.80	-84.18	-73.25
Model 7	-91.70	-86.26	-89.02	-84.21	-83.64	-88.52	-87.84	-92.15
Model 8	-88.51	-83.33	-83.83	-83.52	-76.53	-80.94	-83.47	-84.47
SA model	-83.57	-86.56	-78.47	-91.90	-82.18	-82.95	-93.63	-88.33
OSFA model	-70.10	-54.03	-48.84	-65.42	-71.58	-54.26	-69.45	-65.04

Table A-50: Subject 2: Percentage change of f_d in σ_e^2 when sorted based on run order. Motion disturbance: Surge. Screen direction: Horizontal.

	Run 1	Run 2	Run 3	Run 4	Run 5	Run 6	Run 7	Run 8
Model 1	-90.40	-52.55	-62.44	-65.17	-85.71	-78.22	-79.05	-70.60
Model 2	-78.71	-61.16	-67.80	-47.74	-63.67	-76.01	-75.72	-68.43
Model 3	-90.47	-77.43	-74.29	-79.51	-86.43	-85.89	-88.08	-89.15
Model 4	-83.49	-83.24	-70.98	-65.78	-74.90	-84.23	-83.41	-81.74
Model 5	-88.81	-87.75	-87.90	-77.95	-77.87	-73.16	-80.16	-81.87
Model 6	-83.24	-76.76	-80.51	-77.93	-69.24	-55.44	-76.48	-81.71
Model 7	-91.04	-87.97	-83.36	-85.64	-86.22	-70.39	-66.27	-77.80
Model 8	-77.24	-71.77	-77.54	-71.05	-76.41	-72.07	-69.87	-43.74
SA model	-77.82	-75.49	-89.51	-83.44	-87.83	-80.34	-85.54	-76.23
OSFA model	-78.60	-75.39	-85.48	-78.54	-85.15	-74.75	-79.37	-70.61

Table A-51: Subject 3: Percentage change of f_d in σ_e^2 when sorted based on run order. Motion disturbance: Surge. Screen direction: Horizontal.

	Run 1	Run 2	Run 3	Run 4	Run 5	Run 6	Run 7	Run 8
Model 1	-92.73	-81.13	-88.39	-80.45	-86.09	-80.66	-91.99	-86.76
Model 2	-73.62	-65.19	-72.53	-72.88	-68.98	-73.24	-68.79	-65.00
Model 3	-90.81	-91.50	-90.12	-89.60	-92.39	-86.38	-89.08	-80.92
Model 4	-74.56	-61.59	-70.49	-64.79	-67.68	-70.90	-68.53	-73.88
Model 5	-88.38	-83.21	-83.54	-88.53	-84.05	-85.70	-88.57	-83.58
Model 6	-85.31	-84.15	-80.51	-72.33	-83.17	-73.47	-85.00	-83.89
Model 7	-77.45	-72.39	-76.85	-70.77	-69.66	-78.21	-69.38	-77.31
Model 8	-86.82	-86.30	-83.58	-85.22	-78.23	-78.49	-86.32	-78.20
SA model	-88.15	-73.08	-91.30	-72.55	-88.83	-84.23	-77.12	-85.97
OSFA model	-86.22	-59.24	-74.91	-69.59	-78.26	-64.25	-60.09	-67.34

Table A-52: Subject 4: Percentage change of f_d in σ_e^2 when sorted based on run order. Motion disturbance: Surge. Screen direction: Horizontal.

	Run 1	Run 2	Run 3	Run 4	Run 5	Run 6	Run 7	Run 8
Model 1	-80.09	-70.66	-73.79	-73.14	-67.88	-76.83	-74.33	-79.30
Model 2	-89.87	-88.97	-78.75	-81.18	-81.47	-77.32	-86.83	-82.81
Model 3	-89.97	-85.87	-88.33	-84.94	-73.85	-84.30	-79.68	-86.34
Model 4	-90.76	-85.38	-89.50	-89.94	-82.67	-75.02	-83.60	-83.52
Model 5	-80.21	-81.85	-82.06	-77.59	-77.75	-80.88	-58.47	-78.54
Model 6	-94.70	-81.68	-87.83	-90.68	-90.22	-91.26	-93.25	-88.39
Model 7	-89.52	-80.63	-65.16	-76.24	-75.95	-83.58	-83.74	-75.83
Model 8	-94.11	-81.19	-94.07	-84.93	-89.31	-91.67	-88.82	-89.92
SA model	-77.26	-87.18	-87.53	-88.56	-81.10	-93.15	-81.64	-92.89
OSFA model	-68.73	-79.47	-80.24	-81.05	-75.81	-76.61	-66.12	-78.31

Table A-53: Subject 5: Percentage change of f_d in σ_e^2 when sorted based on run order. Motion disturbance: Surge. Screen direction: Horizontal.

	Run 1	Run 2	Run 3	Run 4	Run 5	Run 6	Run 7	Run 8
Model 1	-56.66	-39.61	-45.18	-41.29	-40.95	-14.94	-33.14	-30.93
Model 2	-77.98	-53.10	-59.43	-67.51	-74.07	-61.24	-71.30	-70.01
Model 3	-76.50	-68.79	-47.01	-68.52	-71.18	-65.99	-38.26	-69.41
Model 4	-85.64	-76.36	-77.17	-44.36	-67.21	-73.81	-72.68	-47.36
Model 5	-79.12	-49.31	-55.37	-72.14	-63.32	-58.02	-61.58	-75.94
Model 6	-77.63	-68.17	-60.51	-69.36	-75.47	-58.00	-67.45	-68.30
Model 7	-68.12	-59.26	-38.30	-58.08	-62.61	-57.80	-48.52	-58.85
Model 8	-65.36	-67.30	-62.24	-39.90	-60.34	-67.89	-59.91	-45.96
SA model	-43.76	-72.02	-69.95	-75.09	-70.49	-74.32	-65.90	-66.29
OSFA model	-4.86	-64.23	-67.82	-83.30	-46.22	-64.84	-54.53	-65.30

Table A-54: Subject 6: Percentage change of f_d in σ_e^2 when sorted based on run order. Motion disturbance: Surge. Screen direction: Horizontal.

	Run 1	Run 2	Run 3	Run 4	Run 5	Run 6	Run 7	Run 8
Model 1	-54.78	5.79	44.76	0.57	32.14	-4.71	120.90	75.41
Model 2	-89.77	-51.85	-85.55	-89.18	-83.42	-87.16	-53.60	-86.50
Model 3	-87.65	-86.08	-41.43	-76.48	-83.14	-75.62	-80.32	-47.25
Model 4	-49.51	-70.58	-72.59	-43.81	-70.17	-72.94	-70.00	-72.48
Model 5	-87.20	-52.32	-84.57	-88.98	-51.33	-86.41	-87.74	-80.14
Model 6	-89.52	-85.08	-59.47	-73.56	-82.02	-63.02	-85.84	-86.45
Model 7	-87.16	-82.04	-85.84	-51.72	-81.88	-87.12	-53.42	-85.67
Model 8	-92.39	-85.76	-86.13	-87.44	-55.85	-67.10	-81.18	-66.96
SA model	10.77	-84.97	-77.25	-71.46	-83.41	-87.82	-83.70	-87.39
OSFA model	-34.77	-75.81	-65.60	-63.40	-74.45	-84.72	-76.40	-87.35

Table A-55: Subject 7: Percentage change of f_d in σ_e^2 when sorted based on run order. Motion disturbance: Surge. Screen direction: Horizontal.

	Run 1	Run 2	Run 3	Run 4	Run 5	Run 6	Run 7	Run 8
Model 1	-56.46	-34.44	-29.77	-21.99	-55.10	-43.64	-46.51	-39.43
Model 2	-37.07	-49.55	-46.88	-19.19	-35.14	-53.27	-33.16	-50.83
Model 3	-35.79	-35.05	-46.94	-27.30	-20.34	-21.22	-44.75	-42.21
Model 4	-28.10	-24.71	-31.15	-1.27	-22.86	-21.79	9.81	-6.95
Model 5	-63.04	-51.63	-51.57	-42.94	-64.76	-40.63	-29.29	-30.55
Model 6	-59.54	-21.48	-24.43	-36.67	-41.03	-13.90	-36.07	-18.11
Model 7	-19.76	25.53	6.34	-21.77	-10.05	-19.14	9.59	-11.20
Model 8	-40.54	-22.34	4.38	-29.61	-31.32	-39.95	-34.12	-24.03
SA model	-45.11	-44.91	-41.14	-29.77	-51.71	-42.72	-14.71	-36.73
OSFA model	1.08	7.97	-39.28	125.53	-42.20	134.01	119.55	80.87

Table A-56: Subject 8: Percentage change of f_d in σ_e^2 when sorted based on run order. Motion disturbance: Surge. Screen direction: Horizontal.

	Run 1	Run 2	Run 3	Run 4	Run 5	Run 6	Run 7	Run 8
Model 1	-65.08	-22.59	-53.77	-48.17	-48.00	-53.46	-23.89	-57.95
Model 2	-75.08	-72.69	-29.41	-73.35	-69.19	-69.30	-74.49	-49.09
Model 3	-82.50	-69.22	-64.64	-17.42	-67.72	-71.67	-73.43	-77.24
Model 4	-64.03	-60.61	-52.16	-48.83	-22.73	-53.55	-64.07	-62.25
Model 5	-87.56	-81.32	-76.53	-71.94	-67.65	-22.72	-74.67	-85.37
Model 6	-56.44	-56.83	-57.00	-54.96	-49.16	-43.42	-19.25	-50.85
Model 7	-62.15	-51.83	-53.77	-56.51	-38.74	-57.21	-43.18	-17.71
Model 8	-22.85	-63.21	-62.08	-62.99	-66.35	-56.27	-62.32	-53.89
SA model	-51.40	-71.14	-71.05	-62.84	-79.80	-55.35	-60.63	-64.48
OSFA model	-14.54	-40.67	-70.40	-60.03	-81.32	-54.47	-31.91	-49.40

Table A-57: Subject 9: Percentage change of f_d in σ_e^2 when sorted based on run order. Motion disturbance: Surge. Screen direction: Horizontal.

	Run 1	Run 2	Run 3	Run 4	Run 5	Run 6	Run 7	Run 8
Model 1	-82.47	-80.73	-81.48	-76.70	-81.20	-73.65	-73.40	-77.78
Model 2	-87.20	-83.10	-82.85	-84.52	-73.53	-84.15	-86.36	-85.89
Model 3	-86.58	-86.98	-84.18	-85.16	-85.91	-73.57	-85.22	-85.20
Model 4	-92.62	-90.89	-90.59	-82.94	-83.42	-86.02	-68.90	-84.54
Model 5	-87.46	-84.10	-88.08	-85.71	-84.70	-86.67	-86.61	-72.29
Model 6	-76.11	-88.03	-91.18	-90.54	-91.59	-87.76	-88.41	-89.82
Model 7	-85.96	-79.99	-85.74	-79.10	-79.55	-82.99	-86.35	-84.67
Model 8	-86.29	-85.94	-70.71	-86.77	-86.98	-90.45	-87.61	-83.53
SA model	-80.79	-85.95	-86.78	-87.47	-86.43	-90.81	-85.41	-86.90
OSFA model	-80.33	-77.96	-79.84	-77.67	-79.50	-83.92	-83.24	-77.55

Table A-58: Subject 10: Percentage change of f_d in σ_e^2 when sorted based on run order. Motion disturbance: Surge. Screen direction: Horizontal.

	Run 1	Run 2	Run 3	Run 4	Run 5	Run 6	Run 7	Run 8
Model 1	-58.65	-49.92	-74.87	-36.86	-70.51	-72.08	-66.31	-55.22
Model 2	-79.25	-68.63	-74.22	-53.63	-38.08	-59.33	-48.64	-62.42
Model 3	-64.83	-52.69	-52.25	-46.97	-67.95	-36.17	-63.21	-64.36
Model 4	-84.58	-73.10	-63.28	-60.89	-56.02	-81.89	-40.71	-78.26
Model 5	-88.05	-77.26	-77.62	-77.10	-79.65	-72.62	-82.57	-47.09
Model 6	-47.13	-3.68	21.93	40.80	-32.15	9.21	-35.20	50.91
Model 7	-86.55	-42.38	-80.73	-84.55	-78.12	-62.45	-64.18	-55.59
Model 8	-69.75	-49.08	-38.37	-60.96	-42.10	-57.30	-71.37	-65.73
SA model	-62.85	-71.81	-62.49	-74.32	-76.49	-0.58	-74.71	-61.19
OSFA model	-68.19	-3.44	-63.34	-74.92	-43.20	133.85	-83.02	7.91

Table A-59: Subject 11: Percentage change of f_d in σ_e^2 when sorted based on run order. Motion disturbance: Surge. Screen direction: Horizontal.

	Run 1	Run 2	Run 3	Run 4	Run 5	Run 6	Run 7	Run 8
Model 1	-68.26	-5.02	69.91	46.71	-0.61	64.93	149.61	202.10
Model 2	-84.90	-40.05	-64.32	-80.64	-78.30	-71.36	-77.05	-79.19
Model 3	-64.84	-54.11	-32.32	-41.60	-55.84	-53.96	-49.41	-55.28
Model 4	-86.27	-72.84	-77.19	-48.55	-79.78	-84.72	-85.44	-82.58
Model 5	-75.28	-74.69	-67.48	-70.21	-47.50	-69.54	-76.86	-76.55
Model 6	-91.85	-86.77	-88.15	-83.52	-87.47	-54.69	-77.86	-92.87
Model 7	-84.83	-83.98	-80.13	-81.02	-76.69	-80.35	-48.75	-73.38
Model 8	-80.73	-80.00	-81.55	-81.24	-82.22	-63.36	-70.83	-47.31
SA model	47.31	-78.29	-54.43	-86.40	-76.99	-91.58	-83.90	-82.71
OSFA model	16.15	-73.59	-56.36	-84.45	-73.96	-88.09	-80.06	-79.55

Table A-60: Subject 12: Percentage change of f_d in σ_e^2 when sorted based on run order. Motion disturbance: Surge. Screen direction: Horizontal.

	Run 1	Run 2	Run 3	Run 4	Run 5	Run 6	Run 7	Run 8
Model 1	-86.72	-5.38	-63.68	-39.49	-51.95	-42.90	-63.75	-69.18
Model 2	-55.44	-62.32	-46.05	-70.78	-55.91	-56.69	-58.37	-68.64
Model 3	-83.09	-68.01	-69.27	-37.30	-78.23	-61.92	-70.16	-58.02
Model 4	-82.86	-66.22	-58.83	-61.02	-80.63	-77.33	-74.33	-73.18
Model 5	-79.18	-80.48	-71.87	-65.63	-67.46	-78.83	-82.22	-79.94
Model 6	-83.81	-80.86	-79.83	-69.42	-66.86	-57.58	-82.12	-79.47
Model 7	-89.16	-88.65	-85.22	-85.69	-78.97	-71.31	-67.77	-86.54
Model 8	-92.08	-83.51	-86.17	-80.70	-86.53	-69.78	-64.52	-61.54
SA model	-65.10	-65.88	-74.17	-75.12	-80.34	-79.92	-87.10	-81.98
OSFA model	-18.24	-63.64	-52.38	-76.74	-77.53	-70.51	-84.93	-86.29

Table A-61: Subject 13: Percentage change of f_d in σ_e^2 when sorted based on run order. Motion disturbance: Surge. Screen direction: Horizontal.

	Run 1	Run 2	Run 3	Run 4	Run 5	Run 6	Run 7	Run 8
Model 1	-16.65	-5.97	-8.77	-11.63	-9.63	-4.01	-6.42	4.71
Model 2	-78.04	-23.92	-44.49	-47.68	-53.07	-50.26	-66.80	-65.84
Model 3	-77.12	-75.51	-31.27	-38.98	-68.78	-66.87	-69.59	-61.14
Model 4	-85.57	-84.57	-83.99	-14.51	-64.42	-71.12	-80.21	-73.46
Model 5	-68.87	-43.79	-66.61	-42.74	-5.71	-31.22	-67.79	-64.79
Model 6	-81.28	-72.54	-75.32	-77.99	-69.46	9.40	-63.93	-71.64
Model 7	-58.89	-59.08	-58.90	-49.60	-61.63	-56.16	-32.16	-36.54
Model 8	-41.41	-64.24	-66.46	-63.21	-39.91	-51.63	-17.18	38.56
SA model	10.77	-54.44	-40.95	-50.65	-13.58	-29.95	-22.53	6.86
OSFA model	14.78	-74.18	-59.21	-67.70	-15.38	-43.63	-37.24	16.25

Table A-62: Subject 14: Percentage change of f_d in σ_e^2 when sorted based on run order. Motion disturbance: Surge. Screen direction: Horizontal.

	Run 1	Run 2	Run 3	Run 4	Run 5	Run 6	Run 7	Run 8
Model 1	-84.44	-71.42	-69.55	-77.46	-81.02	-79.66	-81.47	-62.34
Model 2	-94.24	-63.84	-90.10	-77.42	-74.07	-80.42	-87.27	-77.33
Model 3	-76.88	-65.63	-65.10	-76.78	-69.27	-75.09	-77.74	-78.57
Model 4	-75.88	-71.16	-61.40	-58.87	-74.38	-71.07	-72.78	-75.66
Model 5	-88.73	-88.91	-84.99	-72.44	-76.28	-84.70	-81.99	-84.51
Model 6	-87.19	-90.71	-90.79	-85.07	-75.26	-69.15	-89.04	-88.61
Model 7	-85.52	-77.63	-80.92	-77.87	-70.18	-59.30	-60.46	-72.50
Model 8	-92.11	-80.32	-81.76	-85.98	-90.23	-83.82	-84.97	-64.67
SA model	-81.20	-84.67	-78.58	-75.49	-88.70	-90.65	-78.85	-88.45
OSFA model	-58.18	-82.52	-70.77	-73.13	-79.24	-88.54	-79.82	-87.80

Table A-63: Subject 15: Percentage change of f_d in σ_e^2 when sorted based on run order. Motion disturbance: Surge. Screen direction: Horizontal.

	Run 1	Run 2	Run 3	Run 4	Run 5	Run 6	Run 7	Run 8	Run 9
Model 1	-77.47	-68.15	-63.89	-55.57	-63.94	-55.76	-64.63	-66.15	-75.42
Model 2	-93.35	-81.59	-70.40	-63.14	-54.71	-63.32	-59.79	-64.86	-67.68
Model 3	-69.81	-57.04	-76.83	-71.99	-72.23	-62.03	-72.56	-61.90	-67.52
Model 4	-59.26	-58.98	-50.54	-66.06	-58.35	-58.65	-51.23	-60.20	-48.78
Model 5	-70.96	-55.57	-68.11	-34.50	-65.00	-64.77	-68.23	-63.11	-62.60
Model 6	-79.10	-48.85	-73.59	-66.25	-28.87	-73.16	-71.40	-73.36	-61.05
Model 7	-62.14	-70.27	-53.17	-59.93	-61.89	2.80	-57.91	-63.74	-70.99
Model 8	-54.33	-47.52	-48.12	-46.16	-42.89	-48.61	-19.49	-48.66	-52.85
Model 9	-76.72	-73.92	-56.06	-71.70	-50.23	-62.85	-61.18	-62.70	-74.95
SA model	-72.48	-74.17	-75.62	-63.58	-68.88	-74.29	-65.99	-53.13	-73.43
OSFA model	-75.71	-80.75	-76.64	-63.24	-67.63	-64.57	-55.46	-52.00	-80.53

Table A-64: Subject 16: Percentage change of f_d in σ_e^2 when sorted based on run order. Motion disturbance: Surge. Screen direction: Horizontal.

	Run 1	Run 2	Run 3	Run 4	Run 5	Run 6	Run 7	Run 8
Model 1	-79.68	-37.90	-21.70	-37.23	-68.80	-75.99	-65.87	-71.97
Model 2	-75.43	-65.42	-69.80	-58.97	-68.22	-77.99	-69.55	-78.65
Model 3	-58.17	-53.13	-49.62	-61.67	-57.22	-61.53	-58.41	-50.73
Model 4	-54.65	-60.25	-56.98	-52.41	-55.63	-55.22	-54.66	-59.79
Model 5	-88.61	-80.40	-87.95	-82.33	-78.00	-84.46	-71.45	-82.57
Model 6	-86.72	-79.00	-66.89	-78.28	-70.56	-67.23	-86.22	-84.30
Model 7	-84.63	-80.69	-73.02	-64.20	-72.86	-66.67	-63.90	-79.81
Model 8	-84.63	-84.33	-84.68	-76.80	-65.86	-76.17	-68.35	-65.70
SA model	-63.92	-77.25	-60.03	-61.31	-88.51	-82.08	-77.88	-80.50
OSFA model	-60.86	-75.50	-58.98	-61.38	-87.51	-80.39	-77.54	-79.95

Appendix B

Estimated BDFT Model Parameters

The tables below present the estimated BDFT model parameters in the AIAA Paper for each experiment participant during the system identification session. The BDFT models were identified for two conditions:

HOR: later motion disturbance with horizontal touchscreen input.
VER: vertical motion disturbance with vertical touchscreen input.

The BDFT model was defined by the following transfer function:

$$H_{BDFT}(s) = G_{BDFT} \cdot \frac{\omega_{BDFT}^2}{s^2 + 2\zeta_{BDFT}\omega_{BDFT} \cdot s + \omega_{BDFT}^2} e^{-s\tau_{BDFT}}$$

Four model parameters were therefore identified. Their symbols and units are:

Gain, G_{BDFT} [mm/(m/s^2)]
Natural frequency, ω_{BDFT} [rad/s]
Damping ratio, ζ_{BDFT} [-]
Time delay, τ_{BDFT} [s]

Table B-1: Estimated BDFT parameters Subject 1

	G_{BDFT}		ω_{BDFT}		ζ_{BDFT}		τ_{BDFT}	
	HOR	VER	HOR	VER	HOR	VER	HOR	VER
Run 1	28.97	25.62	5.08	4.88	0.67	0.77	0.10	0.06
Run 2	33.86	21.05	4.79	5.41	0.78	0.86	0.10	0.06
Run 3	22.30	32.25	5.47	4.60	0.55	1.00	0.09	0.07
Run 4	24.57	17.28	4.99	7.08	0.67	1.03	0.10	0.09

Table B-2: Estimated BDFT parameters Subject 2

	G_{BDFT}		ω_{BDFT}		ζ_{BDFT}		τ_{BDFT}	
	HOR	VER	HOR	VER	HOR	VER	HOR	VER
Run 1	25.74	31.41	6.46	4.93	0.59	0.83	0.08	0.06
Run 2	34.68	23.60	6.29	6.77	0.72	1.16	0.09	0.09
Run 3	24.75	22.23	6.89	6.05	0.70	1.07	0.09	0.07
Run 4	34.17	23.15	5.83	6.48	0.82	1.38	0.09	0.08

Table B-3: Estimated BDFT parameters Subject 3

	G_{BDFT}		ω_{BDFT}		ζ_{BDFT}		τ_{BDFT}	
	HOR	VER	HOR	VER	HOR	VER	HOR	VER
Run 1	32.85	21.08	6.09	6.99	0.91	1.21	0.10	0.09
Run 2	29.69	20.56	6.16	5.82	0.81	0.82	0.10	0.06
Run 3	24.18	16.69	6.78	8.11	0.81	1.23	0.09	0.09
Run 4	21.46	16.47	6.79	7.16	0.83	0.96	0.11	0.09

Table B-4: Estimated BDFT parameters Subject 4

	G_{BDFT}		ω_{BDFT}		ζ_{BDFT}		τ_{BDFT}	
	HOR	VER	HOR	VER	HOR	VER	HOR	VER
Run 1	35.00	18.74	7.34	7.26	0.78	0.96	0.11	0.07
Run 2	31.59	18.14	7.44	8.82	0.67	1.02	0.11	0.08
Run 3	35.00	16.43	7.16	8.23	0.67	0.86	0.10	0.08
Run 4	31.08	18.44	7.76	8.60	0.72	0.96	0.11	0.09

Table B-5: Estimated BDFT parameters Subject 5

	G_{BDFT}		ω_{BDFT}		ζ_{BDFT}		τ_{BDFT}	
	HOR	VER	HOR	VER	HOR	VER	HOR	VER
Run 1	19.62	14.39	9.07	15.00	0.92	1.53	0.09	0.11
Run 2	24.18	15.58	8.49	10.10	1.00	0.99	0.10	0.08
Run 3	12.60	12.54	10.52	9.79	0.61	0.81	0.11	0.08
Run 4	20.81	17.03	8.43	11.22	0.84	1.38	0.09	0.10

Table B-6: Estimated BDFT parameters Subject 6

	G_{BDFT}		ω_{BDFT}		ζ_{BDFT}		τ_{BDFT}	
	HOR	VER	HOR	VER	HOR	VER	HOR	VER
Run 1	24.76	12.54	5.82	7.77	0.90	1.23	0.07	0.07
Run 2	25.12	15.08	7.12	6.20	1.24	0.79	0.08	0.05
Run 3	25.67	13.63	6.16	8.96	0.90	1.38	0.07	0.08
Run 4	33.14	12.97	5.79	7.07	1.19	1.06	0.07	0.06

Table B-7: Estimated BDFT parameters Subject 7

	G_{BDFT}		ω_{BDFT}		ζ_{BDFT}		τ_{BDFT}	
	HOR	VER	HOR	VER	HOR	VER	HOR	VER
Run 1	34.69	29.31	6.31	6.00	0.74	1.12	0.10	0.07
Run 2	35.00	22.04	6.26	7.44	0.76	1.09	0.11	0.08
Run 3	34.68	22.66	6.30	7.05	0.71	0.93	0.10	0.07
Run 4	35.00	25.91	6.22	6.32	0.83	1.04	0.11	0.06

Table B-8: Estimated BDFT parameters Subject 8

	G_{BDFT}		ω_{BDFT}		ζ_{BDFT}		τ_{BDFT}	
	HOR	VER	HOR	VER	HOR	VER	HOR	VER
Run 1	29.36	11.91	6.59	5.61	0.66	0.39	0.12	0.05
Run 2	22.57	24.83	7.76	5.58	0.82	0.95	0.13	0.06
Run 3	32.56	30.34	6.78	5.35	0.87	1.12	0.12	0.07
Run 4	23.19	19.04	6.85	7.54	0.62	1.00	0.11	0.08

Table B-9: Estimated BDFT parameters Subject 9

	G_{BDFT}		ω_{BDFT}		ζ_{BDFT}		τ_{BDFT}	
	HOR	VER	HOR	VER	HOR	VER	HOR	VER
Run 1	20.65	9.16	6.49	8.94	0.66	0.99	0.08	0.08
Run 2	17.22	9.18	6.44	6.95	0.50	0.64	0.08	0.06
Run 3	15.81	20.84	7.38	5.96	0.47	0.91	0.09	0.07
Run 4	19.89	10.36	7.08	6.45	0.68	0.42	0.10	0.05

Table B-10: Estimated BDFT parameters Subject 10

	G_{BDFT}		ω_{BDFT}		ζ_{BDFT}		τ_{BDFT}	
	HOR	VER	HOR	VER	HOR	VER	HOR	VER
Run 1	27.80	25.24	6.04	4.76	0.54	0.92	0.10	0.07
Run 2	27.80	29.64	6.06	4.98	0.66	0.93	0.11	0.08
Run 3	30.23	21.25	6.09	5.80	0.71	0.92	0.10	0.07
Run 4	28.86	21.60	6.37	5.65	0.68	0.91	0.11	0.07

Table B-11: Estimated BDFT parameters Subject 11

	G_{BDFT}		ω_{BDFT}		ζ_{BDFT}		τ_{BDFT}	
	HOR	VER	HOR	VER	HOR	VER	HOR	VER
Run 1	18.18	23.51	7.25	4.83	0.49	0.54	0.09	0.04
Run 2	24.91	19.65	6.30	5.90	0.61	0.51	0.10	0.04
Run 3	22.50	21.03	7.26	5.92	0.80	0.69	0.11	0.06
Run 4	24.06	19.54	6.68	5.99	0.70	0.56	0.12	0.05

Table B-12: Estimated BDFT parameters Subject 12

	G_{BDFT}		ω_{BDFT}		ζ_{BDFT}		τ_{BDFT}	
	HOR	VER	HOR	VER	HOR	VER	HOR	VER
Run 1	35.00	16.21	7.31	7.14	0.86	0.75	0.11	0.07
Run 2	24.48	15.66	7.70	7.44	0.63	0.90	0.10	0.08
Run 3	30.63	17.94	7.29	9.34	0.79	1.27	0.10	0.09
Run 4	18.46	10.57	8.23	7.46	0.54	0.61	0.11	0.07

Table B-13: Estimated BDFT parameters Subject 13

	G_{BDFT}		ω_{BDFT}		ζ_{BDFT}		τ_{BDFT}	
	HOR	VER	HOR	VER	HOR	VER	HOR	VER
Run 1	32.87	24.57	6.08	5.00	0.59	0.95	0.11	0.07
Run 2	35.00	19.47	6.07	5.93	0.54	0.79	0.12	0.07
Run 3	29.66	20.74	6.32	6.47	0.56	1.21	0.12	0.09
Run 4	29.13	19.75	6.61	5.62	0.57	0.72	0.12	0.07

Table B-14: Estimated BDFT parameters Subject 14

	G_{BDFT}		ω_{BDFT}		ζ_{BDFT}		τ_{BDFT}	
	HOR	VER	HOR	VER	HOR	VER	HOR	VER
Run 1	28.41	23.22	6.08	6.06	0.57	1.08	0.10	0.09
Run 2	32.48	20.30	5.56	6.31	0.50	0.88	0.10	0.09
Run 3	22.10	23.22	6.78	5.86	0.53	0.89	0.10	0.09
Run 4	33.70	24.18	5.61	5.69	0.70	0.81	0.10	0.09

Table B-15: Estimated BDFT parameters Subject 15

	G_{BDFT}		ω_{BDFT}		ζ_{BDFT}		τ_{BDFT}	
	HOR	VER	HOR	VER	HOR	VER	HOR	VER
Run 1	31.75	25.59	5.67	4.84	0.63	0.68	0.10	0.07
Run 2	25.42	30.01	6.58	5.43	0.68	0.93	0.11	0.08
Run 3	25.02	29.27	6.04	6.59	0.55	1.05	0.10	0.10
Run 4	26.13	29.55	7.52	6.06	0.74	1.08	0.13	0.09

Table B-16: Estimated BDFT parameters Subject 16

	G_{BDFT}		ω_{BDFT}		ζ_{BDFT}		τ_{BDFT}	
	HOR	VER	HOR	VER	HOR	VER	HOR	VER
Run 1	15.63	24.79	7.36	8.36	0.47	0.91	0.10	0.08
Run 2	18.75	19.12	8.03	9.62	0.56	0.76	0.10	0.09
Run 3	15.51	18.38	7.88	9.47	0.45	0.79	0.10	0.10
Run 4	18.39	23.80	8.69	8.95	0.58	0.96	0.12	0.09

Table B-17: Estimated BDFT parameters Subject 17

	G_{BDFT}		ω_{BDFT}		ζ_{BDFT}		τ_{BDFT}	
	HOR	VER	HOR	VER	HOR	VER	HOR	VER
Run 1	22.97	12.53	6.71	7.07	0.62	1.11	0.09	0.07
Run 2	22.85	10.37	6.50	7.51	0.70	1.03	0.09	0.07
Run 3	22.31	8.69	6.99	8.07	0.67	1.00	0.08	0.07
Run 4	21.89	7.95	7.23	6.87	0.77	0.58	0.09	0.04

Table B-18: Estimated BDFT parameters Subject 18

	G_{BDFT}		ω_{BDFT}		ζ_{BDFT}		τ_{BDFT}	
	HOR	VER	HOR	VER	HOR	VER	HOR	VER
Run 1	34.70	23.64	6.44	6.99	0.60	1.30	0.11	0.10
Run 2	35.00	24.26	6.65	7.08	0.59	1.38	0.11	0.10
Run 3	34.31	21.34	6.78	7.56	0.60	1.34	0.11	0.10
Run 4	30.99	20.58	7.02	6.80	0.65	0.99	0.11	0.08

Appendix C

Between-Subject Variability

In an effort to find a cause for between-subject differences as presented in the AIAA Paper, several scatter plots are presented in this appendix. Because variables with different scales and units are compared, normalization was necessary. All variables was normalized according to Equation (C.1), where x is the vector to be normalized.

$$x_{norm} = \frac{x - \min x}{\max x - \min x} \tag{C.1}$$

Results are reported for lateral motion disturbance with horizontal touchscreen input (HOR) and vertical motion disturbance with vertical touchscreen input (VER). The numbered labels next to the data points, which have been averaged cross runs, represent each participant.

C-1 BDFT Vs. Anthropometric Measures

A potential cause for differences in magnitude of BDFT observed between people is the variation in the anthropometric measures of height, weight and BMI. In Figure C-1 and Figure C-2 the normalized BDFT are plotted against these anthropometric measures for HOR. In Figure C-3 and Figure C-4 the VER conditions are shown. In Figure C-1 and Figure C-3 the BDFT is from the system identification session of the experiment. In Figure C-2 and Figure C-4 the BDFT is taken from the BDFT cancellation session. No strong relationship is observed between the between the anthropometric measures and the magnitude of BDFT.

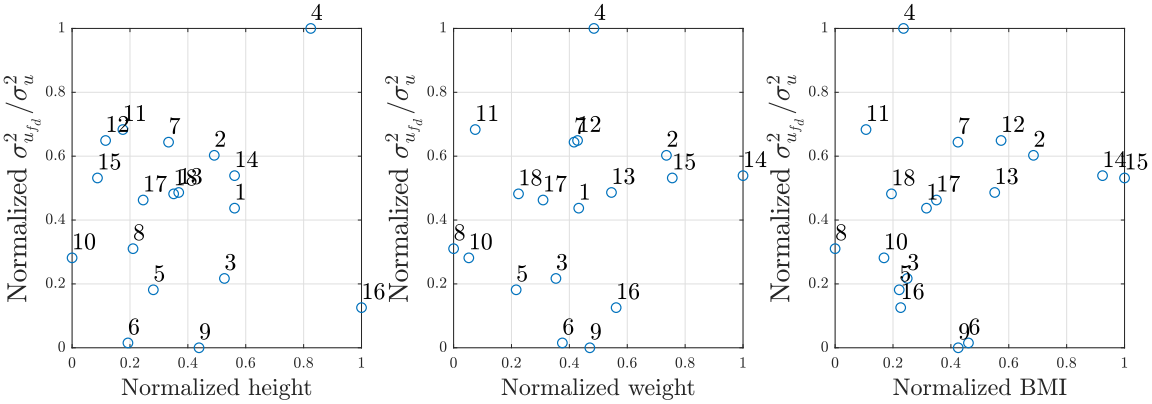

Figure C-1: Scatterplots of anthropometric measures (height, weight and BMI) against BDFT ($\sigma^2_{u_{f_d}}/\sigma^2_u$) in the system identification experiment session for each subject. Condition: HOR.

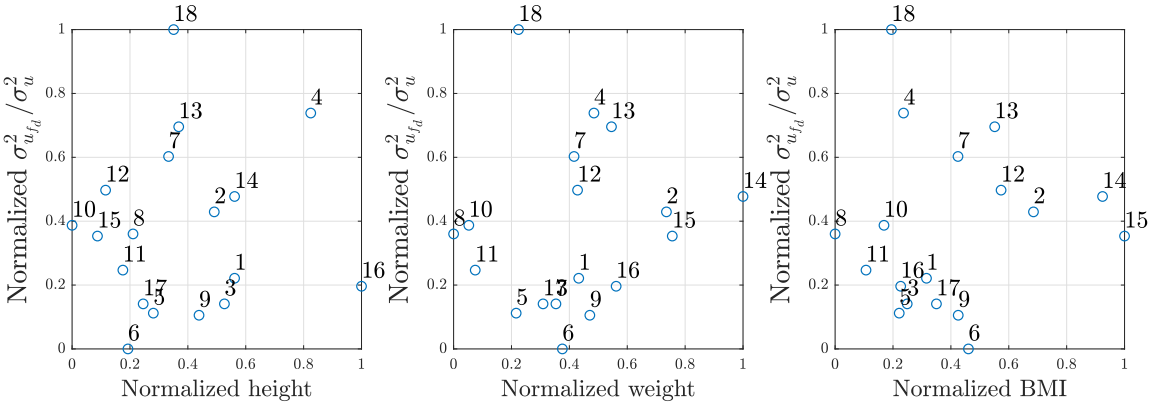

Figure C-2: Scatterplots of anthropometric measures (height, weight and BMI) against BDFT ($\sigma^2_{u_{f_d}}/\sigma^2_u$) in the BDFT cancellation experiment session for each subject. Condition: HOR.

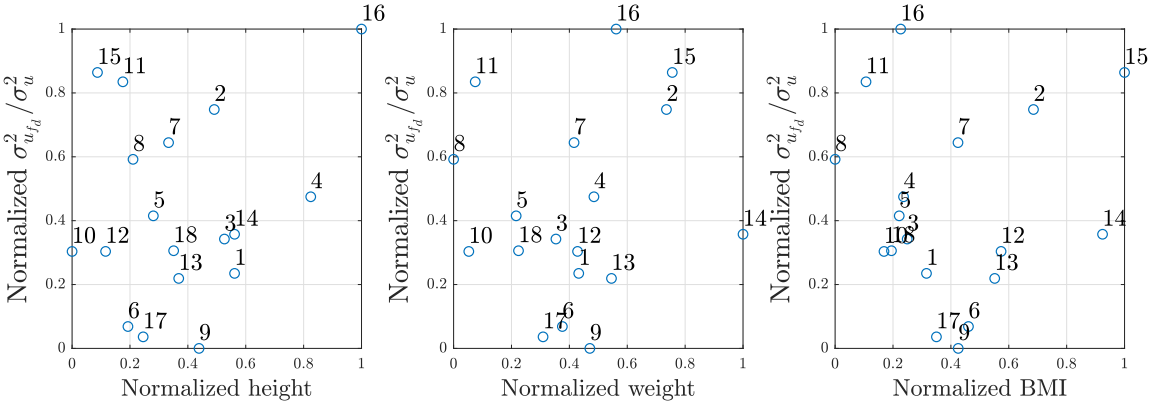

Figure C-3: Scatterplots of anthropometric measures (height, weight and BMI) against BDFT ($\sigma^2_{u_{f_d}}/\sigma^2_u$) in the system identification experiment session for each subject. Condition: VER.

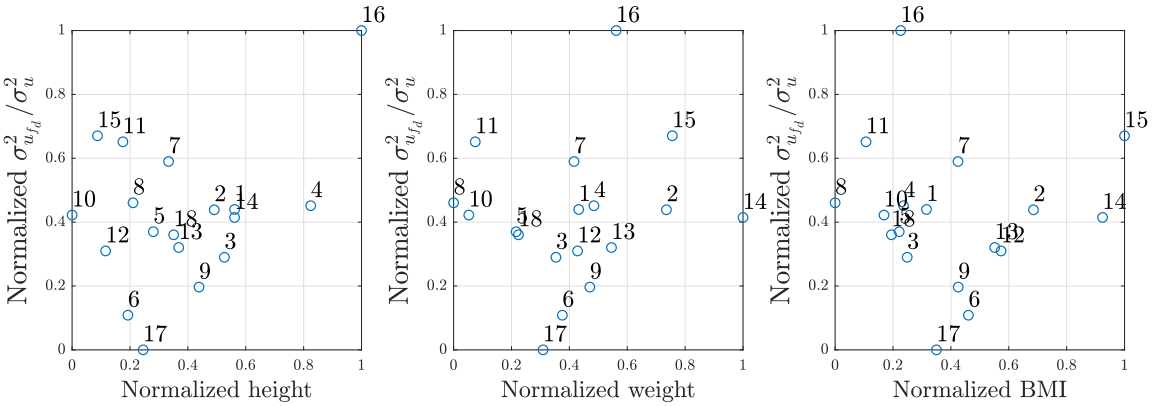

Figure C-4: Scatterplots of anthropometric measures (height, weight and BMI) against BDFT ($\sigma^2_{u_{f_d}}/\sigma^2_u$) in the BDFT cancellation experiment session for each subject. Condition: VER.

C-2 BDFT Model Parameters Vs. Anthropometric Measures

The following figures show the normalized BDFT model parameters estimated from the system identification against the normalized BDFT. The results for HOR are shown in

Figure C-5 while the VER condition is seen in Figure C-6. The only strong relationship is observed between G_{BDFT} and the BDFT. Since the gain models the magnitude of BDFT this is an expected result.

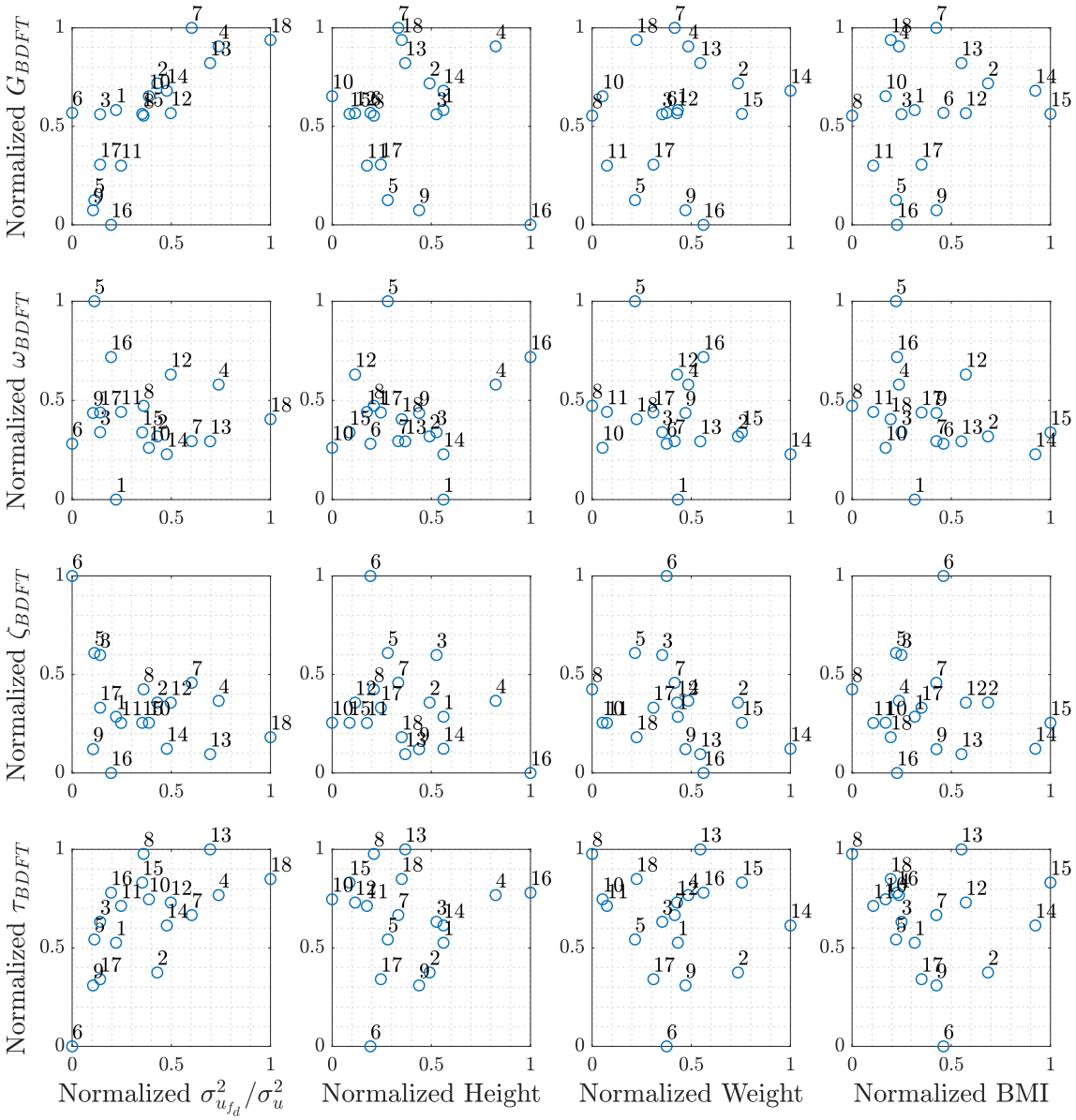

Figure C-5: Scatterplots of normalized BDFT model parameters against BDFT ($\sigma^2_{u_{f_d}}/\sigma^2_u$) in the system identification experiment session, and anthropometric measures (height, weight and BMI) for each subject. Condition: HOR.

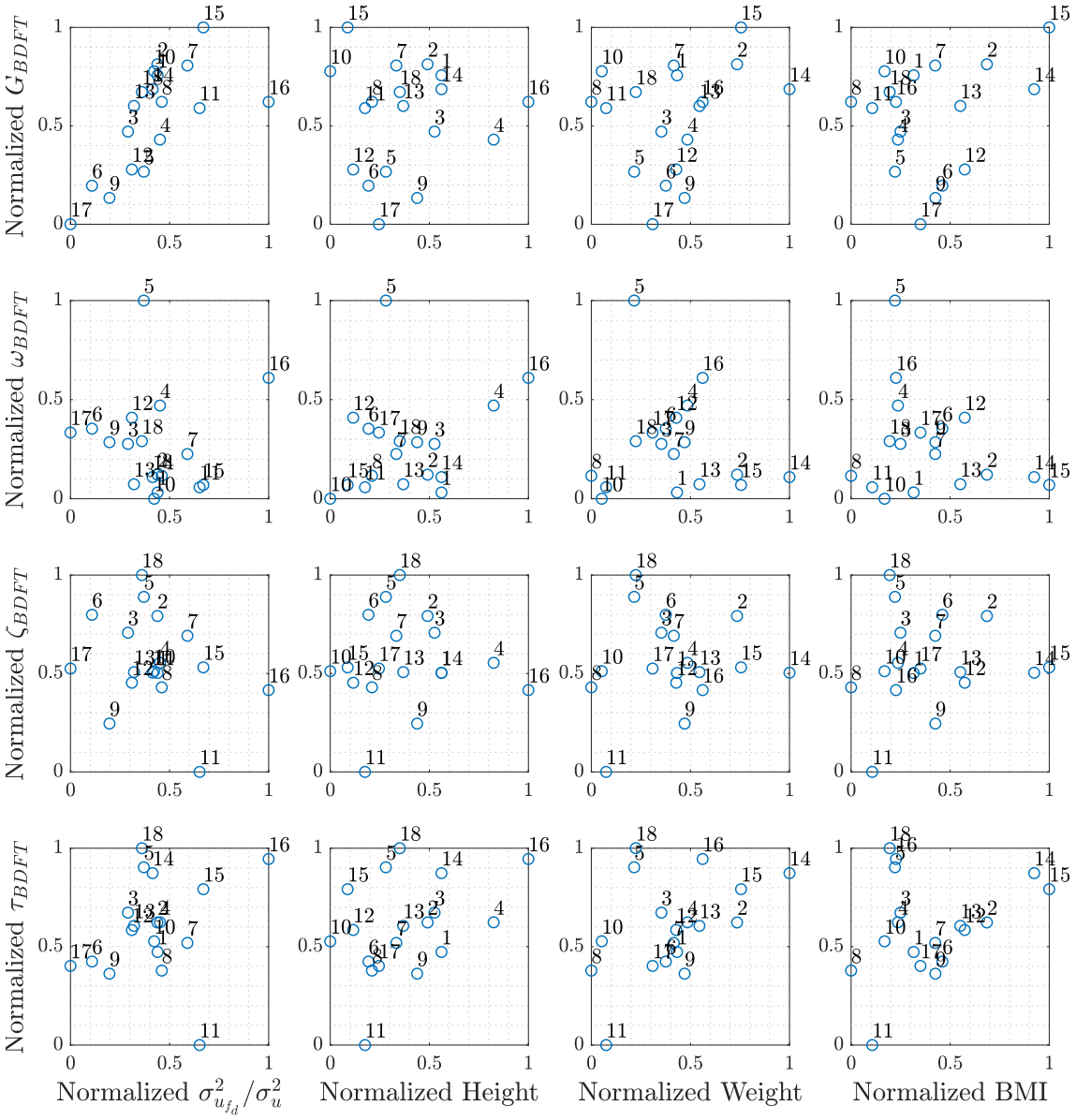

Figure C-6: Scatterplots of normalized BDFT model parameters against BDFT ($\sigma^2_{u_{f_d}}/\sigma^2_u$) in the system identification experiment session, and anthropometric measures (height, weight and BMI) for each subject. Condition: VER.

C-3 BDFT Vs. Days Between Experiment Sessions

Each participant had to be present for two experiment session over two days. The goal of day 1 was to gather data which was later used for identifying BDFT models. The second day used the identified models for model-based BDFT cancellation. However, there was a range of 3-14 days between these sessions, which can have an impact on the magnitude of the observed BDFT. In Figure C-7 and Figure C-8 it is shown that this large range of days between session did not have a considerable impact on BDFT on the two sessions. The difference in BDFT between sessions is plotted against the amount of days between sessions for each participant. A positive difference means the system identification session had a higher feedthrough, while a negative difference means the the second evaluation day had a higher magnitude BDFT. It is clear that the second session overall has less

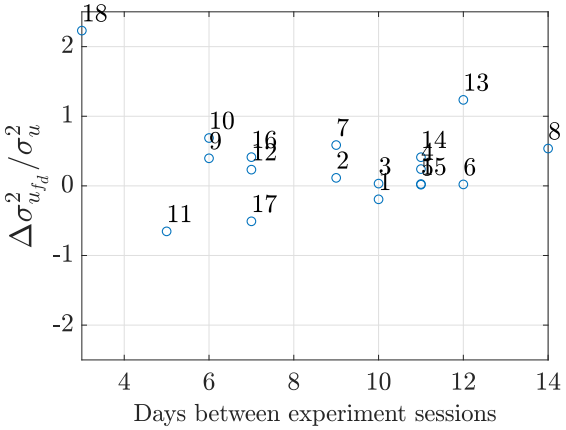

Figure C-7: Correlation between BDFT and days between experiment session for HOR

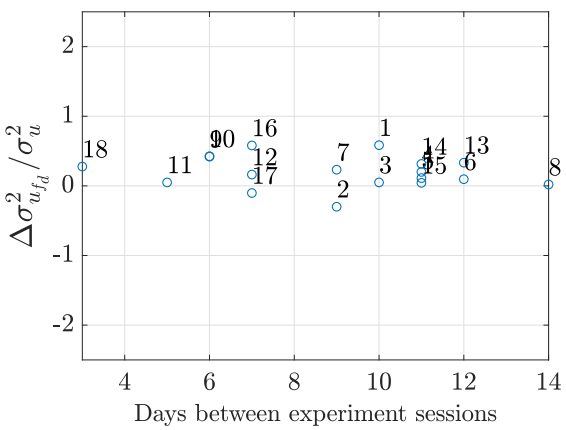

Figure C-8: Correlation between BDFT and days between experiment session for VER

feedthrough than the first day. But any relationship between BDFT and days between sessions is nonexistent.

Appendix D

Experiment Briefing and Consent Form

The following pages show the experiment briefing and consent form that was sent to participants before the experiment. On the day of the two experiment sessions the briefing contents were carefully explained to the participants and the consent form signed before commencing the experiment. Contact information has been redacted or removed due to privacy reasons.

Effect of turbulence on touchscreen dragging tasks

Experiment Briefing

Purpose

Turbulence is an everyday occurrence for pilots and in most cases not considered a danger neither to passengers or the aircraft. With the ongoing introduction of touch sensitive displays on the flight deck the old switches, knobs and buttons are being replaced with their virtual counterparts on the screen. Previous research has shown the difficulty of using a touchscreen under turbulent conditions. This experiment therefore focuses on the the effect of turbulence on touchscreen use.

Apparatus

The research simulator SIMONA (SImulation, MOtion and NAvigation Institute) at the faculty of Aerospace Engineering at the TU Delft is used for the experiment (Figure 1). A touchscreen placed in front of the seat is the only input method and all other screens and outside visuals will be turned off. This screen is placed where the Primary Flight Display (PFD) of a typical aircraft is located. The simulator motion system will be turned on for parts of the experiment to simulate turbulent conditions.

Figure 1

Experiment Task

In total you will perform two different screen tasks. The first task is a pursuit tracking task. Your goal is to minimize the error between your finger and the target you are following. In Figure 2 the white triangle is the target while the purple circle is your finger position. The target will have a smooth motion across the entire screen.

For the second task the same graphics are used as in the first session. This time the target doesn't move in a smooth way, but jumps between different locations. This is called the step task. Your goal is to reach the target location (white triangle) in a smooth way using natural movements. Once you reach the target keep as close to the white triangle as possible until it jumps to the next location.

Because of the touchscreen technology used the the marker indicating your current finger position might be lagging behind your actual position. This might be confusing during the first runs. However, it's your finger position that is important, the marker is just there as an aid.

During both sessions you should only use your index finger and you should not lean on the frame of the screen or rest your elbow anywhere. Additionally, you finger should always be in contact with the screen during the experiment run.

Experiment Procedure

The experiment is split over two days. On the first day only the pursuit task is performed as shown in the table on the following page. Even when the turbulence condition changes you will do the same task. In total day 1 consist of 16 runs of 90 seconds each. It will take around 2 hours to complete including a break of around 15 minutes.

On the second day both the pursuit and step task is used with a total of 24 runs. You will perform different combinations of the tracking task and turbulence condition in a randomized order. There will also be a condition with no motion. That means after every run both the tracking task can change as well as the turbulence condition. Day 2 will also take around 2 hours with a break of around 15 minutes.

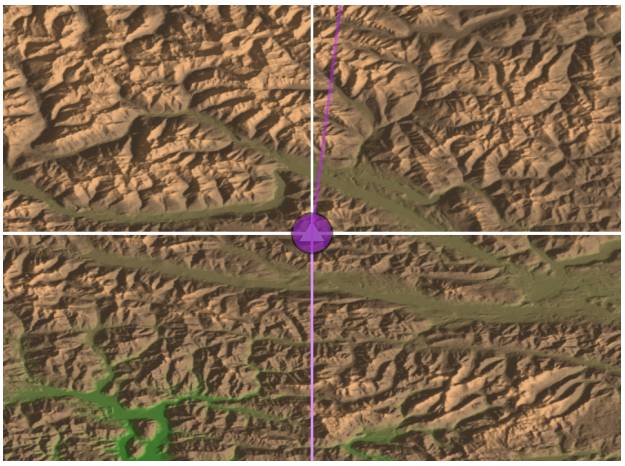

Figure 2: The graphics you will see during the experiment

After meeting at the coffee area in the SIMONA building you will first read this briefing. Any questions you will have will be answered by the experimenter. You will then be asked to sign a consent form. Before the experiment starts you will be given a safety briefing of the simulator and your seating position will be adjusted.

Participation in the experiment is voluntary. Although unlikely, the disturbance can induce motion sickness, it is perfectly fine to request a break at any time during the experiment. You can also stop taking part in the experiment for any reason and at any time by letting the researcher know you don't want to continue.

	Taks	**Motion Condition**	**Runs**
Day 1	Pursuit Task	Different motion	16
Day 2	Pursuit Task Step	Different motion No motion	24

Table 1

Experiment Execution

For each tracking run, the subsequent procedure will be followed:

1. The researcher applies the settings for the next run.
2. The researcher checks whether the participant is ready to proceed and initiates the run after a countdown from 3 (3-2-1-go).
3. The participant performs the 90 second tracking task.

Experiment Consent Form

Effect of turbulence on touchscreen dragging task

I hereby confirm that:

1. I volunteer to participate in the experiment conducted by the researcher (**Arwin Khoshnewiszadeh**) under Supervision of **dr.ir. Daan Pool** from the Faculty of Aerospace Engineering of TU Delft. I understand that my participation in this experiment is voluntary and that I may withdraw and discontinue participation at any time, for any reason.
2. I have read the experiment briefing. Also, I affirm that I understand the experiment instructions and have had all remaining questions answered to my satisfaction.
3. I understand that my participation involves performing a simple manual control task in a moving simulator setup
4. I agree that the researcher collects the following data: age, sex, weight, height, and which hand is your dominant one.
5. I confirm that the researcher has provided me with detailed safety and operational instructions for the hardware (simulator setup, touchscreen) used in the experiment. 6
6. I understand that the researcher will not identify me by name in any reports or publications that will result from this experiment, and that my confidentiality as a participant in this study will remain secure.
7. I have been given a copy of this consent form.

My Signature	Date
My Printed Name	Signature of researcher

Contact information researcher:
Arwin Khoshnewiszadeh
[redacted]

Contact information research supervisor
dr. ir. Daan Pool
[redacted]